TOPFARM - next generation design tool for optimisation of wind farm topology and operation

Larsen, Gunner Chr.; Aagaard Madsen , Helge; Troldborg, Niels; Larsen, Torben J.; Réthoré, Pierre-Elouan; Fuglsang, Peter; Ott, Søren; Mann, Jakob; Buhl, Thomas; Nielsen, Morten; Markou, Helen; Sørensen, Jens Nørkær; Hansen, Kurt Schaldemose; Mikkelsen, Robert Flemming; Okulov, Valery; Shen, Wen Zhong; Heath, Malcolm; King, John; McCann, Graeme; Schlez, Wolfgang; Carlén, Ingemar; Ganander, Hans; Migoya, Emilio; Crespo, Antonio; Jiménez, Angel; Prieto, J.L.; Stidworthy, Amy; Carruthers, Davis; Hunt, Julian; Gray, Stephanie; Veldkamp, Dick; Mouritzen, Anders S.; Jensen, Leo; Krogh, Thomas; Schmidt, Björn; Argyriadis, Kimon; Frohböse, Peter

Publication date:
2011

Document Version
Publisher's PDF, also known as Version of record

TOPFARM - NEXT GENERATION DESIGN TOOL FOR OPTIMISATION OF WIND FARM TOPOLOGY AND OPERATION

Risø-R-Report

Gunner C. Larsen, Helge Aa. Madsen, Niels Troldborg, Torben J. Larsen, Pierre-Elouan Réthoré, Peter Fuglsang, Søren Ott, Jakob Mann, Thomas Buhl, Morten Nielsen, Helen Markou, Jens N. Sørensen, Kurt S. Hansen, Robert Mikkelsen, Valery Okulov, Wen Zhong Shen, Malcolm Heath, John King, Graeme McCann, Wolfgang Schlez, Ingemar Carlén, Hans Ganander, Emilio Migoya, Antonio Crespo, Angel Jiménez, J.L. Prieto, Amy Stidworthy, Davis Carruthers, Julian Hunt, Stephanie Gray, Dick Veldkamp, Anders S. Mouritzen, Leo Jensen, Thomas Krogh, Björn Schmidt, Kimon Argyriadis and Peter Frohböse

Risø-R-1805(EN)
February 2011

Risø DTU
National Laboratory for Sustainable Energy

Author: Gunner C. Larsen, Helge Aa. Madsen, Niels Troldborg, Torben J. Larsen, Pierre-Elouan Réthoré, Peter Fuglsang, Søren Ott, Jakob Mann, Thomas Buhl, Morten Nielsen, Helen Markou, Jens N. Sørensen, Kurt S. Hansen, Robert Mikkelsen, Valery Okulov, Wen Zhong Shen, Malcolm Heath, John King, Graeme McCann, Wolfgang Schlez, Ingemar Carlén, Hans Ganander, Emilio Migoya, Antonio Crespo, Angel Jiménez, J.L. Prieto, Amy Stidworthy, Davis Carruthers, Julian Hunt, Stephanie Gray, Dick Veldkamp, Anders S. Mouritzen, Leo Jensen, Thomas Krogh, Björn Schmidt, Kimon Argyriadis and Peter Frohböse

Title: TOPFARM - NEXT GENERATION DESIGN TOOL FOR OPTIMISATION OF WIND FARM TOPOLOGY AND OPERATION

Division: Wind Energy Division

Abstract:
The present report is the p*ublishable final activity report* for the EU project TOPFARM. The project has been running from 1st December 2007 to 30th November 2010, and has successfully addressed *optimization of wind farm topology and control strategy based on aero-elastic modeling of loads as well as of power production* as seen in an economical perspective. Crucial factors in this regard are the overall wind climate at the wind farm site, the position of the individual wind turbines, the wind turbine characteristics, the internal wind farm wind climate, the wind turbine control/operation strategy for wind turbines interacting through wakes, various cost models, the optimization strategy and a priori defined constraints imposed on the wind farm topology. In TOPFARM, the object function used in the optimization platform is formulated in economical terms, thus ensuring the optimal balance between capital costs, operation and maintenance costs, cost of fatigue lifetime consumption and power production output throughout the design lifetime of the wind farm. The report describes the project consortium and the project activities, which has been organized in 9 Work Packages. A summary description of the results is given, and reference is made to a large number of publications resulting from the project.

Risø-R-1805(EN)
February 2011

ISSN 0106-2840
ISBN 978-87-550-3964-3

Contract no.:
TREN07/FP6EN/S07.73680/038641

Group's own reg. no.:
1110062-01

Sponsorship:
European Commission in the framework of the
NonNuclear Energy Programme
Sixth Framework

Pages: 94
Tables: 7
References: 147

Information Service Department
Risø National Laboratory for Sustainable Energy
Technical University of Denmark
P.O.Box 49
DK-4000 Roskilde
Denmark
Telephone +45 46774005
bibl@risoe.dtu.dk
Fax +45 46774013
www.risoe.dtu.dk

1 INTRODUCTION

Establishment of large wind farms requires enormous investments putting steadily greater emphasis on *optimal topology design and control* of these. Today, the design of a wind farm is based on an optimization of the power output only, whereas the load aspect is treated only in a rudimentary manner, in the sense that the wind turbines are required only to comply with the design codes. However, in order to achieve the *optimal economic output* from a wind farm during its life time an optimal balance between - on the one hand - capital costs, operation and maintenance costs, costs related to component fatigue lifetime consumption and - on the other hand - power production output is to be determined on a rational background. This is not a trivial problem.

The TOPFARM project addresses this problem. The *power production* and *loading* patterns, related to turbines placed in a wind farm, deviate significantly from the production- and loading of similar stand-alone wind turbines subjected to the same (external) wind climate. Crucial factors in this connection are the relative position of the individual wind turbines and the wind turbine control/operation strategy for wind turbines interacting through wakes. Compared to a standalone turbine, a turbine located within a wind farm typically experiences higher loading and produce less energy. This would in principle imply that a wind farm should be designed with turbine spacings sufficiently large to essentially eliminate the wind turbine mutual interactions. However, due to area constraints and financial costs associated with the grid (and civil engineering) infrastructure this is not an attractive approach, and consequently more sophisticated strategies must be developed.

Such strategies require formulation of advanced in-stationary flow models that include dynamic wake effects for a realistic description of the wind farm flow field, advanced (and fast) aeroelastic models for load and production prediction, dedicated cost and control strategy models, and a subsequent synthesis of these models in a layout optimization algorithm subjected to various kinds of constraints, as e.g. area constraints and turbine interspacing constraints. The TOPFARM project thus clearly requires a multidisciplinary effort.

Because optimization algorithms in general are iterative procedures that need a huge number of iterations before convergence to the global optimum is achieved, a major challenge for the project has been to develop fast approximate models and yet preserve the essential physics of the problem. This computational challenge inevitably had to be met on all levels ranging from the wind farm wind field simulation to the aeroelastic simulation and the optimization strategy.

2 CONSORTIUM

The consortium behind the TOPFARM project is a balanced group with representatives from different European countries; it represents Universities, Research institutions, Utilities, wind turbine manufacturers private consultancies and Certification bodies. The consortium of universities, research institutions, consulting engineers, certification agencies and manufactures, turned out to be uniquely well placed to tackle the challenges of the technical program.

Details of the consortium participants, with a short description of their expertise's and contributions to the project activities, appear in Table 1.

Table 1: Consortium specifications.

Organ. Name	Type	CC	Activity	R&D Function in the project
The Technical University of Denmark (Participant ID: RISOE.DTU)	HE	DK	Wind energy experts, R&D, Aeroelasticity experts, CFD experts	WP1: Formulate turbulent wake wind field models WP2: Develop load prediction tools WP3: Modelling of control strategies WP4: Verification of model toolbox WP5: Cost model formulation WP6: Formulate optimisation method, test algorithms WP7: Optimal design of Middelgrunden wind farm WP8: Optimal design of Coldham and Stags Holt wind farms WP9: Co-ordination, workshop and management
Cambridge Environmental Research Consultants ltd. (Participant ID: CERC)	OTH	UK	CFD experts, Turbulence experts	WP1: Formulate turbulent wake wind field models WP8: Optimal design of Coldham and Stags Holt wind farms
The Technical University of Denmark (Participant ID: MEK.DTU)	HE	DK	Wind energy experts, R&D, Aeroelasticity experts, CFD experts	WP1: Formulate turbulent wake wind field models WP2: Develop load prediction tools WP4: Verification of model toolbox WP7: Optimal design of Middelgrunden wind farm
DONG Energy Power A/S (Participant ID: DONG)	IND	DK	Utility, Developer	WP1: Formulate turbulent wake wind field models WP2: Develop load prediction tools WP4: Verification of model toolbox
Vestas Wind Systems A/S (Participant ID: VESTAS)	IND	DK	Wind turbine manufacturer	WP4: Verification of model toolbox WP5: Cost model formulation WP6: Formulate optimisation method, test algorithms
Garrad Hassan and Partners ltd. (Participant ID: GH)	OTH	UK	Wind energy experts, Consultancy	WP2: Develop load prediction tools WP3: Modelling of control strategies WP4: Verification of model toolbox WP5: Cost model formulation WP7: Optimal design of Middelgrunden wind farm
Germanischer Lloyd Industrial Services GmbH (Participant ID: GL)	IND	DE	Certifying body	WP2: Develop load prediction tools WP3: Modelling of control strategies WP4: Verification of model toolbox
Teknikgruppen (Participant ID: TG)	IND	SW	Wind energy experts, Aeroelasticity experts, Consultancy	WP2: Develop load prediction tools WP3: Modelling of control strategies WP4: Verification of model toolbox WP6: Formulate optimisation method, test algorithms
Universidad Politécnica de Madrid (Participant ID: UPM)	HE	ES	Wind energy experts, CFD experts, Turbulence experts	WP1: Formulate turbulent wake wind field models

3 PROJECT ACTIVITIES

The TOPFARM project is organized in eight work packages focusing on different technical topics (WP1-WP8) plus an additional work package (WP9) dedicated to project management and dissemination of results. The work packages and their interdependencies are schematically illustrated in Figure 1.

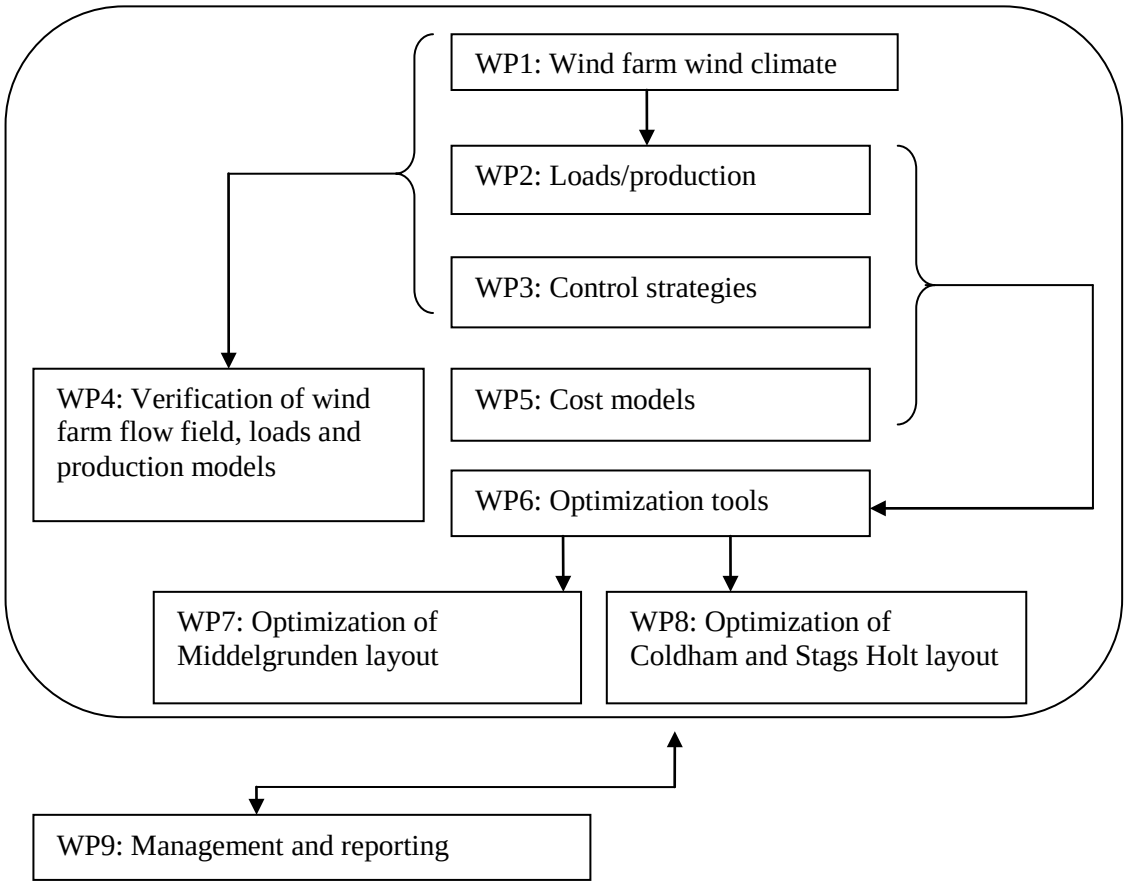

Figure 1: Project work packages and their interdependencies.

In the following sub-sections the technical work packages are briefly described, and the work package responsible project partners are indicated.

3.1 WP1 – Wind farm wind climate

WP1 is a fundamental WP dealing with characterization and modeling of the wake affected flow field inside a wind farm. The responsible of this WP is RISOE.DTU. The goal is a model complex that is sufficiently fast to allow for an optimization application and, at the same time, sufficiently detailed for achieving reliable prediction of power production and wind turbine loads, as based on aero-elastic simulations, given the ambient wind climate at the location of interest as boundary condition. More specifically, this implies derivation of models describing the *wake deficit* (incl. attenuation and expansion with downstream position), the *added (inhomogeneous) wake turbulence* caused by turbines located upstream, and the *wake meandering* caused by large scale turbulence structures in the atmospheric boundary layer.

Because meandering is presumed to be driven by the large scale turbulence structures, it is important to investigate a possible *feed-back* on these large-scale structures originating from the presence of wind turbines. This question is addressed by analysis of full-scale wind farm measurements.

The wake deficit and the added wake turbulence are ultimately related to the aerodynamics as well as to the control strategy of the wake generating rotor. The added wake turbulence is *small-scale* turbulence with characteristic eddy seizes up to approximately one rotor diameter (D), and include contributions from conventional mechanically generated turbulence, caused by the shear associated with the wake deficit, as well as from the blade bound vorticity consisting mainly of tip and root vortices. These vortices initially have the form of organized coherent flow structures, but later gradually break down due to instability phenomena and approach the characteristics of conventional (isotropic) turbulence with a length scale shorter than that of atmospheric turbulence.

Because the ultimate goal of the TOPFARM project is to develop a tool for *optimization* of wind farm layout – involving a computationally demanding iterative process – it is, as mentioned in Section 1, of crucial importance that the resulting models of the complex wind field within a wind farm can be "condensed" into *fast*, though accurate, flow simulation tools. The basic strategy for achieving this goal goes through a *chain of flow models* of various complexities, where the advanced and computational very demanding (RANS based) CFD-based models, together with available experimental evidence, are used to formulate, calibrate and verify simpler models ranging from simplified CFD models to more engineering (stochastic) type of models.

3.2 WP2 – Aero-elastic simulation of loads and power production

In WP2 the detailed three dimensional dynamic wake wind field modeling, resulting from WP1, is used to model wake inflow characteristics to state of the art aeroelastic codes (Bladed [122], HAWC2 [133] and VIDYN [142], respectively) to facilitate full aeroelastic load- and production calculations of wind farms. The coupling of the advanced wake wind field description with aeroelastic codes enables us to get a correct and detailed estimation of wind turbine (fatigue) loads as well as of wind turbine production. This is contrary to today's more rudimentary modeling possibilities where challenges as e.g. wake meandering, near wake situations and wake effects caused by a yawed turbine are insufficiently described. The responsible of this WP is GH.

3.3 WP3 - Control strategies

The development of control concepts for wind turbines to be placed in a wind farm may have several different targets. The primary goal is usually to achieve high power production, good power quality, and low levels of fatigue loading in vital turbine components. In wind farms the flow in the wakes of upstream turbines is often characterized by high levels of turbulence and frequent periods of asymmetric wind loading over the rotor. If a control system of an *individual turbine* is designed to reduce the effects of wake operation inside the farm, then it is also likely that some information about wake transport directions can be extracted and communicated to a master controller at all times. This kind of information is essential when developing

successful concepts for wind farm control strategies as e.g. *Wind Sector Management.* WP3 deals with control algorithms both for individual turbines in wind farms and options for wind farm control strategies. The responsible of this WP is TG.

3.4 WP4 - Verification of load and production sub-models

Work packages 1-3 encompass a range of advanced sub-models. The objective of WP4 is to verify these, as well as their interaction, in full-scale environments. Model predictions are compared with available *power production*- and *structural measurements* as well as with detailed *flow measurements*. In addition to existing full-scale experiments, new *dedicated* full-scale experiments are performed within WP4 with the primary aim of analyzing wake turbulence and wake-wake interaction. The responsible of this WP is MEK.DTU.

3.5 WP5 - Cost models

The two main objectives of WP5 are to develop a cost model describing the *capital costs* relevant for the wind farm topology optimization, and to develop an *operation and maintenance* cost model primarily linking these costs to the turbine fatigue lifetime consumption. The overall philosophy is to consider only costs that depend on wind farm topology and/or control philosophy, because only these are relevant for the wind farm optimization. The responsible of this WP is GH.

3.6 WP6 - Optimization platform

The objective of this work package is to develop an *optimization procedure* that, based on the models and methods resulting from WP's 1, 2, 3 and 5, allows for optimization of a wind farm layout considering energy production, turbine degradation (fatigue loads) and total installation costs. The optimization problem may be subjected to various types of constraints (area, minimum distances between turbines etc.). The responsible of this WP is RISOE.DTU.

As already mentioned, an optimization study of a wind farm will involve a huge number of complex and time consuming analyses. In order to make such a study at all possible, focus must be put on *all* different possibilities to reduce computational costs. A priori, there are (at least) two optimization philosophies of particular interest in this respect – the use of *variable fidelity* modeling, and the use of *structured optimization grids*.

Variable fidelity modeling is an approach often seen in applied aeronautics. It means e.g. that an *approximate and fast* model is used for a vast majority of the parameter evaluations needed for a design study, while a more *detailed and accurate* model is used in regions of specific interest. It is, however, important that the *low fidelity* describes the same physics as the *high fidelity* model, albeit in a coarser and more approximate way.

A schematic illustration of a two level fidelity approach is shown in Figure 2, with parameters (and gradients) associated with the two involved models denoted by f (∇ f) and a (∇ a), respectively.

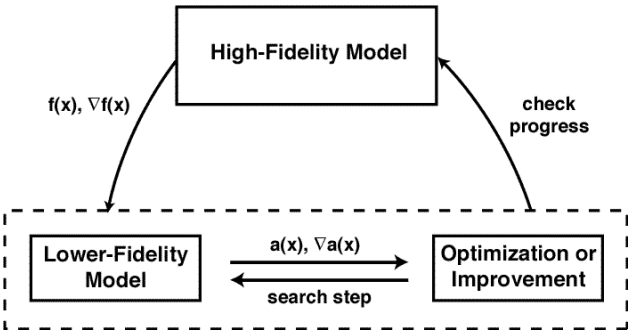

Figure 2: Two level fidelity optimization.

The methodology is easily generalized to more fidelity levels. For this particular application, a three level fidelity approach is suggested, with Level 1 being related to production optimization as based on simple analytical or linear numerical (CFD) models; Level 2 being optimization based on table look-up and interpolation in data, which is generated prior to the optimization for a limited number of generic load cases (based on the complex model); and Level 3 being the level of highest complexity characterized by full aero-elastic load calculations combined with wake meandering, etc..

The second reduction philosophy – i.e. the use of structured grids – relates to reduction of the design variable space, however, on the cost of the resolution of the design domain.

3.7 WP7 - Optimization of the Middelgrunden wind farm

The objective of this work package is to demonstrate the potential of the developed optimization method on an *offshore* site. This is achieved by re-designing the famous Danish Middelgrunden offshore wind farm just off the coast of Copenhagen. It is composed of 20 Bonus B80 2MW wind turbines with a rotor diameter of 76 m and a hub height of 64 m. In the original design, the wind turbines are arranged in an arc with 2.3D turbine inter-spacing.

3.8 WP8 - Optimization of the Coldham and Stags Holt wind farms

The objective of this work package is to demonstrate the potential of the developed optimization method in layout of *onshore* wind farms. This is achieved by re-designing the topology of the Coldham/Stags Holt wind farms consisting of 8+9 Vestas V80 turbines with 60m hub height. The Coldham site is a flat onshore terrain close to March (north of London), and prior to the layout optimization the ambient wind climate for the site must be characterized.

4 PROJECT RESULTS

In the present Section a summary description of the results is given. The results are presented work package by work package.

4.1 WP1 – Wind farm wind climate

As mentioned in Section 3.1 the activities in WP1 encompasses a hierarchy of flow models ranging from very detailed – and computational very demanding – CFD-based models to simplified and fast models. These codes are either developed or refined within the framework of the TOPFARM project, and are briefly described in the flowing sub-sections.

UPMPARK model (UPM)

UPMPARK model is a CFD code that describes the diffusion of multiple wakes in the atmospheric surface layer parameterized by Monin-Obukhov scaling [124]. The equations describing the flow are the conservation equations of mass, momentum, energy, turbulence kinetic energy, and the dissipation rate of the turbulence kinetic energy. The modeling of the turbulent transport terms is based on the k-ε method for the closure of the turbulent flow equations. Formerly, the code was steady because it would be supposed that the air crosses the park faster than the ten minutes averaged measured time. The convective term is simplified because the boundary layer approximation is employed; then the diffusion length in the main direction is higher than diffusion length in the transversal and vertical direction. Besides, viscous stress term and heat molecular diffusion term are supposed lower than the turbulent stress term and the heat turbulent diffusion term in the momentum and energy equations respectively. Therefore, a parabolic approximation was obtained. The code has two options. There is a simplified option in which only the convective terms containing the main flow velocity are retained. In the more advanced version the convective terms, containing the velocity components perpendicular to the main flow direction, are also retained. In any way, the set of equations has been solved numerically using the SIMPLE algorithm. Finite difference methods were used in the discretization of the equations and the equations were solved numerically by using an alternate-direction implicit (ADI) method. The developed wake model is three dimensional and pressure variations in the cross-section have to be retained in order to calculate transverse velocities.

Within the framework of the TOPFARM project, UPMPARK has been modified in order to retain the non-steady terms for the simplified version of the code. Unsteady terms have been incorporated considering convection only in the main flow direction, x-axis, which is not the instantaneous wind direction; otherwise it's the averaged direction of the wind turbines. In a first version of the unsteady code, the program runs for a wind whose direction changes with time in a sinusoidal way. A stochastic simulation, based on Shinozuka [138], has been implemented to take into account the meandering wake. Changes in the wind characteristics due to large sale turbulence have been retained and incorporated simultaneously to UPMPARK. Kaimal and Von Kármán expression could be employed to obtain spectrum for x and y directions, IEC-61400. Both of them use as data the average and variance incident wind speed, average incident wind direction and a scale parameter of turbulence. Stochastic time series generators are based on the integration of velocity spectrum. Therefore, summations of harmonics, with a random phase and amplitudes, which follow one of the previously mentioned spectral density function, are used.

Linearized mixed spectral model (Fuga; RISOE.DTU)

A model for offshore wakes based on linearized CFD equations has been developed. The model is based on a set of RANS equations with some kind of closure. At the moment we can handle k-ε mixing length closure and the simple closure with the eddy viscosity set equal to $\kappa u_* z$. A perturbation expansion is made with the wind turbine drag force acting as a 'small' perturbation.

There exists a wealth of linearized flow models. Most often these models use simplified equations where only the most important terms are kept. Which terms to keep, depends on in which layer you are in (two or three layers are typical). Analytical solutions are derived for the various layers and these are pieced together by asymptotic matching. The present model uses a different strategy. All terms, large or small, are kept and numerical solutions are made. This means that the same, linear solver, in principle, can be used for all orders, because we do not have to worry about how to divide into layers for higher orders.

The zero order equations are simply the original equations with no drag force, and, although non-linear, they are easily solved due to the simple boundary conditions (a flat sea surface at the bottom and a specified velocity at some height z_i). The equations for all other, higher orders are linear and have the same form except for a source term. The source term depends on lower order perturbations in a non-linear way, but when the calculations proceed from lower to higher orders, this is known. The same, linear solver can therefore be used for all orders higher than zero. At the moment we have, however, not attempted to go beyond first order.

A *mixed-spectral formulation* is used, which leads to a de-coupling into finite sets of coupled, ordinary differential equations. There is one independent set of equations for each horizontal wave vector.

Solving the equations proves, however, to be surprisingly difficult. Unfortunately all state-of-the-art solvers we have come across fail to do the job properly. It is the fact that it is a two-point problem (boundary conditions both at the top and at the bottom) that makes the equations hard to solve. A new method had therefore to be developed. It is based on the chasing method, also employed in Mathematica, but with some tricks added. In the chasing method a boundary condition is moved to another location by solving auxiliary equations. In this way all boundary conditions can be moved e.g. to the top. This changes the problem to an initial value problem, which can be solved marching down from the top to the bottom. This should reproduce the lower boundary conditions, but in practice this does not happen. This is because the accuracy needed to specify the top boundary conditions and the subsequent solution is exorbitant. 50 decimal places may not be enough. The trick is to make stations on the way up where the boundary conditions calculated by the auxiliary equations is changed into an equivalent set that improves the numerical inaccuracy in the subsequent calculation.

The principle of superposition is used intensively. Thus the combined wake of many turbines can be obtained from the wake of a solitary turbine. The solitary wake is in turn made from Fourier components stored in pre-calculated look-up-tables (LUTs). Lately we have extended this principle to what we refer to as preliminary LUTs, or preLUTs. These are look-up-tables

that can be used to make look-up-tables. The preLUTs do not depend on wind farm layout, wind speed and direction, surface roughness or inversion height. They can therefore be calculated at installation time once and for all.

A Fortran program that calculates preLUTs and processes them into LUTs has been made. It is called Preludium. Preludium is Latin (or Danish) for prelude, and it is not an acronym. A C program was also made that can make wakes from LUTs. It is called Trafalgar, for obscure reasons named after a sea battle. Finally, a Windows application called Fuga (meaning fugue, often following a prelude) was made using Delphi. Fuga is a GUI that controls Preludium and Trafalgar and interfaces with the WAsP world. Thus Fuga gives the user access to WAsP wind climate files, wind farm layout files and wind turbine data. Output from Fuga is in terms of energy production for specific wind conditions and individual turbines as well as estimates of total annual production. These programs were developed under a separate contract with Carbon Trust, but on the basis of methods and Mathematica implementations developed in the TOPFARM project.

One of the outcomes of the TOPFARM project is that 'industrial standard' RANS CFD models do not seem to work reliably when it comes to wakes, and there is no reason to expect linearized versions of them to do any better. It is possible to tune a k-ε to match wake data to some degree, but the tuned constants will depend on the surface roughness. This lack of universality indicates an inability of the model to properly represent the physical phenomena. In light of this it was decided to use the simplest possible approach. For mean flow calculations the only input from the closure model is the eddy viscosity ν_t, which can be determined in various ways. In the k-ε model ν_t is made up from k and ε, and in the mixing length closure it is determined by a predefined local mixing length and the rate of strain of the mean flow. The simplest choice is to set ν_t equal to the unperturbed value $\kappa u_* z$. This approach works surprisingly well and is preferred until turbulence theory comes up with something better.

A linearized model is much faster than the non-linear CFD model on which it is based. With the speed ratios exceeding 10^4 the advantage is clear: CFD calculations taking one week take less than one minute with linearized CFD.

The Actuator Line Method (ACL; MEK.DTU and RISOE.DTU)

The CFD ACL approach has been intensively used for verification and calibration of the Dynamic wake Meandering model at RISOE.DTU. Basically, the wind turbine rotor is simulated using the actuator line model developed by Sørensen and Shen [139]. This model combines a three-dimensional Navier-Stokes solver with a technique in which body forces, determined from the local angle of attack and a look-up table of aerofoil data, are distributed along lines representing the blades of the wind turbine using a suitable smearing function. The computations of the flow field have been carried out with the 3D flow solver EllipSys3D [139], [136], [140] using Large Eddy simulations (LES).

The atmospheric boundary layer is modeled using a technique [137], [141] where body forces applied to the entire computational domain are used to prescribe a given steady wind shear profile, while free-stream turbulence is modeled by superimposing synthetic turbulent velocity fluctuations to the

mean flow in a cross-section upstream of the rotor. The introduced turbulence field was generated in advance with the Mann algorithm [135].

Parabolic Navier-Stokes solver (ParaSol; MEK.DTU)

In order to speed up CFD simulations of wake affected flow fields MEK.DTU has developed a new parabolic Navier-Stokes solver (ParaSol). The solver is based on the parabolised Navier-Stokes equations, where gradients in the flow direction of the diffusion as well as the pressure gradient in the flow direction are neglected, whereby the velocity and pressure in each plane can be coupled dynamically. The code uses staggered grid arrangements and integrates plane by plane from upstream to downstream.

The final parabolised Navier-Stokes equations read

$$\frac{\partial(\rho u)}{\partial x}+\frac{\partial(\rho v)}{\partial y}+\frac{\partial(\rho w)}{\partial z}=0 \tag{1}$$

$$\frac{\partial(\rho u)}{\partial t}+\frac{\partial(\rho uu)}{\partial x}+\frac{\partial(\rho vu)}{\partial y}+\frac{\partial(\rho wu)}{\partial z}=-\frac{\partial p}{\partial x}+\frac{\partial}{\partial x}\left[(\mu+\mu_t)2\frac{\partial u}{\partial x}\right]+\frac{\partial}{\partial y}\left[(\mu+\mu_t)\left(\frac{\partial u}{\partial y}+\frac{\partial v}{\partial x}\right)\right] \tag{2}$$

$$\frac{\partial(\rho v)}{\partial t}+\frac{\partial(\rho uv)}{\partial x}+\frac{\partial(\rho vv)}{\partial y}+\frac{\partial(\rho wv)}{\partial z}=-\frac{\partial p}{\partial y}+\frac{\partial}{\partial x}\left[(\mu+\mu_t)\left(\frac{\partial v}{\partial x}+\frac{\partial u}{\partial y}\right)\right]+\frac{\partial}{\partial y}\left[(\mu+\mu_t)2\frac{\partial v}{\partial y}\right] \tag{3}$$

$$\frac{\partial(\rho w)}{\partial t}+\frac{\partial(\rho uw)}{\partial x}+\frac{\partial(\rho vw)}{\partial y}+\frac{\partial(\rho ww)}{\partial z}=\frac{\partial}{\partial x}\left[(\mu+\mu_t)\frac{\partial w}{\partial x}\right]+\frac{\partial}{\partial y}\left[(\mu+\mu_t)\frac{\partial w}{\partial y}\right] \tag{4}$$

The equations are solved with the fractional step or projection method. In the prediction step, the parabolised Navier-Stokes equations are solved without the pressure terms. In the correction step, pressure is obtained from the pressure equation

$$-\frac{1}{\delta t}\left[\frac{\partial(\rho u^*)}{\partial x}+\frac{\partial(\rho v^*)}{\partial y}+\frac{\partial(\rho w^*)}{\partial z}\right]=-\left(\frac{\partial^2 p}{\partial x^2}+\frac{\partial^2 p}{\partial y^2}\right). \tag{5}$$

When the pressure is available, the velocity in each plane is corrected according to

$$\begin{aligned}\rho u &= \rho u^*-\delta t\frac{\partial p}{\partial x}\\ \rho v &= \rho v^*-\delta t\frac{\partial p}{\partial y}\end{aligned} \tag{6}$$

In order to simulate wind turbine wakes, an Actuator Line (ACL) model is implemented in the ParaSol code. The ParaSol code is about 8 times faster than the corresponding full elliptic code EllipSys3D code.

Atmospheric Dispersion Modeling System (ADMS 4; CERC)

ADMS 4 is a practical, short-range dispersion model that simulates a wide range of types of releases to the atmosphere either individually or in combination. It is a "new generation" dispersion model using two parameters, namely the boundary layer height h and the Monin-Obukhov length L_{MO} to describe the atmospheric boundary layer and using a skewed Gaussian concentration distribution to calculate dispersion under convective conditions. The model is applicable up to 60 km downwind of the source and provides useful information for distances up to 100 km.

Wind turbine wakes are modeled in ADMS 4 as an initial wake deficit with the dimensions of the fully-expanded wake; this is then dispersed according to the characteristics of the atmospheric boundary layer. The magnitude of the initial wake deficit is $2aU$, where a is the calculated axial induction factor and U is the inflow wind speed at the turbine hub height. The axial induction factor a may be calculated either by iterative solution of the Blade Element Momentum (BEM) equations, or from the relationship between thrust coefficient and a, depending on the user's choice. Zero yaw is assumed. The ADMS 4 turbulent fluctuations model calculates the additional turbulence generated by the meandering of the wake.

Turbines are automatically modeled in order, starting with the most upstream turbine, and finishing with the most downstream turbine. The vertical wind and turbulence profile used to characterize the flow dispersing each wake includes the effect of all upwind turbines.

Entrainment into the wake is delayed for turbines not inside the wake of another turbine; a turbine is defined as being inside a wake if its hub is less than $2\sigma_y$ from the centerline of the wake behind any upstream turbine. The time delay before entrainment starts is:

$$t_E = t_{u_{\min}} + 3 \times \frac{D}{U} \times \exp(-20 \times \max(I - 0.05, 0)); \tag{7}$$

where $t_{u_{\min}} = \frac{2D}{U}$ (D is turbine diameter, I is turbulence intensity).

An additional term is added to the turbulent velocities to account for the effect of the flow gradient (or 'shear') at the edge of the wake. For turbines not inside an upstream wake, this added shear-induced turbulence at a downstream distance x is:

$$\sigma_{shear} = \begin{cases} 0.1 \times |\Delta U_{\max}| & 7D \le x \\ \left(\frac{x - 2D}{5 \times D} \right) \times 0.1 \times |\Delta U_{\max}| & 2D \le x \le 7D \\ 0 & x \le 2D \end{cases} \tag{8}$$

For a turbine inside a wake, the added shear-induced turbulence is $\sigma_{shear} = 0.1 |\Delta U_{\max}|$.

Dynamic wake meandering model (DWM; RISOE.DTU)

The development of the Dynamic Wake Meandering (DWM) model was initiated in 2003. The background was the need in the industry for a wake model that could predict more details of the increased loading in wake operation than the equivalent turbulence method which is the standard method for computation of increased loading in wakes. The DWM model computes also the decrease in power production, and the model forms therefore a good basis for a thorough optimization of the layout of new wind farms, taking into account both power production and loading.

The DWM model was developed with the objective to model the basic wake flow mechanisms with sufficient accuracy while keeping the model as simple as possible. The DWM model complex is based on the combination of three elements: 1) modeling of quasi-steady wake deficits; 2) a stochastic model of the downwind wake meandering; and 3) added wake turbulence.

The *wake meandering* part is based on the fundamental assumption that the transport of wakes in the atmospheric boundary layer can be modeled by considering the wakes to act as passive tracers driven by the large-scale turbulence structures in lateral and vertical directions. Modeling of the meandering process consequently includes considerations of a suitable description of the "carrier" stochastic transport media as well as of a suitable definition of the cutoff frequency defining large-scale turbulence structures in this context. For the stochastic modeling of wake meandering, we imagine a wake consisting of a cascade of wake deficits, each "emitted" at consecutive time instants in agreement with the passive tracer analogy [47], [48]. We subsequently describe the propagation of each of the emitted wake deficits, and the collective description of these constitutes the wake meandering model.

Adopting Taylor's hypothesis, the down-stream advection of these wakes is assumed to be controlled by the mean wind speed of the ambient wind field. With this formulation the wake momentum in the direction of the mean flow is invariant with respect to downstream displacement. This is a considerable simplification allowing for a straight-forward decoupling of the wake along wind deficit profile (and its expansion) and the wake transportation process. As for the dynamics in the lateral- and vertical directions, each considered wake cascade element is displaced according to the large-scale lateral- and vertical turbulence velocities at the position of the particular wake cascade element at each time instant.

The choice of a suitable stochastic turbulence field, that in turn defines the stochastic wake transport process, is not mandatory, but may be guided by the characteristics of the atmospheric turbulence at the site of relevance. These characteristics encompass in principle not only turbulence standard parameters such as turbulence intensity, turbulence length scale and coherence properties, but also features like degree of isotropy, homogeneity of the turbulence, Gaussianity of the turbulence etc.. The meandering mechanism in the DWM model has been successfully verified by correlating DWM predictions with direct full-scale measurements of the instantaneous wake position obtained from LiDAR recordings [5].

The turbulence box for the meandering process is generated using a transverse resolution of one rotor diameter. Further, a second order time filter

on the transverse wind speed is applied in order to remove smaller turbulence scales than two rotor diameter. The filter cut-off frequency, f_c, is defined as

$$f_c = \frac{U}{2 \times D} \tag{9}$$

where U denote the mean wind speed, and D is the diameter of the wake producing turbine rotor.

A detailed description of a recent calibration of the DWM model can be found in Madsen et al. [82], where also some validation cases are included.

GH Bladed with dynamic wake meandering model (BLADED; GL)

GH Bladed [122] is a state of the art aero-elastic wind turbine simulation code with fully coupled modal dynamic modeling. The dynamic wake meandering model allows a dynamic wake deficit to be superimposed on top of ambient turbulence. The sections below describe the components of the dynamic wake meandering model.

Meandering time history generation: Within Bladed, the wind file governing the meandering motion is generated from a low pass filtered turbulence spectrum. The wind file velocities resulting from the reverse Fourier transform of this turbulence spectrum are therefore those associated with the low frequency components of the turbulence. The low pass frequency suggested by Risø-DTU [47] for ambient turbulence-wake interaction is defined as

$$f_c = \frac{U}{2 \times D} \tag{10}$$

The low frequency components of the turbulence govern the lateral and vertical transportation of the wake deficit downstream. Since the wind file has been generated to only include the velocities that interact with the wake, no further filtering or processing of the velocities is required.

The meandering displacement time history is based on the ‘cascade of deficits’ model reported by Risø-DTU [47]. This assumes a deficit is released at each time step within a frozen turbulent wind field. The transportation of each deficit is governed solely by the velocity that it encounters as it is released into a *given* plane (y,z) of the frozen turbulent wind field. Therefore the lateral (y) and vertical (z) wake displacements at downwind position L_d is equal to

$$\begin{aligned} y(t) &= \int_{t-L_d}^{t} v_c\left(y, z, t, t - L_d / U\right) dt \\ z(t) &= \int_{t-L_d}^{t} w_c\left(y, z, t, t - L_d / U\right) dt \end{aligned} \tag{11}$$

where ($t - L_d/U$) is the release time of the deficit arriving at the downstream position L_d at time t, and v_c and w_c denote the filtered turbulent velocities.

Wake deficit velocity profile is determined using the existing Eddy Viscosity Model proposed by Ainslie [118] initialized with an induced pressure-expanded velocity deficit. The Ainslie model is based on the thin shear layer

approximation of the Navier-Stokes equation. The Reynolds stress terms governing the transfer of momentum from the ambient turbulence to the wake at each downwind position are approximated with an eddy viscosity proportional to the width of the deficit shear layer and the shear velocity gradient.

4.2 WP2 – Aero-elastic simulation of loads and power production

WP2 deals with full aeroelastic load- and production modeling of the individual wind turbines constituting the wind farm, as based on detailed three dimensional in-stationary wake wind field modeling resulting from WP1.

Because computational speed is a critical issue in relation to the ultimate optimization application, the interfacing of aeroelastic models and the flow field models requires selection of flow models that are suitable in this respect. In the framework of TOPFARM it was decided to base the aeroelastic computations on the DWM wake wind field model, basically because this model is both fast and capable of model the required in-stationary/intermittent characteristics of wake affected flow fields, which is essential for realistic load predictions. In addition to fast flow models, fast aeroelastic codes are equally essential, and a study on profiling such codes has therefore also been conducted.

Even with fast models, a complete aeroelastic simulation of the whole wind farm in each interative step of the optimization loop is a computational challenge, and therefore simpler, more approximate, approaches based on table look-up in databases of generic wake load cases have been investigated. Finally, load predictions resulting from the WP2 approach have been compared with load predictions as based on the IEC code recommendations.

Implementation of the DWM model in state of the art aeroelastic codes

The DWM model has been implemented in three state of the art aeroelastic codes – Bladed [122], HAWC2 [133] and VIDYN [142], respectively – in order to facilitate full aeroelastic calculations of wind farms. The coupling of the advanced in-stationary wake wind field description with aeroelastic codes enables us to get a realistic and detailed estimation of wind turbine (fatigue) loads as well as of wind turbine production, which both are essential elements in the intended thorough topology optimization.

Basic elements of the DWM model are briefly described in Section 4.1, and a more detailed description of the DWM philosophy can be found in [47]. The final calibration of the model and the specific principles applied for the implementation in an aeroelastic code are described in detail in [82].

The basic principle for the implementation is to define a coarse grid – typically with a grid size of the order of a rotor diameter – to resolve the large scale turbulence driving the meandering of the *quasi-steady wake deficit* along with its self-generated small scale *wake turbulence*. For the present implementation, a turbulence field obtained from the Mann spectral tensor [84] has been used, but this choice is not mandatory. The quasi-steady wake deficit is computed using the Blade Element Momentum (BEM) theory in

combination with the boundary layer approximation of the Navier-Stokes in their rotational symmetric form.

Databases of generic wake load cases

Even with fast flow- and aeroelastic models available, it is a challenge to keep computational costs on a reasonable level in an optimization context. A possible simplified approximate approach to deal with this challenge is to base the fatigue load calculations on a database of pre-calculated generic load cases for turbines in wake operation. Total lifetime equivalent fatigue loads can then be found by interpolating and summing contributions from these individual load cases.

One such database was created using the aeroelastic code, HAWC2 [133], [134] with the DWM implemented to simulate 7436 generic load cases of each of 600 seconds as based on UPWIND 5 MW turbine [132]. The type of generic inflow situations covered is illustrated in Figure 3.

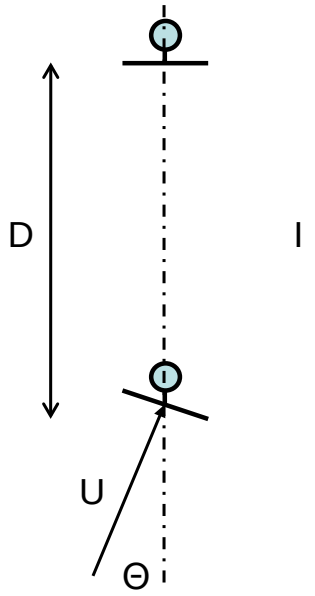

Figure 3: Definition of inflow parameters for the turbine being in wake of an upstream turbine.

The resulting database contains the following parameter variations:

1. Mean wind speed, U, varied from 4 m/s to 26 m/s in steps of 2 m/s;
2. Ambient turbulence intensities I = {1%, 5%, 10%, 15%};
3. Azimuth angles Θ = {0^o, 0.5 ^{o}, 1^o, 2^o, 3^o, 4^o, 5^o, 10^o, 15^o, 20^o, 25^o, 35^o, 45^o}; and
4. Distances from the closest upstream turbine (in rotor diameters) D = {1, 2, 3, 4, 5, 6, 7, 8, 9, 10, 12, 16, 20}.

The subsequent data processing of these aeroelastic simulations involved extraction of statistical information as well as a quantification of the fatigue loading of selected structural elements. The fatigue evaluation was based on a traditional Rainflow counting [147] of the load cycles combined with a S-N formulation of the fatigue loading using representative Wöhler curve exponents for the components in question.

The sensors in Table 2 were defined. In addition to the six load sensors, the electrical power was included in the statistical analysis to enable estimation of annual energy yield (AEP) on basis of the results.

Table 2: HAWC2 sensors defined for look-up database.

Sensor	**Wöhler curve exponent**
Tower base over turning bending moment, Mx_{Tower}	4
Tower base transverse bending moment, My_{Tower}	4
Nacelle (tower top) tilt moment, $Mx_{Nacelle}$	8
Nacelle (tower top) yaw moment, $Mz_{Nacelle}$	8
Blade root flapwise bending moment, My_{Blade}	12
Blade root edgewise bending moment, Mz_{Blade}	12
Electrical power, P_{Elec}	-

As the database is based on the UPWIND 5MW turbine, it is not directly applicable for wind farms consisting of other wind turbines. However, a first order approximation is suggested to adapt the current load and production set to different turbine types. The suggested scaling is valid for geometrically similar turbines equipped with a power and load control system comparable with that of the applied 5MW turbine. In such cases, the scaling can be simplified to depend on the rotor radius, R, as:

- *Tower moments*: Only the aerodynamic loading is taken into account, and we thus assume that the rotor load scales with R^2, while the moment arm scales with R because the tower height scales with R for geometrically similar turbines. This makes the static tower moment to scale with R^3, and in the present context we assume that the fatigue life equivalent moments scale likewise.
- *Blade moments*: For the blade, we distinguish between flap- and edgewise moments. The edgewise moments are dominated by the blade gravity loading, while the flapwise moments are dominated by the aerodynamic loading.
    - *Flapwise moments:* The aerodynamic load scales with R^2. The blade chord, and obviously also the blade length, scale with R. In conclusion the static aerodynamic flapwise moment scales with R^3. In analogy with the tower moments, we assume that the flapwise fatigue life equivalent moments scale with R^3.
    - *Edgewise moments:* The blade gravity loading scales with R^3, and the moment arm scales wit R. Consequently, the edgewise moment static as well as fatigue life equivalent moments scale with R^4.
- *Drive train and main shaft:* The static moment scales with the rotor power, P, and we assume that this holds also for the life equivalent loads.
- *Rotor power:* The rotor power obviously scales with the nominal power of the turbine.

Comparison of load predictions

In order to evaluate possible differences in load predictions, we have compared loads calculated according to the Frandsen method, as recommended in the present edition of the IEC61400-1 standard, with loads simulated using the DWM model. We have chosen a simple quadratic wind farm layout for the study and further assumed a uniform wind direction distribution. We have moreover chosen an ambient turbulence intensity of 6%, since this value is quite typical for offshore wind farm conditions. This type of comparative load study has previously been performed by Thomsen [146] and Larsen [74]. The DWM model was, however, later further calibrated in [82], and in addition a time domain low-pass filter on the meandering process, as specified in [77], was introduced in relation to the present study, which has improved the predicted load levels considerably for especially tower loads compared to the results presented in [74].

As illustrated in Figure 4 a wind farm configuration with equal row/column spacing is assumed. Influence of the 8 closest turbines, as well as from the neighboring turbines of these, results in at total of 24 turbines to be taken into account for the study. However, due to symmetry reasons, only wind directions from 0 to 45 deg are investigated causing only wake influence from the five turbines in this 45 deg sector (down-wind placed turbines are automatically ignored). Three configurations are investigated with 3, 7 and 11 diameter (D) spacing distance, respectively. For each wind speed three turbulence boxes, each with their own random seed number, are used. Identical sets of seeds are, however, kept for the different wind directions included in the study.

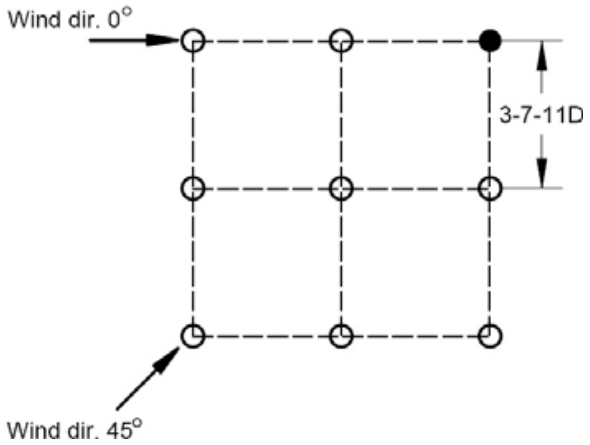

Figure 4: The wind farm layout is a quadratic grid with distance of 3D and 8D spacing.

Selected loads as function of wind direction are shown in Figure 5 for the three different turbine distances 3, 7 and 11D. Starting with the 7D configuration, the wake effects are clearly seen to cause large variations in loads depending on the wind direction. At wind directions of 10-17 deg. (the free direction) the turbine experiences no or very limited influence from wake effects, where a significant contribution to loading is seen especially for full- and half wake situations in the wind direction intervals 0-5 deg. and 40-45

deg., respectively. The variation in the tower fatigue loading is considerable, and a factor of 2.5 between the highest and lowest loaded wind direction is observed. The corresponding factor is in the range 1.6 - 2.5 for blade loads and tower torsion.

Looking at the similar results for the 3D configuration in Figure 5 a slightly different variation pattern of the loads is seen. For the flapwise bending moment rather little variation is seen for the fatigue loads, clearly indicating that the turbine *never experiences any free flow condition*. When the wind direction is 12 deg., which for other spacing scenarios is the free flow situation, the wake loaded turbine is in half wake situation of one of the upstream turbines. This effect is only seen because the wake source is modeled for several turbines simultaneously using the same meandering turbulence field; hence the meandering paths of the individual wakes are correlated. Also for the tower torsion a high load level is observed, especially corresponding to wind direction 15 deg., where the turbine experiences a half wake situation from three turbines (2 at roughly 3D distance and one at 6D distance).

For the 11D configuration, it is mainly the closest turbines at 0 and 45 deg. that cause an increase in load levels. The wake effects in these sectors are quite noticeable and comparable to the 7D case, though the increase in wake loads are less severe than for the 7D case. Wind directions in the interval from 10 to 35 deg. correspond to almost free conditions.

The comparison of fatigue loads obtained from the DWM and IEC simulations are shown in Figure 6 for all wind speeds and wind directions. When comparing the fatigue loads between the DWM and IEC loads there seem to be a general pattern that the IEC loads are conservative for small spacings (3D), in good agreement at intermediate distances (7D) and non-conservative for larger spacings (11D).

The analog comparisons of extreme loads are displayed in Figure 7. The maximum loads for the IEC method is obtained using the turbulence intensity corresponding to the maximum wake situation in agreement with the IEC61400-1 recommendation. Similar to the fatigue loads, the IEC loads seem conservative for small spacings, in good agreement for intermediate spacings, and non-conservative for large spacings. The largest difference is seen for the tower yaw loads at 3D spacing, where the IEC loads are 1.8 times higher than the DWM loads. At 11D spacing the DWM loads are 1.5 times higher than the IEC loads for the tower bending moment. For the tower bending moment it is also interesting to see, that in the DWM results the maximum tower loads increase for increased spacing in contradiction to the IEC results. This effect is explained by the influence of the meandering process especially affecting tower loads.

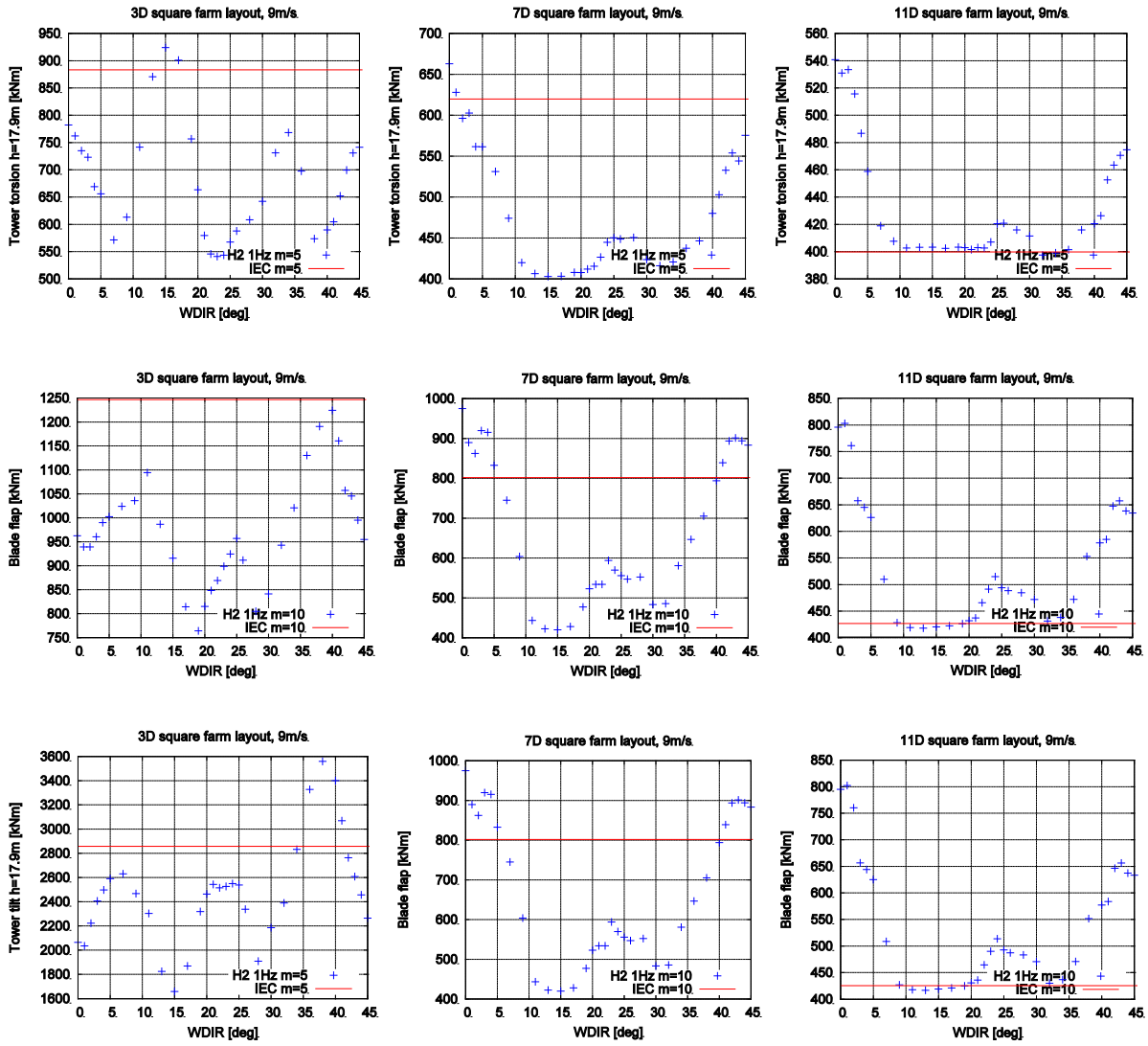

Figure 5: Comparison of DWM model with Frandsen model at 9m/s for a quadratic wind farm layout with 3, 7 and 11D spacing.

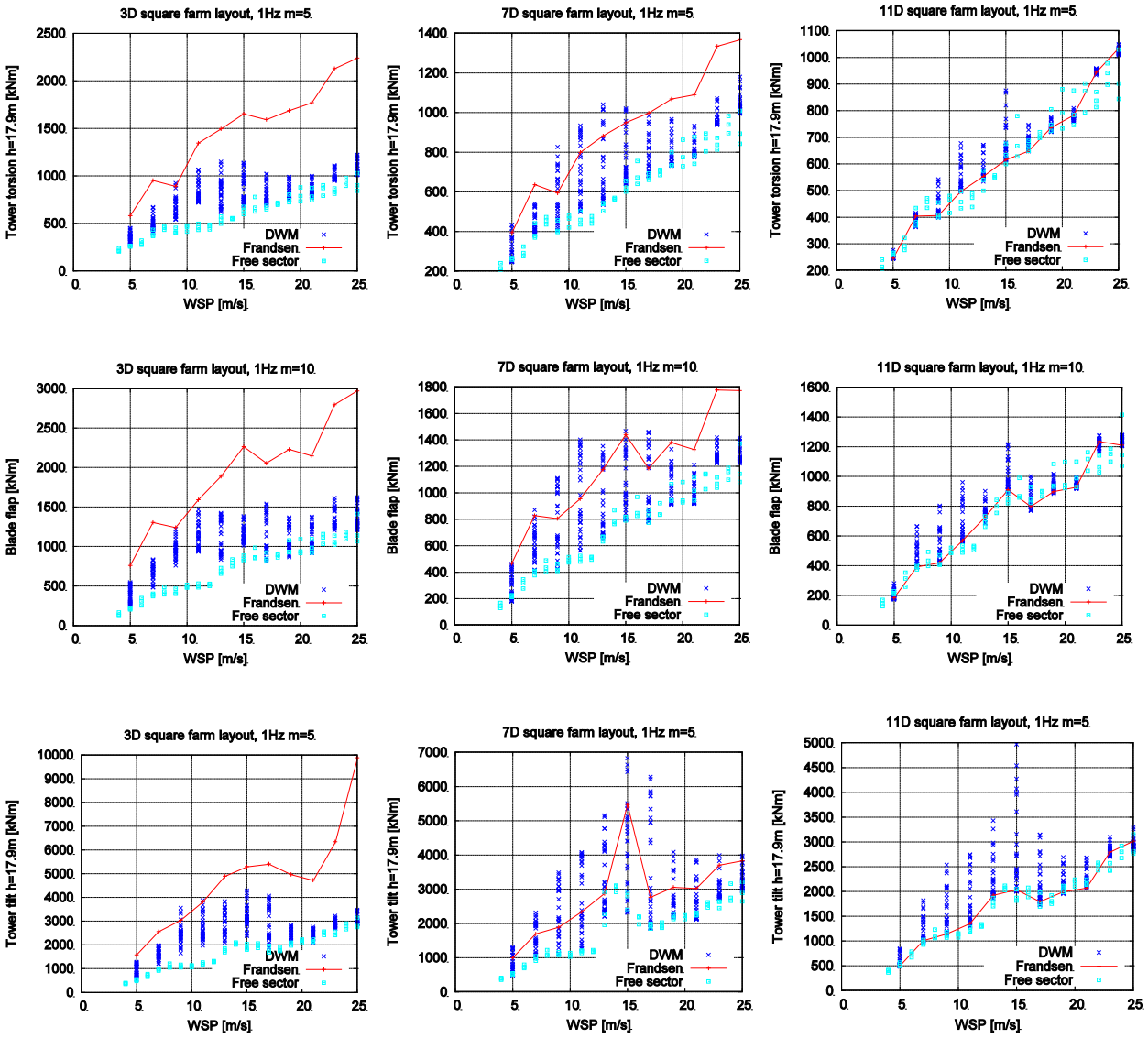

Figure 6: Fatigue load comparison of DWM model with Frandsen model at all wind speeds for a quadratic wind farm layout with 3, 7 and 11D spacing. In the DWM results all wind directions are included.

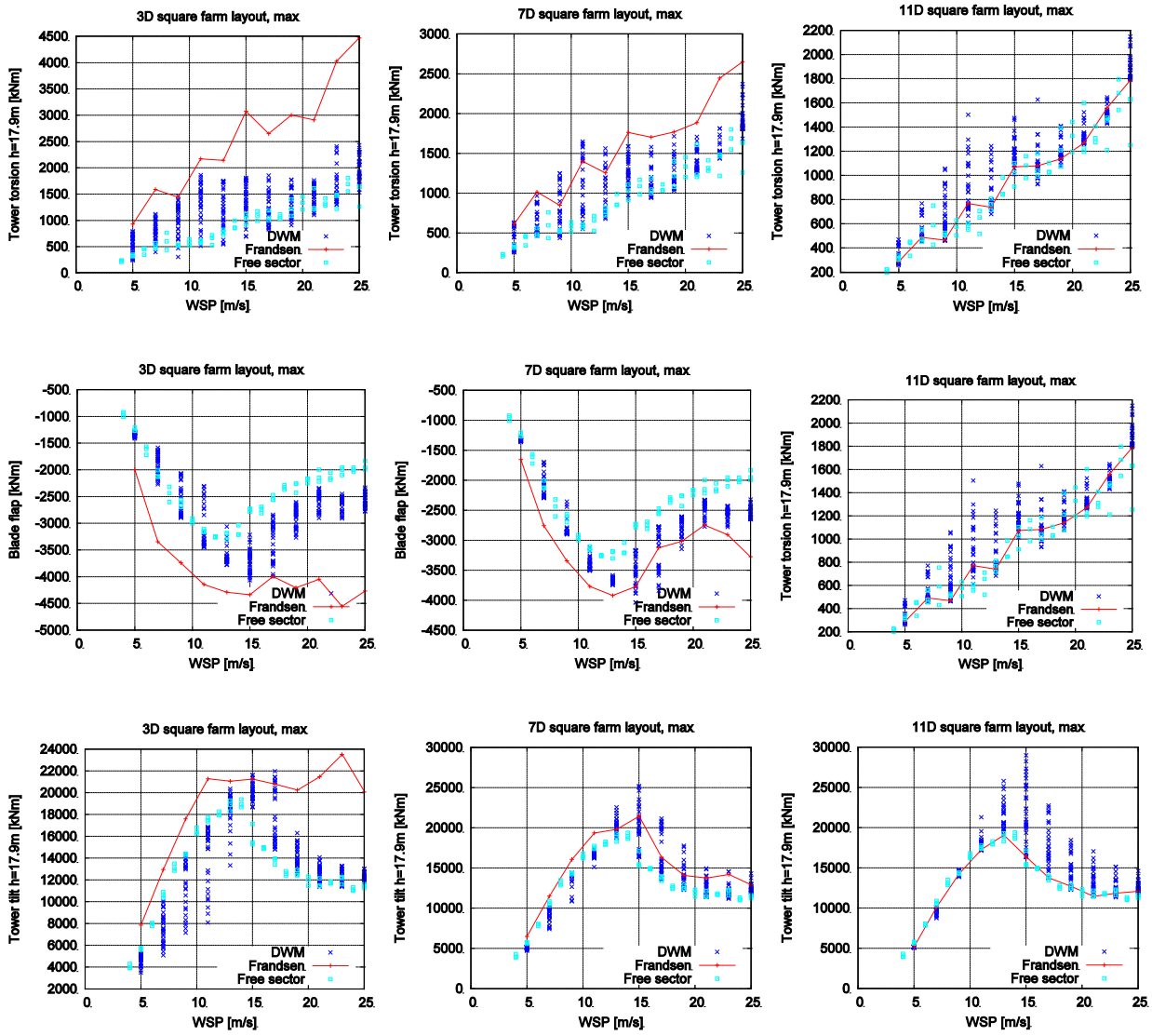

Figure 7: Maximum load comparison of DWM model with Frandsen model at all wind speeds for a quadratic wind farm layout with 3, 7 and 11D spacing. In the DWM results all wind directions are included.

Profiling of aeroelastic codes

The investigation of "stream-lining" aeroelastic codes has been split into two sub-activities – 1) reduce runtime of detailed aeroelastic simulations, and 2) further reducing runtime through simplification of models at the expense of accuracy.

For this study, the aeroelastic simulation software Vidyn [142] has been used. The profiling activities pointed out the parts of the code where most of the CPU-time was consumed. Based on this knowledge, tasks were outlined in order to focus the efforts towards increased performance, without sacrificing accuracy.

The most important areas of work were:

a) ***Linear solver*:** The routines previously used to solve the linear system of equations were replaced by modern open source software. The

CPU-time used for these steps was reduced significantly. There is though still a potential to achieve further savings through optimization of other linear algebraic operations in various parts of the source code.

b) ***Equations of motion*****:** In Vidyn, the equations of motion are derived using symbolic computing software (Mathematica™), and the result is automatically written to Fortran subroutines. In the final step, a code optimization is performed where identical common sub-expressions are matched in linear time. This approach thus avoids matrix-vector operations, which proves to be very efficient for large systems of dynamic equations (derived using energy principles of analytical mechanics). The only drawback is that the subroutines tend to get very large in size. During the present work, the symbolic manipulations in the derivation process were improved, linearization of some higher order terms was introduced, and some optional settings for the code optimization step were explored.

c) ***Compiler*****:** In parallel with a major compiler upgrade, an evaluation of compiler settings/options was performed, in order to find the optimal combination for the automatically generated subroutines discussed under b). This combined effort resulted in a total speedup of almost a factor of two.

d) ***Internal time steps*****:** Time integration of the wind turbine simulation model basically means updating of structure, control, and aerodynamics. By using different time step sizes for these different parts of the aeroelastic model, the total simulation time can be significantly reduced. The obvious continuation of this work will be to implement algorithms for adaptive time-stepping.

Initial results for the overall speedup of an ordinary 10 min load calculation (normal operation, turbulent wind input) are presented in Figure 8. Further linearization of the equations of motion, introduction of adaptive time-stepping procedures, a tailored linear solver, simplification of the aerodynamic model, and finally a more efficient output format, will most likely open up for and additional performance enhancement of a factor of 2-4 (i.e. typical runtimes of around 5 seconds). Several of the changes mentioned above might lead to some reduction of accuracy for the calculated output. However, the tradeoff between accuracy and runtime will be different for each situation.

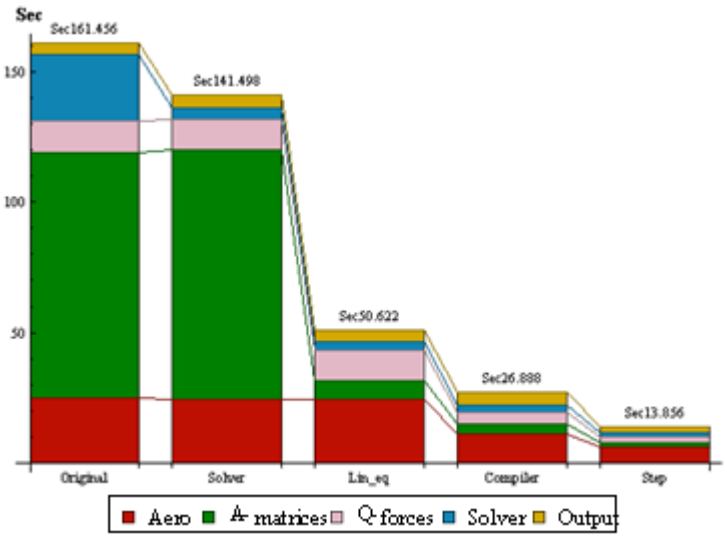

Figure 8: Example of the total time reduction achieved for a typical 10 min aeroelastic simulation (IEA 5MW benchmark turbine), divided into four main steps: 1) new linear solver; 2) +linearization of selected terms in the equations of motion (and other improvements in the symbolic manipulations); 3) +upgrading of the compiler; and 4) +differentiation of internal time steps (i.e. structure-control-aero).

4.3 WP3 – Control strategies

The development of control concepts for wind turbines to be placed in a wind farm may have several different targets. The primary goal is usually to achieve high power production, good power quality, and low levels of fatigue loading in vital turbine components. In wind farms the flow in the wakes of upstream turbines is often characterized by high levels of turbulence and frequent periods of asymmetric wind loading over the rotor. If a control system of an *individual turbine* is designed to reduce the effects of wake operation inside the farm, then it is also likely that some information about wake transport directions can be extracted and communicated to a master controller at all times. This kind of information is essential when developing successful concepts for *Wind Sector Management.* Wind sector management is an example of control on wind farm level, and WP3 in TOPFARM deals with control of the *individual turbine* operating in wind farm conditions as well as control on the *wind farm level*.

Wind farm control

When considering the level of complexity already reached during the implementation of the *DWM* model described in previous chapters, it is evident that full representation of *dynamic* wind farm control, including all turbines of a large wind farm, is not yet feasible. However, the multi-fidelity approach taken to the general optimization problem means that also results from simplified (quasi-static) analyses can provide valuable results.

In the present context, a *de-rated* turbine is a turbine for which a certain amount of power is *traded* for a lower thrust (e.g. less momentum taken out

from the flow). Two concepts for wind farm control have been investigated, where individual turbines are de-rated (operating below maximum C_p) - the *Power Balance* control and the *Pattern* control algorithms, respectively (see Figure 9). The latter is here mainly chosen to represent the *trivial reference* case (as monkeys were throwing darts at the stock pages).

In the following it will be assumed that flow behind the de-rated turbines will in general expose less wake induced turbulence together with lower magnitudes of wind shear over the rotor, while the fatigue loading of de-rated turbines will be reduced. The main target for the developed control algorithms has been an assumed first loop of a wind farm optimization study, where the topology of a parametric farm layout is to be settled.

The *Power Balance* control concept can be briefly described by the following iterative procedure (see also [16], [17]):

- All pairs of interacting turbines are identified.
- If the downstream turbine of a pair is producing less power than the upstream turbine, then the upstream turbine is de-rated δP by adjusting pitch angles and/or rotor speed (an optimal strategy is worked out through evaluation of thrust and power curves).
- If the entire wind farm is producing less power than a reference value (i.e. the production for the unmanaged wind farm), then all turbines are again up-rated ΔP.

It is here obvious that certain *dead-bands* need to be introduced as control parameters, and that smart filtering is required for any dynamic implementation. The parameters of this algorithm can also be used for wind farm power control (e.g. power reduction ordered from the grid). A power reduction for the wind farm (within certain limits) is then achieved without imposing unnecessary shut down of turbines.

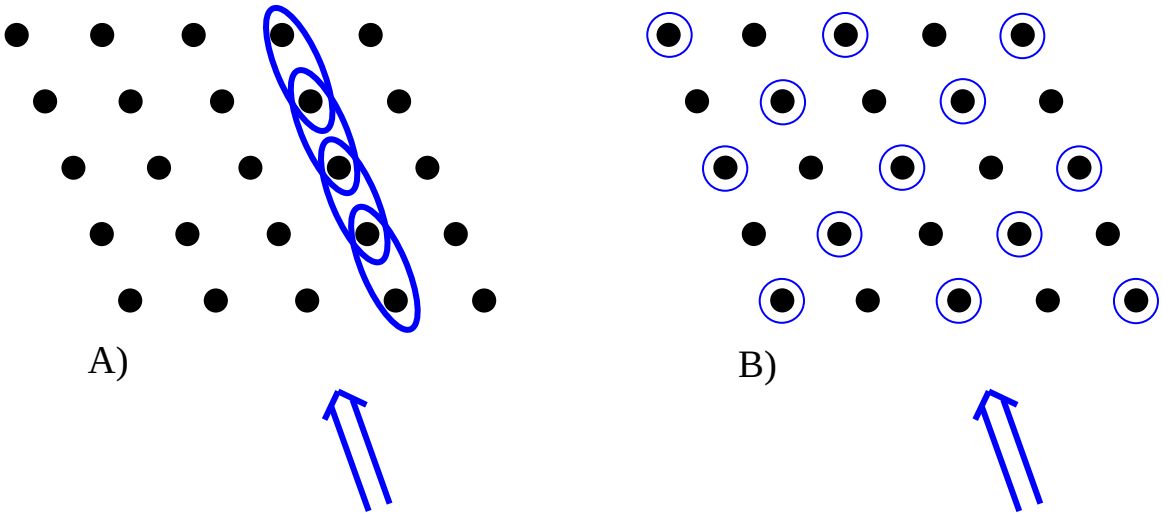

Figure 9: Examples of concepts for Wind Sector Management: A) "Power Balance" (upstream de-rating), and B) "Pattern" (downstream de-rating).

A typical result of *Power Balance* control is illustrated in Figure 10. A straight row of 6 turbines with 6 diameters spacing is de-rated using the *Power Balance* algorithm as outlined above. Here the *engineering* wind farm tool presented in [57] was used.

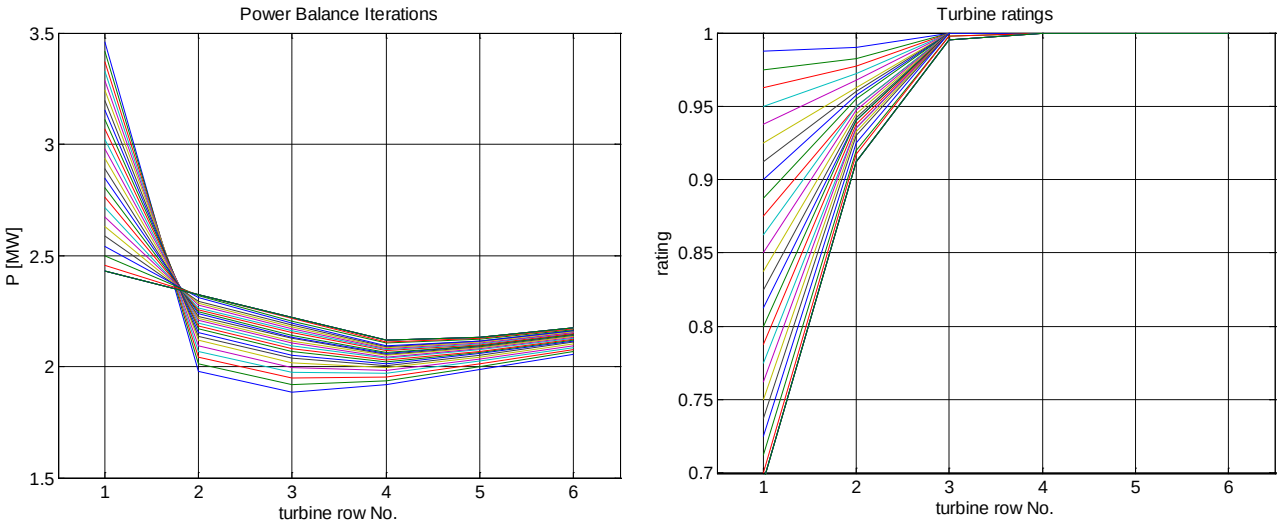

Figure 10: Power production and rating for a straight row of 6 turbines throughout the iteration (U_a=10 m/s , I_a=10% , S=6D).

For some configurations, simplified wind farm models have previously suggested that the total power output can be maintained (or even increased) while achieving a significantly better production balance between individual turbines. The corresponding power output from the 6 turbine farm referred to above, is presented in Figure 11.

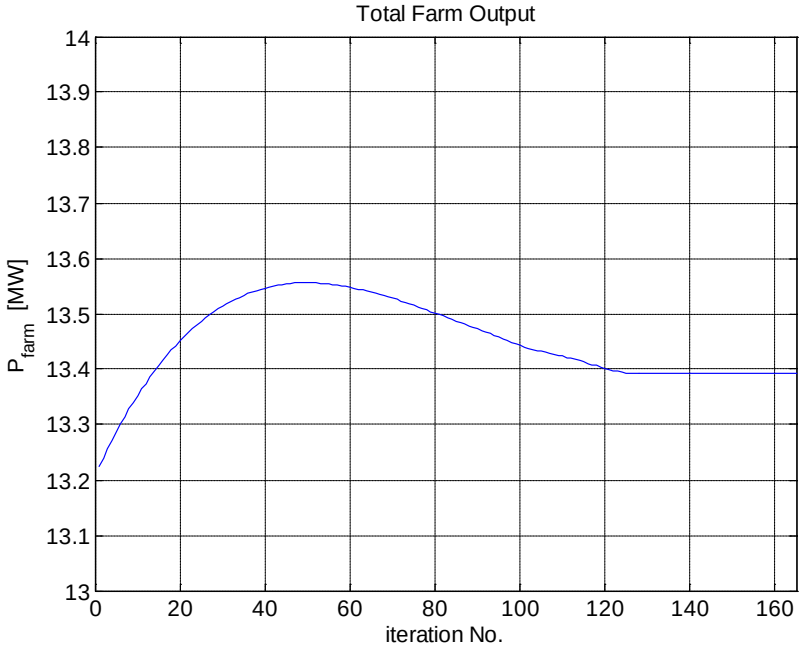

Figure 11: Total farm output (U_a=10 m/s , I_a=10% , S=6D).

For the straight row of 6 turbines row it is then straight forward to run the *trivial test-case* (i.e. *Pattern* control). This is here accomplished by equally de-rating turbines 1, 3, and 5. The resulting total farm output is presented in Figure 12.

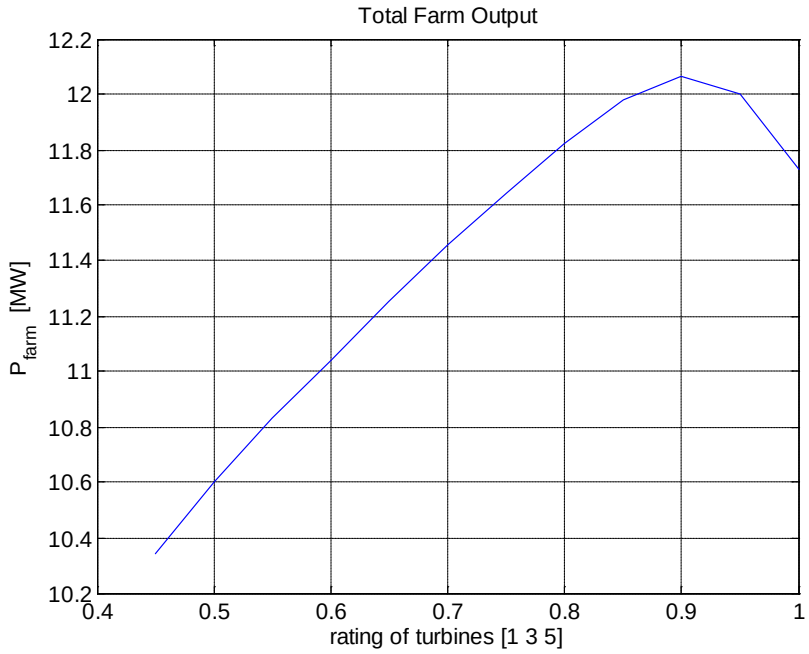

Figure 12: Total output from the straight row of 6 turbines when turbines 1, 3 and 5 are equally de-rated (U_a=10 m/s , I_a=10% , S=6D).

It is seen that de-rating turbines 1, 3 and 5 to 0.78 gives the same total farm production as for the unmanaged wind farm, and that there also here might be a potential to even increase the total production (by de-rating to 0.9).

It should be pointed out that the simple examples given here should be extended to include also extensive load analysis, before any overall conclusions can be drawn.

Individual wind turbine control

Asymmetric structures in the inflow field to a wind turbine will often result in higher levels of fatigue loading. Especially for turbines operating in a wind farm, partial wake operation can result in substantial and frequent asymmetric loading over the rotor of a downstream turbine. It is well known that some of these effects can be reduced by using an approach to rotor blade control where each blade is treated individually.

Therefore WP3 has investigated/developed strategies for individual blade control in combination with wind farm operation. Blade root load measurements as well as pitot tube flow information have been used as main input signals, while full span pitch systems and trailing edge flaps were used as control devices. Three strategies were developed – one based on "traditional" individual pitch control, one based on a so-called wake compensator approach (i.e. a dedicated version of individual pitch control adjusted for wake affected flows), and one based on trailing edge flap actuators. The philosophies and potentials of these strategies are briefly described in the following.

Individual pitch control

The load alleviating benefits of *individual pitch control (IPC)* within a meandering wake flow was investigated by combining the IPC controller [143] developed for the NREL 5MW test turbine model [132] by the GH control group, and the dynamic wake meandering model [47], [82] recently implemented within GH Bladed [122].

To quantify the benefits of IPC over collective pitch control, a load comparison study was conducted for a two-turbine wind farm. The turbines were aligned along the north-south direction vector, with a wind rose consisting of equally weighted bins of 2 degrees width ranging ±30deg from North; see Figure 13. Five inter-turbine spacings have been considered: 3D, 4D, 6D, 8D and 10D. Two ambient mean wind speeds of 12 m/s and 20 m/s have been considered to study the possible load alleviation at rated and above rated operating conditions.

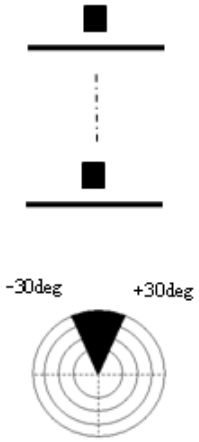

Figure 13: Wind farm layout and wind rose.

Damage equivalent fatigue loads for five design driving components (hub thrust force, blade root flapwise bending moment, yaw bearing torsion moment, tower base overturning moment and tower top moment) were compared for the two pitch control regimes. The full study, results and conclusions have been reported in [88].

Figure 14 and Figure 15 display a sample of the study results; the percentage change in damage equivalent loading due to the implementation of IPC for blade root flapwise bending moment and tower base overturning moment, respectively. The change in yaw bearing and tower top loading due to IPC are characteristic of the blade root load. The change in hub thrust force due to IPC is characteristic of the tower base load.

Figure 14 shows that at rated wind conditions there is an increase in the magnitude of load reduction with turbine spacing in blade root flapwise bending moment. Blade root flapwise bending loads reduce by 15% at 10D spacing. This indicates that the potential benefits of IPC on these load components are magnified for farms with large turbine spacing. Under rated wind conditions, the tower base overturning moment load does not reduce significantly due to the addition of IPC; it remains within ±1.5% of the collective pitch datum loads.

Above rated conditions, the benefit of IPC is increased for blade root flapwise bending moment. Figure 14 shows the reduction in fatigue loading is largest at 4D spacing where loads are reduced by approximately 25%. Figure 15 shows that above rated conditions, IPC causes an increased tower base overturning moment which increases with turbine spacing. At 10D, IPC shows a load increase of approximately 7%.

The loading benefits of IPC at rated and above rated conditions seen by the yaw bearing torsion, tower top overturning and blade root flapwise loads may be outweighed by the exacerbation of the hub thrust and tower base overturning loads at wind speeds above rated.

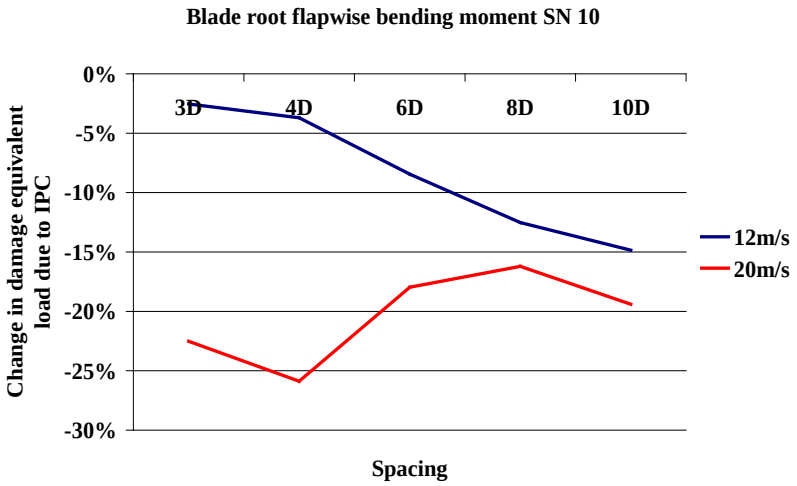

Figure 14: Change in damage equivalent blade root flapwise bending load due to IPC.

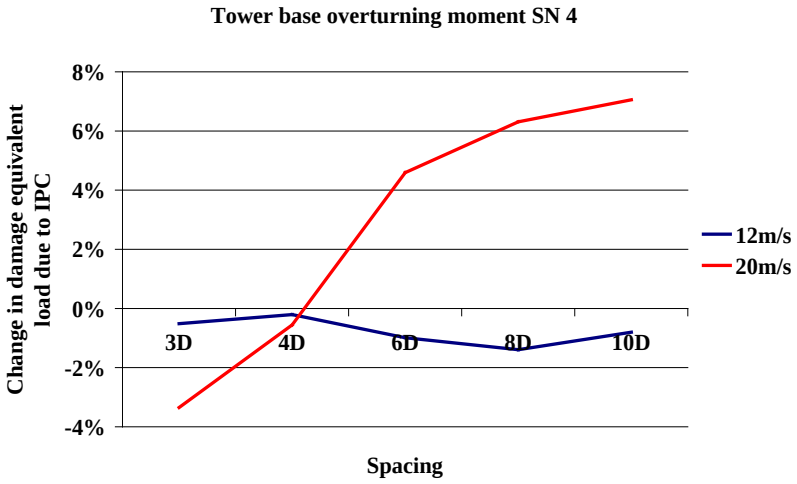

Figure 15: Change in damage equivalent tower base overturning moment due to IPC.

Figure 16 and Figure 17 display the contribution to the damage equivalent fatigue load over the wind rose for blade root flapwise bending moment and tower base overturning moment. Both the collective pitch and IPC loads have been plotted for comparison.

Figure 16 shows that IPC has a significant effect at reducing the peak wake affected blade flapwise loads for all spacing above rated wind conditions.

Figure 17 shows that the benefit of IPC over collective pitch on the tower base overturning moment is almost negligible for all turbine spacings.

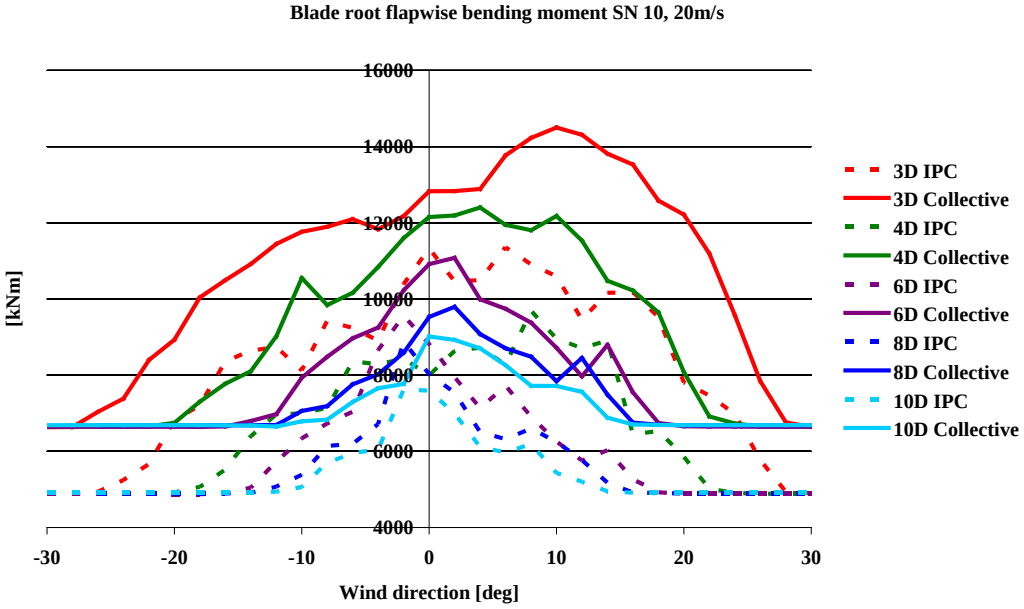

Figure 16: Distribution of blade root flapwise bending load with wind direction, 20 m/s ambient mean wind speed.

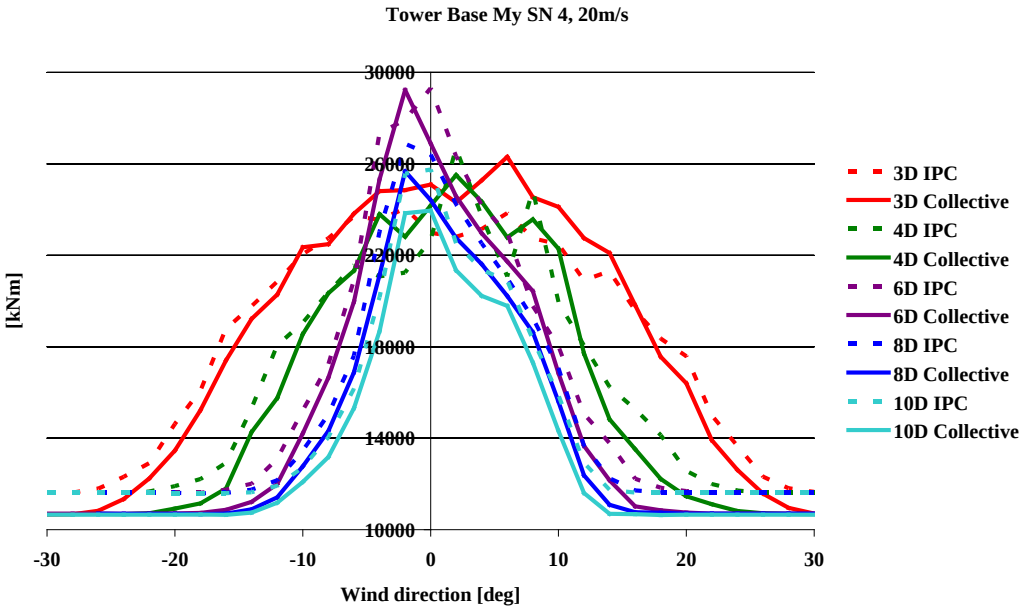

Figure 17: Distribution of tower base overturning moment with wind direction, 20 m/s ambient mean wind speed.

Wake compensator and deflecting trailing-edge flaps approach

The controllers based on the wake compensator approach and the deflecting tailing edge approach, respectively, were developed and analyzed using the

multi-body aero-servo-elastic tool HAWC2 [133] developed at Risø-DTU. As a reference, the "traditional" cyclic pitch approach was included in the investigation.

The wake compensator belongs to the group of individual pitch controllers, however, with significantly different characteristics compared to a "traditional" cyclic pitch approach. These differences concerns both the sensor signals (the control input) and the control algorithm itself.

The sensor input for a *"traditional" cyclic pitch* algorithm is the blade root flap moment, transformed into tower-top, non-rotating, co-ordinates, M_{flap_tt}, and the aim of the control algorithm is to reduce the *average* yaw and tilt moment and partially the blade root loads. The cyclic pitch controller thus only alleviates loads resulting from the 1P deterministic loading of the blades. Any 3P component in the input to the controller is filtered out.

The sensor input for the *wake compensator* is the measured angle of attack of the flow around the blade profile. The aim of this controller is to keep the instantaneous angle of attack the same on all three blades, and equal to the average instantaneous angle of attack of all three blades. The wake compensator does not only alleviate deterministic loading on the blade, as the cyclic pitch does, but will also alleviate loading from low-frequency turbulence structures in the wind direction e.g. meandering wakes. A potential additional advantage in using a direct measurement of the inflow angle instead of the blade root moment is that if there is not much of a phase-delay between the measurement and the controller response, the response to changes in the inflow is of course much faster.

The different input sensors used for each of these approaches and the key characteristics of these are:

- *Individual Pitch control:* The output is an additional pitch angle demand to each blade, using the existing pitch actuators.
    - Cyclic pitch: the input is the blade flap moment (e.g. strain gauge);
    - Wake compensator: the input is the angle of attack measurement (e.g. pitot tube).
- *Deflecting trailing-edge flaps*: the output is an angle demand to the trailing edge flaps. The optimum positioning and length of the flap has been investigated in previous works [144] and not dealt with here. Three different controller designs have been investigated.
    - Controller A: the input is the blade flap moment (e.g. strain gauge);
    - Controller B: the input is the angle of attack measurement (e.g. pitot tube);
    - Controller C: two inputs are used – the blade root flap moment and the blade angle of attack.

As with the traditional individual pitch controller, these load controllers are implemented and tested for the 5MW UPWIND reference turbine [132]. The turbine is in the wake of another 5MW turbine which is located 2.4D directly upstream. The wake is modeled in HAWC2 using the Dynamic Wake

Meandering (DWM) model, facilitating prediction of both structural loads and production of the turbine. In both controller approaches, the power/speed regulation of the turbine is identical and a description of this is given in [145].

The load reductions achieved by controllers are summarized for the individual pitch type of controllers in Table 3 and for the trailing edge flaps controllers in Table 4, respectively. The load reductions achieved are presented for the main component sensors that see, or should see, an affect from the controllers (blade flapwise moment, yaw and tilt moment, and tower bottom fore-aft moment) and for one simulation case only – i.e. an average wind speed of 11 m/s (near rated power), with no yaw error or topography inflow.

Table 3: fatigue loads for blade, yaw, TILT moment and mean electrical power production for the Individual pitch controllers.

sensor [unit]	**material param.**	**power control only**	**Cyclic Pitch**	**Wake comp.**
Blade flapwise root moment [kNm]	10	8768.2 (0.0%)	6954.5 (21%)	7980 (10%)
Yaw moment [kNm]	4	5292.6 (0.0%)	5085.0 (4%)	4643 (12%)
Tilt moment [kNm]	4	5346.3 (0.0%)	5249.4 (3%)	4620 (14%)
Mean electrical power [kW]	-	4793 (0.0%)	4761 (-0.7%)	4795 (0.0%)

Table 4: fatigue loads for blade, tower and yaw moment and mean electrical power production for the deformable trailing edge Flaps.

sensor [unit]	**mate-rial param.**	**power control only**	**flap control A**	**flap control B**	**flap control C**
Blade flapwise root moment [kNm]	10	5974 (0.0%)	2433 (59.3%)	2595 (56.6%)	2278 (61.9%)
Yaw moment [kNm]	4	4968 (0.0%)	2027 (59.2%)	2164 (56.4%)	1732 (65.1%)
Tower flowwise root mom. [kNm]	4	11980 (0.0%)	4745 (60.4%)	5813 (51.5%)	4892 (59.2%)
Mean electrical power [kW]	-	4832 (0.0%)	4789 (-0.9%)	4746 (-1.8%)	4734 (-2.0%)

In summary the results indicate that there is a significant potential for load reduction in vital cross-sections and components, but the consequences of the extra work done by the control devices needs more attention.

4.4 WP4 – Verification of load and production sub-models

Work packages 1-3 encompass a range of advanced sub-models. The objective of WP4 is to verify these, as well as their interaction, in full-scale environments. Model predictions are to be compared with available power

production- and structural measurements as well as detailed flow measurements.

Data classification

To meet the objectives of WP4, three characteristic data classes have been identified: *i*) Wind turbine – mast interaction; *ii*) Wind turbine – wind turbine interaction; and *iii*) Wind turbine – direct wake measurement.

Data category *i*) is characterized by having the mast located on a fixed position, which in turn results in a limited sector with applicable measurements. A huge amount of measurements is available from [125], which are useful for investigations of (mean) wake characteristics as e.g. wind speed deficits.

For data category *ii*), the power and load response of a downwind turbine are used to identify the wake properties. Such data is useful for analysis of directional wake behavior inside large wind farms.
Data category *iii*) offers the possibility for analysis of *instantaneous* wake properties. The wake is measured directly with a laser Doppler based measuring device (LiDAR) mounted at the nacelle of the wake generating wind turbine.

Identification of existing data

A report on existing available and relevant measurements, [24], was compiled to facilitate part of the WP4 verifications, and the resulting potential data sources were subsequently categorized in agreement with the classification system defined in the previous section with the following result:

- *Wind turbine – mast interaction*: The mast is located on a fixed position, which results in a limited sector with applicable measurements. This group of data is represented with 9 different sites ranging from small to large wind turbines located in Denmark, Sweden and the Netherlands. Some of the measurements are available as time series [125], which are useful when investigating the wake properties, while the remaining part of measurements only are available in a compiled version e.g. as mean value plots.
- *Wind turbine – wind turbine interaction*: The response of the downwind turbine(s) is used to determine the wake properties. This category is useful for the analysis of directional wake behavior inside large wind farms and is represented by 8 different wind farms ranging from small to large wind farms located in Denmark, the Netherland and in UK.
- *Wind turbine – direct wake measurement:* The wake characteristics are measured directly with a LiDAR mounted on the wake generating wind turbine and offer the possibility for analysis of instantaneous wake properties. This data category is represented both with a dataset from a 95 kW experimental wind turbine placed in Denmark and a new dataset from a full scale experiment on an 80m/2.5MW wind turbine located in Tjæreborg, DK.

In addition, structural wind turbine loads measured on wind turbines located inside wind farms are available from a limited number of projects.

Some of the datasets have been restricted due to confidentiality agreements, but all dataset have been transferred to servers at DTU for quality screening and have subsequently been used for code validations within the TOPFARM environment in a compiled form. The remaining datasets are available from the "Database on Wind Characteristics" [125] without restrictions imposed.

Additional full scale tests

As a supplement to the existing detailed TELLUS wake flow measurements [120], [121], [5], [114] represented in data category *iii*), a full scale experiment at the Danish Tjæreborg site was conducted within the framework of TOPFARM. Where the existing data sets might be useful in verification of large scale properties of wake affected flows (i.e. wake meandering models), the new experiment is a dedicated experimental investigation of wake deficit characteristics as well as (small scale) wake turbulence characteristics resolved in the meandering frame of reference.

The experimental activities were conducted within a coordinated collaboration between RISOE.DTU and MEK.DTU. The experimental campaign was carried out in a small wind farm in Tjæreborg Enge, Denmark, consisting of 8 2.5 MW wind turbines. The full scale measurements were coordinated with other research activities on the same wind turbine and could therefore benefit from additional experimental recordings.

The total recording system consisted of 6 sub-recording-systems:

1) LiDAR measurements of the wind field across the wake at focal distances of either 40, 80, 120, 160 or 200m;
2) Basic meteorological statistics from a 93 m mast;
3) Wind turbine operational parameters, e.g. power, yaw position, rotor speed, pitch angle;
4) Wind farm statistics from 7 nearby wind turbines recorded as SCADA data;
5) Measurement of the incoming wind speed and gusts with a spinner mounted LiDAR;
6) Flow characteristics in the rotor plane recorded by using an instrumented blade quipped with pressure sensors.

The initial wake measurements have been recorded with sub-system 1), and these measurements were subsequently synchronized with measurements recorded by sub-systems 2), 3) and 4).

Sub-system 5) has been successfully operating during April 2009, but is primarily used in other research projects as part of RISØ.DTU's ongoing wind scanner project.

Sub-system 6) consists of a dedicated blade equipped with 4 × 5-hole pitot tubes distributed span-wise to measure the wind speed in the rotor plane during rotation. Furthermore, the blade was equipped with surface pressure taps, a surface microphone in combination with traditional strain gauges and accelerometers.

The full-scale campaign, with dedicated recording of the wake dynamics associated with an 80m diameter 2.5MW wind turbine, was performed during January to September 2009. The test wind turbine was located inside the

small wind farm, and the campaign resulted in more than 1000 hours of measurements covering both *single* and *multiple wake* situations.

A robust procedure to determine the coordinates of the meandering wake deficit center as function of time was developed and implemented, which in turn are used to define the meandering frame of reference and thus facilitate a description of the wake deficit (and wake turbulence) in this frame of reference. As a result a characterization of the quasi-steady wake properties (i.e. the wake deficit and the wake turbulence properties expressed in the meandering frame of reference) behind the operating wind turbine was obtained for single wake flow cases [60]. The results from the analysis confirmed the inhomogeneous character of wake turbulence, which was previously identified from numerical studies based on detailed CFD simulations [62]. Summarizing, these results show that the length scale of wake turbulence is significantly less than the length scale of conventional atmospheric turbulence, and furthermore that the coherence decays much faster than for conventional atmospheric turbulence.

Model validations

A large number of model validations were performed during the project. This section presents a selected number of essential validation examples based on full-scale wake measurements. An overview of the verifications performed is given in Table 5.

Table 5: Selected model verifications performed in TOPFARM.

TOPFARM WP4.4: verifications	RISØ.DTU	UPM	DTU.MEK	CERC	GL
4.4.1.1.Maximum power deficit vs TI	X	X		X	
4.4.1.2.Nordtank (1&2D flow field)		x			
4.4.1.3.Tjæreborg D=60m (2-D flow field)	X		X	X	
4.4.1.4.Tjæreborg NM80, wake deficit	X	X			
4.4.1.5.Sexbierum (2D Flow field)		x	X		
4.4.1.6.Nibe (2-D flow field)			X		
4.4.1.7.Alsvik (2-D flow field)					
4.4.1.8.Vindeby (2-D flow field)		X			
4.4.1.9.Tjæreborg NM80 (2½-D flow field; LiDAR)	X	X		X	
4.4.2.1.NoordZee, fatigue loads	X				
4.4.2.2.Horns Rev, fatigue loads					X
4.4.3.1.NoordZee, park performance	X			X	
4.4.3.2.Nørrekær Enge, park performance			X		
4.4.3.3.Nysted, park performance	X			X	
4.4.3.4.Horns Rev, park performance	X		X		

Flow case 4.4.1.1 is a general flow case resolving the power deficit resulting from two (large) turbines operating “on line” under different atmospheric conditions quantified in terms of ambient turbulence intensity.

Flow cases 4.4.1.2-9 represent selected recordings of wind speed deficits behind various operating wind turbines.

Flow cases 4.4.2.1-2 represent flow cases suitable to validate the accumulated fatigue loading of various structural turbine components of turbines subjected to both wake affected- and undisturbed inflow fields.

Flow cases 4.4.3.1-4 represent flow cases where the power deficit is determined for two nearby turbines operating “on line”.

A variety of codes developed or refined in WP1 and WP2 have been validated, and the results are presented in the following sub-sections with reference to the flow cases specified in Table 5.

UPMPARK model (UPM)

UPMPARK has been validated against 6 different flow cases ranging from single wind turbine wake deficits to power deficits inside wind farms.

Case 4.4.1.1 Maximum power deficit as function of turbulence intensity (Figure 18):

This exercise tries to clarify the influence of ambient turbulence on power deficits. The wind turbine has 5MW nominal power, and the results refer to three different downstream distances: 3.8 diameters (blue lines); 7 diameters (green lines); and 10.3 diameters (red lines). UPMPARK results are full lines and “filled” symbols, and experimental results are dashed lines and “open” symbols. The UPMPARK ambient turbulence, I_{amb}, can be imposed modifying the upstream terrain roughness, z_0, and using the approximation $I_{amb}=1/ln(z/z_0)$. The UPMPARK simulations start in the expanded wake regime one rotor diameter behind the position of the wake generating turbine.

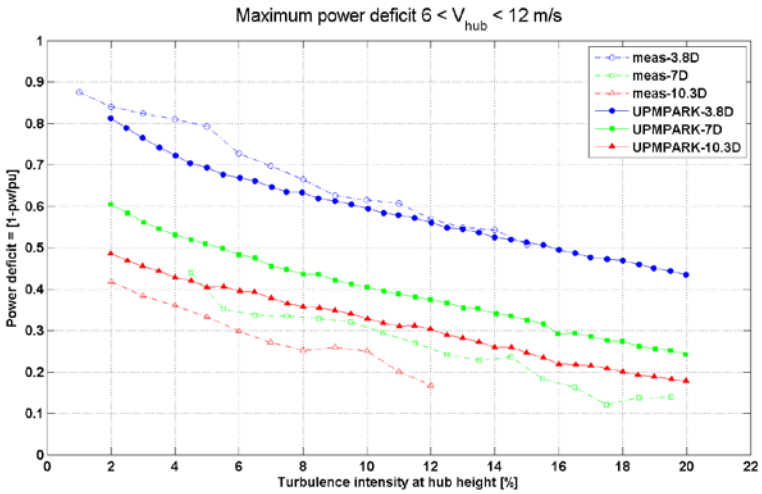

Figure 18: Maximum power deficit for 5MW wind turbines with 3.8D, 7D and 10.3D spacing simulated with UPMPARK.

Case 4.4.1.2: Wind speed deficit behind 500 kW Nordtank wind turbine (Figure 19):

The Nordtank 500W wind turbine has a diameter of 41m and is located at Risø-DTU campus, [24]. The results obtained by UPMPARK are the velocity distributions in the wake for ambient upstream velocities equal to 6 and 8 m/s, respectively. The ambient wind inflow wind speed at hub height (i.e. the wind speed denoted HUB) are represented with blue lines, the sensor in the wake region 55m downstream (i.e. the wind speed denoted WSP) with green

lines, and the sensor 99m downstream (i.e. the wind speed denoted WS35) with red lines. UPMPARK results are presented with “filled” symbols and lines, whereas experimental results are presented with dashed lines and “open” symbols. UPMPARK results show a nucleus of constant deficit, which is included in the boundary conditions of the model and affects the near wake region. The results with unsteady UPMPARK reproducing meandering have not been included. However, for the present verification example wake meandering is not likely to contribute significantly to the flow conditions, because the amplitude of the meandering at such a short distances downstream is small.

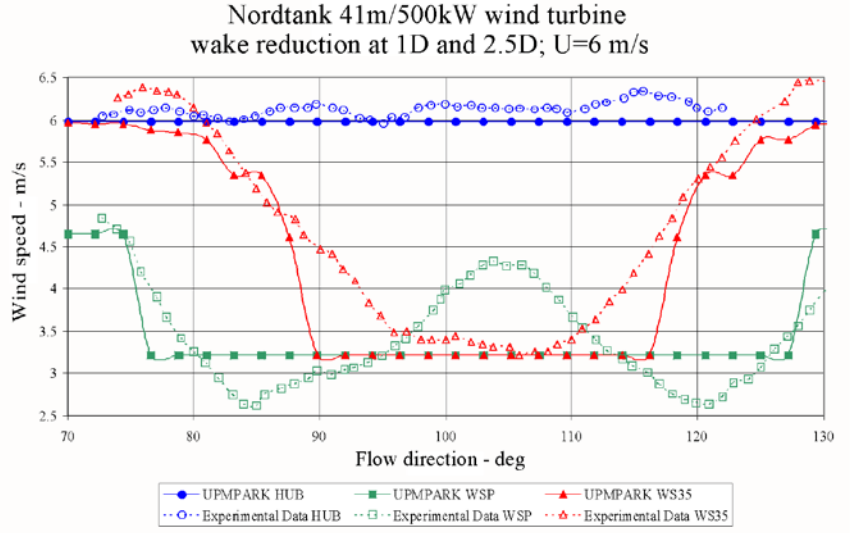

Figure 19: Wake reduction behind 500kW Nordtank wind turbine; where WSP=1D and WS35=2.5D spacing, calculated with UPMPARK.

Case 4.4.1.4. TJÆREBORG NM80 wake deficit (Figure 20):

The NM80 wind turbine is located in Tjæreborg Enge wind farm Denmark [24], together with seven other 80m turbines In this case, the simulations focus on the power deficit distributions for turbine 3 (in the wake) normalized with the power production of the upstream turbine wt01. The spacing between the turbines is 4.6 D. Upstream velocity is 8 m/s, and UPMPARK results are full lines and “filled” symbols, whereas experiments are identified by dashed lines and “open” symbols.

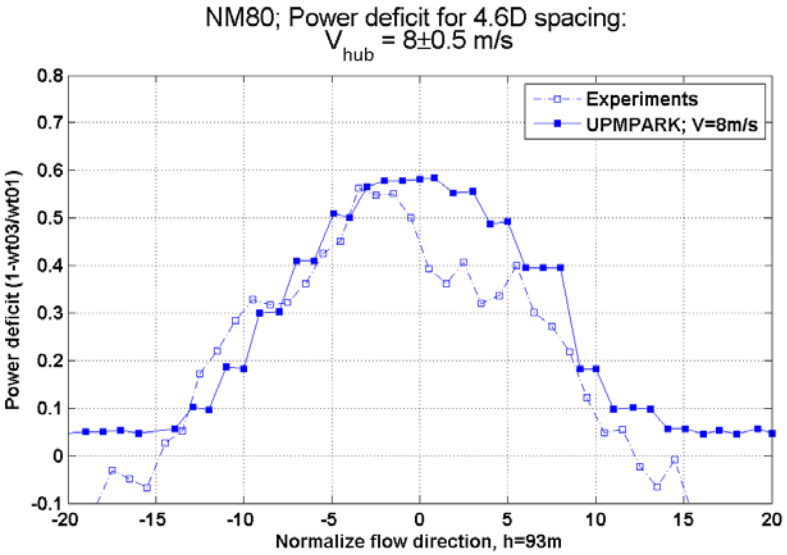

Figure 20: NM80 power deficit for 4.6 D spacing, calculated with UPMPARK.

4.4.1.5. SEXBIERUM, 2-D flow field (Figure 21):

The Sexbierum wind farm was located in the Netherlands and consisted of 18x0.3MW Holec wind turbines, each with a diameter of 30m [24]. Wind speed deficits have been evaluated for the Sexbierum wind farm. Figure 21 shows the wind speed deficit at three downstream distances: 2.5D (blue lines); 5.5 D (green lines); and 8 D (red lines). UPMPARK results are represented by full lines and "filled" symbols, and experimental results are plotted with dashed lines and "open" symbols. The Sexbierum data have been obtained from Figures 4-8 in [123]. The figures show aggregated results from 5m/s to 10m/s, whereas the UPMPARK results represents the 10m/s case. The roughness employed to UPMPARK calculations is 0.002m instead 0.05m mentioned in the TNO document – otherwise the ambient turbulence would not be consistent with the experimental observations. The UPMPARK calculations start in the expanded wake 2.25D behind the wake generating turbine.

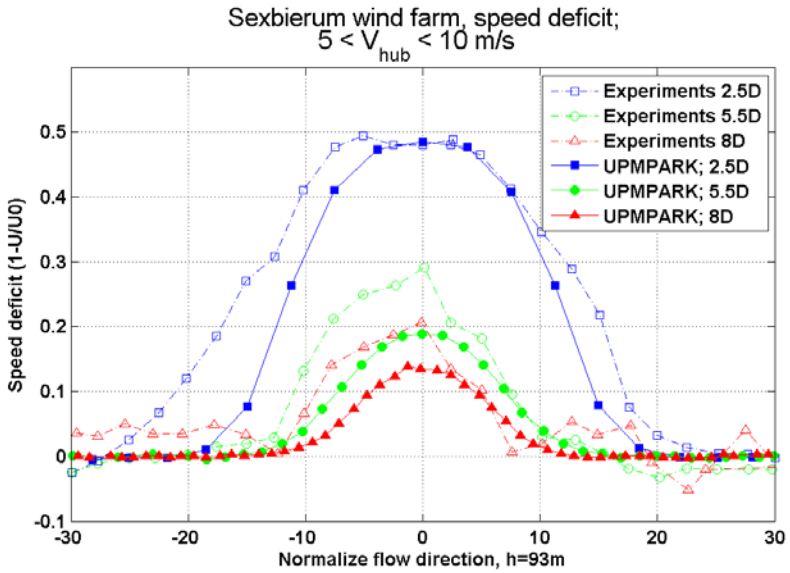

Figure 21: Sexbierum; Wind speed deficits for 2.5D, 5.5D and 8D spacing calculated with UPMPARK.

4.4.1.8. VINDEBY; 2D flow field (Figure 22):

The Vindeby offshore wind farm is located in Denmark and consists of 11x450 kW Bonus wind turbines arranged in two rows. Many calculations have been performed on the Vindeby wind farm. However, UPMPARK need a free inflow, and consequently only the flow case representing 140º mean inflow direction could be used. Besides, only results from turbine 4w and 5e were available. The figure compares the averaged velocity deficits results, with and without meandering, along the lines joining the wind turbines in both the northern turbine row, with 6 turbines, and the southern turbine row with 5 turbines. The turbine 4w is in the northern turbine row, and the turbine 5e is in the southern turbine row. The differences are very small, and the two sets of simulated results are almost undistinguishable from the scarce experimental results. On this basis, it is therefore difficult to elucidate whether retaining the meandering effect really improves the results.

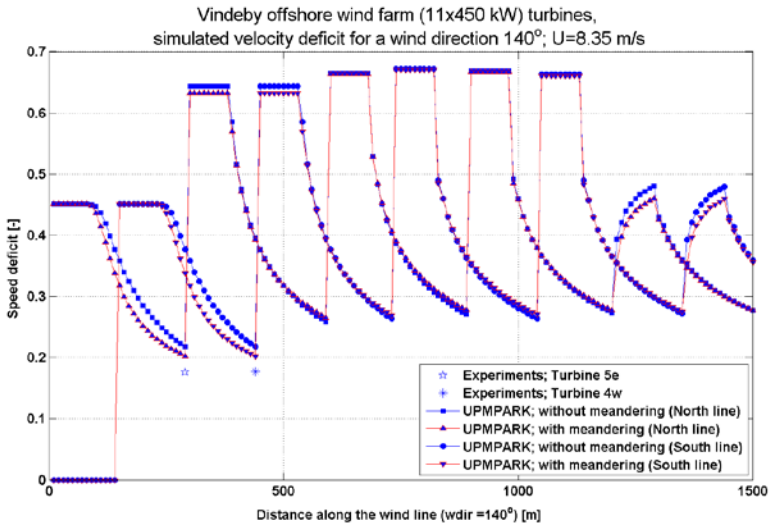

Figure 22: Vindeby; Simulated speed deficit along the two rows of operating turbines calculated with (UPMPARK) for U_∞=8.35 m/s.

4.4.1.9. TJÆREBORG NM80; 2½D flow field; LiDAR (Figure 23):

The NM80, 2.5MW wind turbine is located in Tjæreborg Enge wind farm in Denmark [24] together with seven other 80m turbines. This analysis shows four wake flows in terms of speed deficit and turbulence distributions across the wake at hub height and 2.5D downstream, corresponding to a 200m focus distance of the LiDAR. The four flow cases have been recorded in a narrow inflow sector, where the NM80 wind turbine has been operating under free undisturbed wind conditions. Figure 23 presents simulation results obtained assuming neutral atmospheric stratification and shows comparisons at four mean hub wind speeds: 5.2 m/s (blue lines); 7.2 m/s (green lines); 9.1 m/s (red lines); and 11.4 m/s (black lines). UPMPARK results are plotted with full lines and “filled” symbols, and experiments are plotted with dashed lines and “open” symbols. The large discrepancies observed for the 5.2 m/s and 11.4 m/s cases, respectively, may be due to an incorrect estimation of the thrust coefficient.

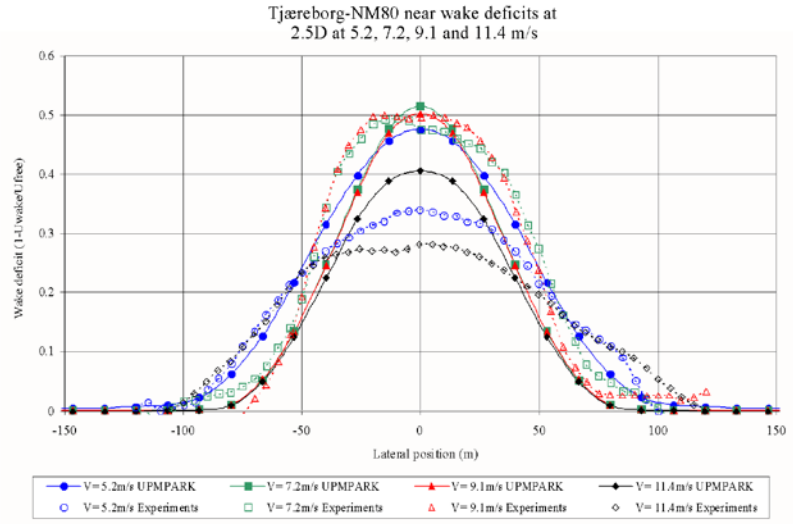

Figure 23: NM80 wake deficits at 2.5D spacing calculated with UPMPARK.

Linearized mixed spectral model (Fuga; RISOE.DTU)

As mentioned in Section 4.1 a linearized model is much faster than the non-linear CFD model on which it is based. A linearized model therefore provides a quick overview, and the question is of course whether the results are quick-and-dirty or quick-and-reliable. For this purpose validations have been made against data from offshore wind farms. These include OWEZ, Vindeby, Nysted and Horns Rev I. Figure 24 and Figure 25 show two examples. Results are shown for relatively broad sectors around a wind direction where the turbines are aligned. Data for narrower, 5 degree sectors are available, but are not shown. This is because such a narrow range of wind directions is not likely to be representative for the whole farm area and also because wind direction fluctuations larger than the bin width are likely.

Case 4.4.3.3: Nysted Park performance (Figure 24):

The Nysted offshore wind farm in Denmark consists of 72 2.3 MW Bonus 82m wind turbines arranged in a regular layout. The wind farm includes 4 masts located outside the wind farm, which can be used to determine the inflow conditions [24]. The power deficit along row of turbines has been determined for the western flow sector and compared to simulation results in Figure 24 for three different sectors.

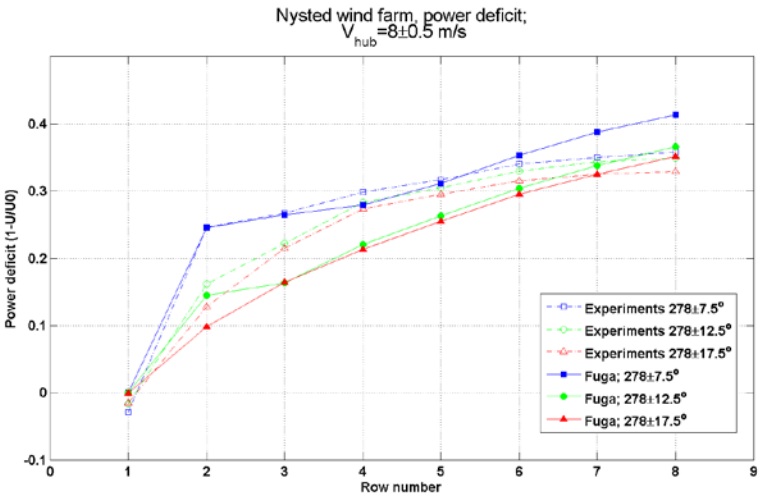

Figure 24; Power deficit inside Nysted wind farm, along a row of turbines, calculated with Fuga.

Case 4.4.3.4: Horns Rev Park performance (Figure 25):

Horns Rev offshore wind farm is located west of Denmark and consists of 80 2MW Vestas V80 80m wind turbines arranged in a regular layout. The power deficit along row of turbines has been determined for the western flow sector and compared to simulation results in Figure 25 for three different sectors.

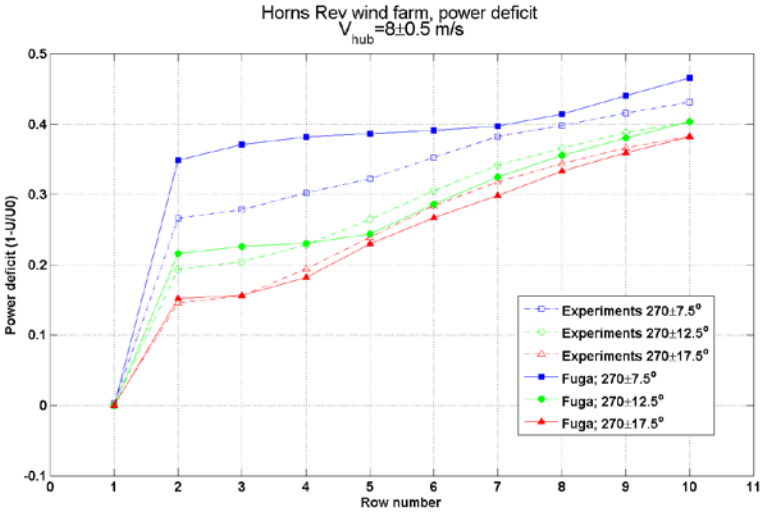

Figure 25: Power deficit inside Horns rev wind farm, along a row of turbines, calculated with Fuga.

The Actuator Line Method (ACL; MEK.DTU and RISOE.DTU)

All computations used for the full-scale based verification of the ACL model have been conducted in Cartesian computational domains. Generally, grid points were distributed equidistantly in the region around and downstream of the simulated turbines at a resolution which fulfill the basic demands for a well resolved LES [113].

Case 4.4.1.3: 2MW/60m Tjæreborg turbine (Figure 26 and Figure 27):

The 2MW/60m wind turbine, surrounded by two masts, was previously operating in Tjæreborg Enge [24]. A detailed wake analysis based on measurements has been used for this validation. The comparison is carried out at a mean wind speed at hub height of V_∞ = 6 m/s. In the computations the ambient turbulence intensity was approximately 9%, and the shear coefficient in a power law representation of the shear profile was 0.2.

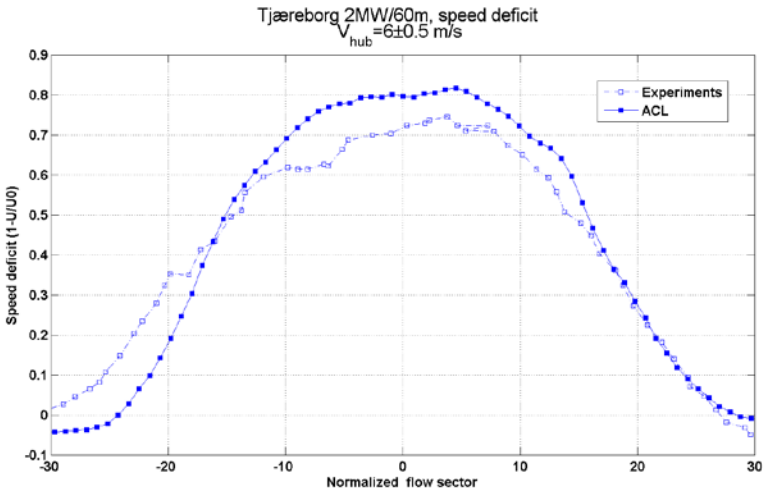

Figure 26: Comparison of measured and computed (ACL) velocity deficit at hub height, 2D downstream of the turbine.

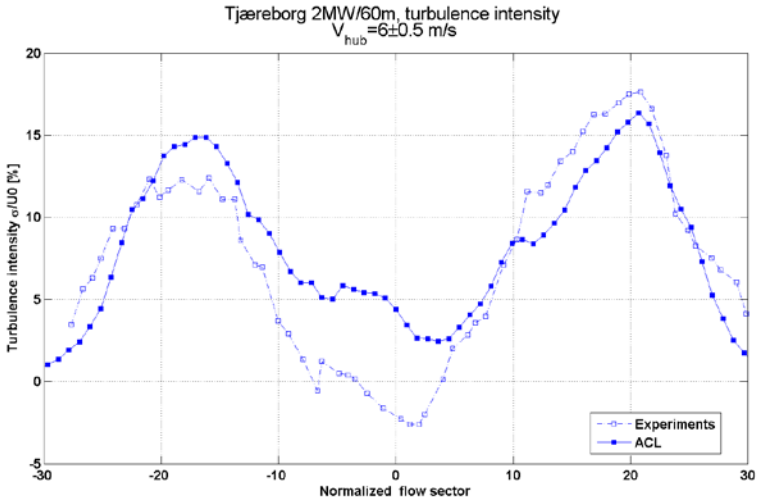

Figure 27: Comparison of measured and computed (ACL) added turbulence intensity at hub height 2D downstream of the turbine.

Further comparisons, based on measurements from this site, are presented in [113].

Case 4.4.1.5: Sexbierum - 2D flow in wind farms (Figure 28):

The Sexbierum wind farm was located in the Netherlands and consisted of 18 300kW Holec wind turbines with a diameter of 30m [24]. The measured and simulated speed deficit and turbulence have been compared for 2.5D, 5.5D and 8D spacing. The free-stream velocity is 8.4 m/s at hub height, and the ambient turbulence is approximately 13%.

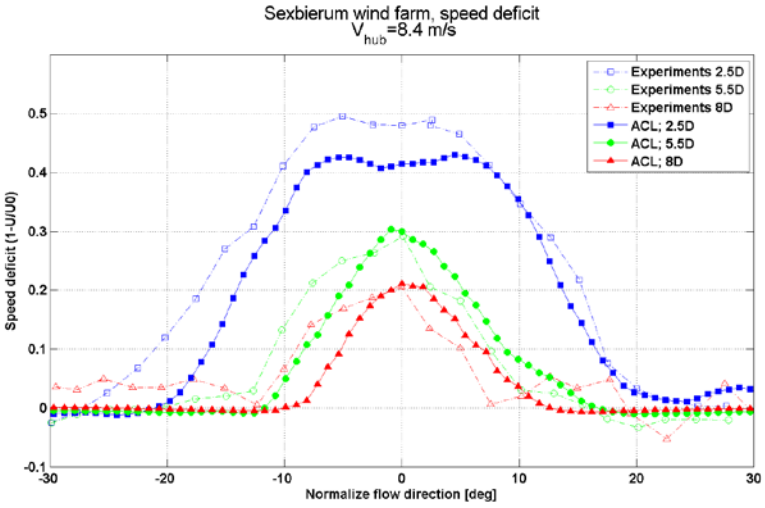

Figure 28: Comparison of measured and computed (ACL) mean velocity deficit at hub height downstream for 2.5D, 5.5D and 8D spacing.

Case 4.4.1.6: Wake flow validation at the Nibe turbines (Figure 29):

Two 40m/0.63MW wind turbines located in Nibe, Denmark was supplied with 4 masts for measuring wake properties.

Mean axial velocity profiles at hub height for various downstream positions have been measured behind the Nibe B wind turbine. Figure 29 shows both measured and simulated mean speed deficit across the wind turbine wake with 2.5D, 4D, 6D and 7.5D spacing, respectively. The ambient velocity and turbulence intensity were approximately 8.5 m/s and 9%.

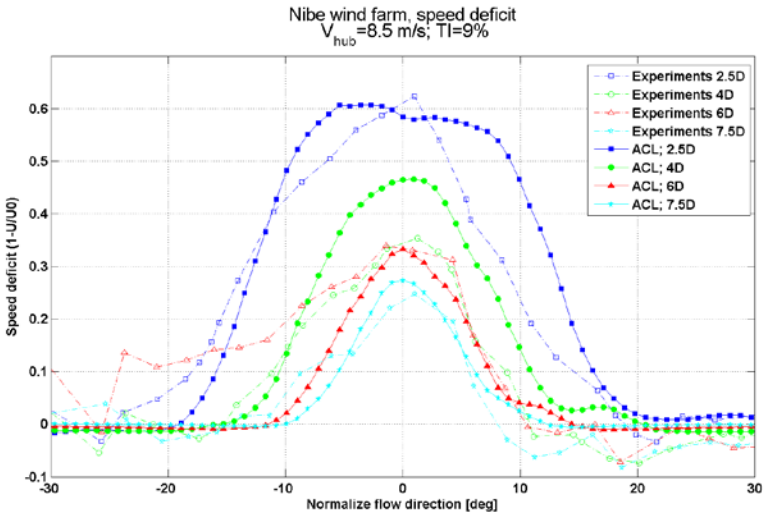

Figure 29: Comparison of measured and computed (ACL) mean velocity deficit at hub height downstream for 2.5D, 4D, 5.5D and 7.5D spacing.

Case 4.4.3.2: Wake flow Nørrekær Enge wind farm (Figure 30 and Figure 31):

The Danish Nørrekær Enge onshore wind farm consisted of 42 330 kW Nordtank stall regulated wind turbines with a diameter of 28m, and the turbines were distributed in regular rows [24].

The wind speed measured at hub height with 2D spacing inside the wind farm was used for validation. Figure 30 shows the measured and simulated wind speed deficit, and Figure 31 shows turbulence intensity for a 60 degree inflow sector.

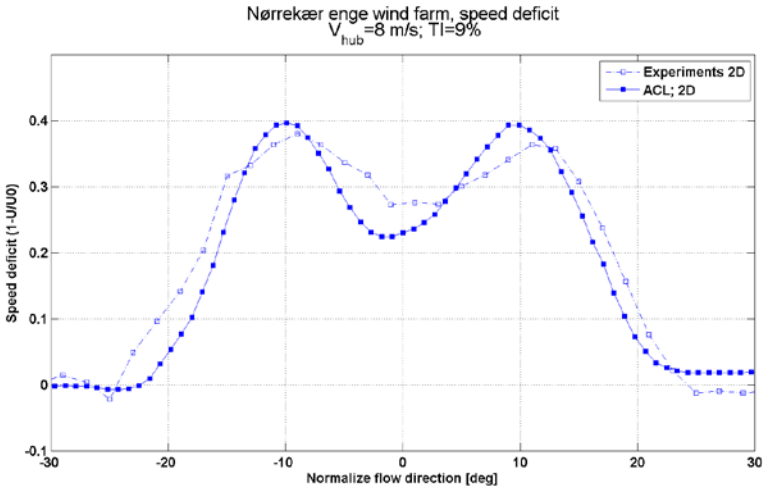

Figure 30: Comparison of measured and computed (ACL) velocity deficit at hub height 2D downstream of the turbine.

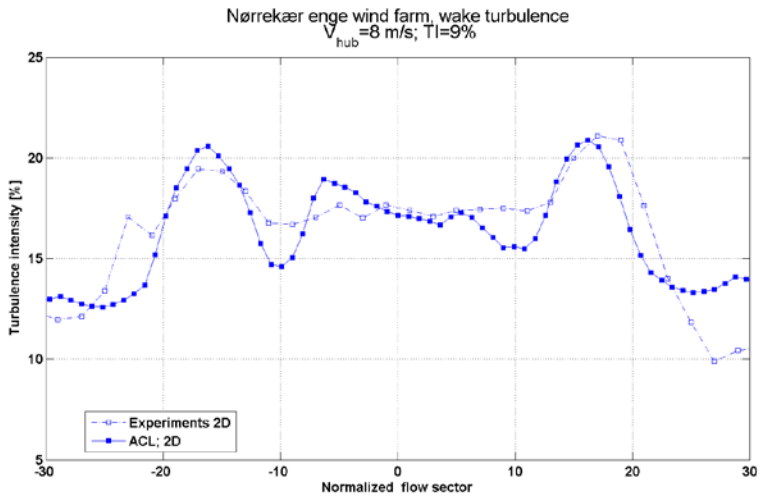

Figure 31: Comparison of measured and computed (ACL) turbulence intensity at hub height 2D downstream of the turbine.

Case 4.4.1.4: 2.5MW NM80 turbine flow field and power deficit (Figure 32, Figure 33 and Figure 34):

The NM80 2.5MW wind turbine is located in the Danish Tjæreborg Enge wind farm, consisting of 8 80m wind turbines and one meteorological mast [24]. The near wake flow field 2.4D behind the NM80 wind turbine has been measured on the mast – as function of wind direction. Furthermore, the power deficit for the NM80 turbine has been determined for different flow directions and spacings. More results have been published in [113]. Figure 32 shows the measured and simulated speed deficit, and Figure 33 shows the turbulence intensity for a 50 degree inflow sector.

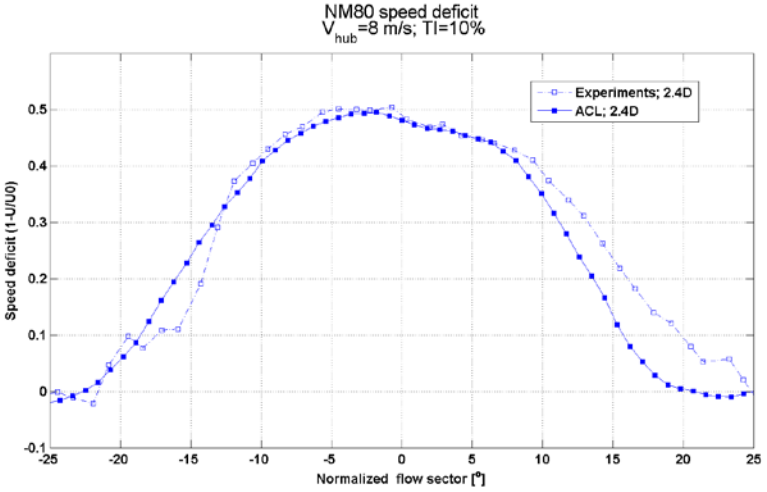

Figure 32: Comparison of measured and computed (ACL) velocity deficit at hub height 2.4D behind the turbine.

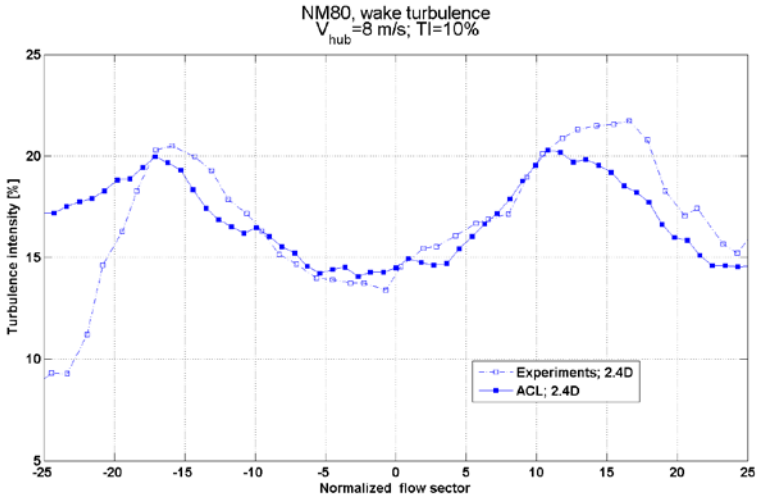

Figure 33: Comparison of measured and computed (ACL) wake turbulence intensity at hub height 2.4D downstream of the turbine.

The simulated and measured power deficit at respectively 3.3D and 6.6D spacing are compared with experiments in Figure 34.

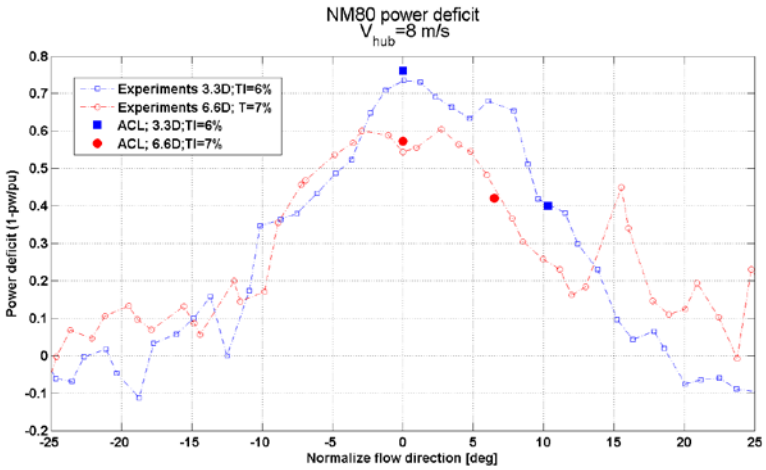

Figure 34: Comparison of measured and computed (ACL) power deficit at V_{hub}= 8m/s for two different turbine spacing 3.3D and 6.6D.

Case 4.4.1.9: 2.3 MW NM80; 2.5D flow field from LIDAR (Figure 35 and Figure 36):

The NM80 2.5MW wind turbine, which is located in the Danish Tjæreborg Enge wind farm, was in an experimental campaign equipped with an adapted LIDAR for measuring the wake characteristics [24].

A comparison of the wake deficit and turbulence intensity, as expressed in the meandering frame of reference, 2.5D downstream of the 80m turbine has been performed in Figure 35 and Figure 36, respectively.

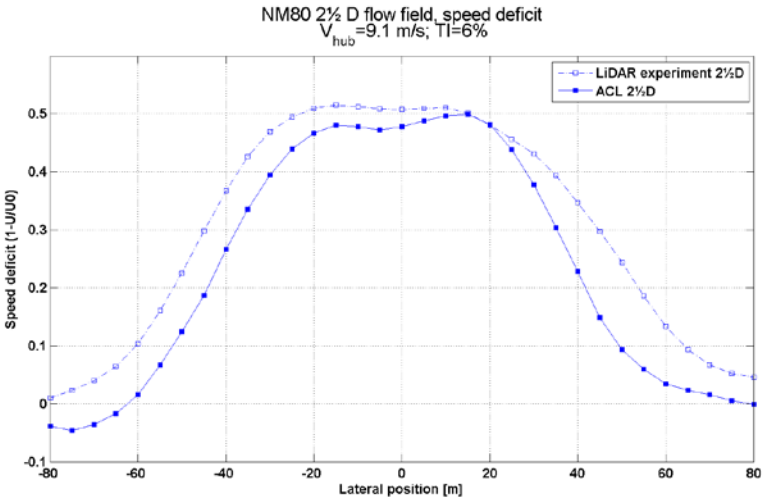

Figure 35: NM80 wake deficits in the meandering frame of reference at 2.5D spacing, compared and calculated with ACL.

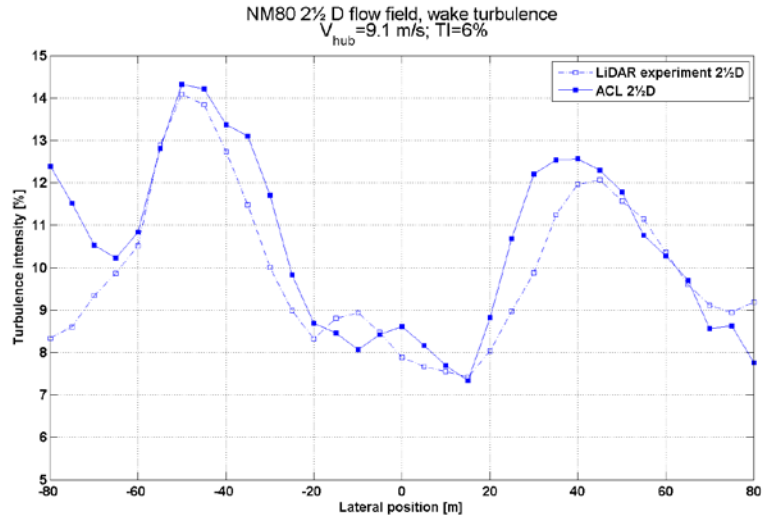

Figure 36: NM80 wake turbulence in the meandering frame of reference at 2.5D spacing, compared and calculated with ACL.

Parabolic Navier-Stokes solver (ParaSol; MEK.DTU)

The performance of the ParaSol code was analyzed by comparing with solutions obtained from a full elliptic Navier-Stokes code, EllipSys3D, combined with an actuator line method. For each time-step, the ParaSol code was about 8 times faster than the EllipSys3D code, and deviations in predicted normalized axial and tangential force coefficients were moderate. The performance of the new code has been further analyzed using the Tjæreborg wind turbine where the computations were carried out on a mesh of 144×144×200 using a mixed-scale sub-grid scale model. The performance of the parabolic code is evaluated by comparing code predictions to results from full-scale measurements.

The results are shown in Figure 37 and Figure 38. Both laminar and turbulent inflow conditions are investigated. The turbulent inflow is generated using the

Mann turbulence generator model. It is seen that there is a significant difference between laminar and turbulent inflow conditions, which clearly demonstrates the need for simulating ambient turbulence in this type of calculations. The axial velocity is reasonably well predicted when based on turbulent inflow conditions, whereas significant deviations appear for the axial standard deviation.

Case 4.4.1.3 Tjæreborg, D=60m, 2-D flow field (Figure 37 and Figure 38):

The 2MW/60m wind turbine, surrounded by two meteorological masts, was previously operating in Tjæreborg Enge [24]. A detailed wake analysis based on these measurements has been used for this validation.

Wind speed measurements recorded in the wake of the wind turbine at hub height were compared with simulated results in Figure 37 and Figure 38. The figures are presenting results for a free inflow hub wind speed equal to 10 m/s.

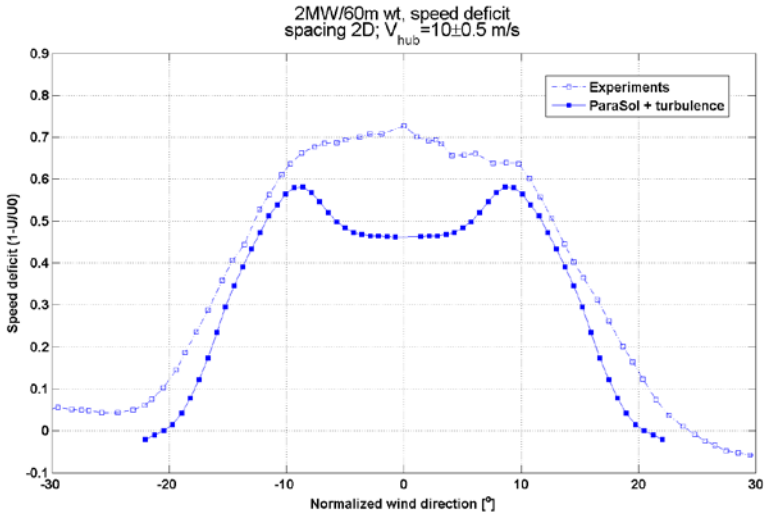

Figure 37: Comparison of measured and calculated (ParaSol) axial velocities at hub height with 2D spacing.

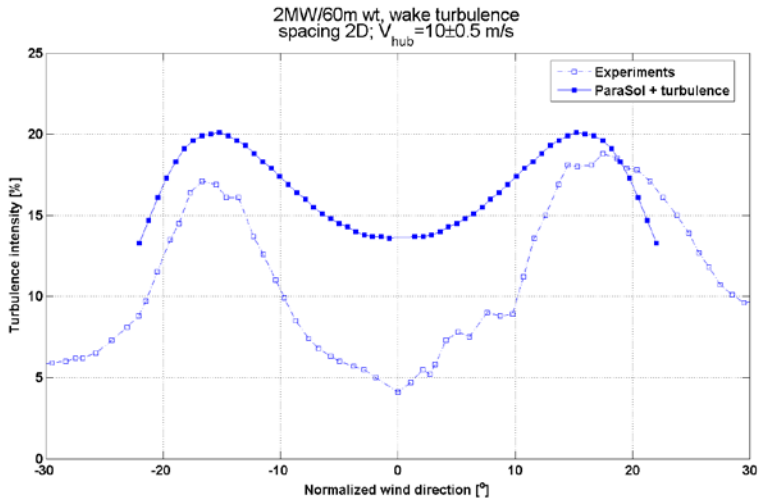

Figure 38: Comparison of measured and calculated (ParaSol) axial turbulence at hub height with 2D spacing.

Atmospheric Dispersion Modeling System (ADMS 4; CERC)

ADMS 4 has been tested against two sets of full scale measurements.

4.4.1.1. Maximum power deficit vs. TI (Figure 39):

This basic simulation tries to clarify the influence of ambient turbulence on power deficits. The wind turbine has 5MW nominal power. Results are representing three downstream distances: 3.8D (blue lines); 7D (green lines); and 10.3D (red lines). ADMS 4 results are represented by full lines and "filled" symbols, and experimental results are represented by dashed lines and "open" symbols.

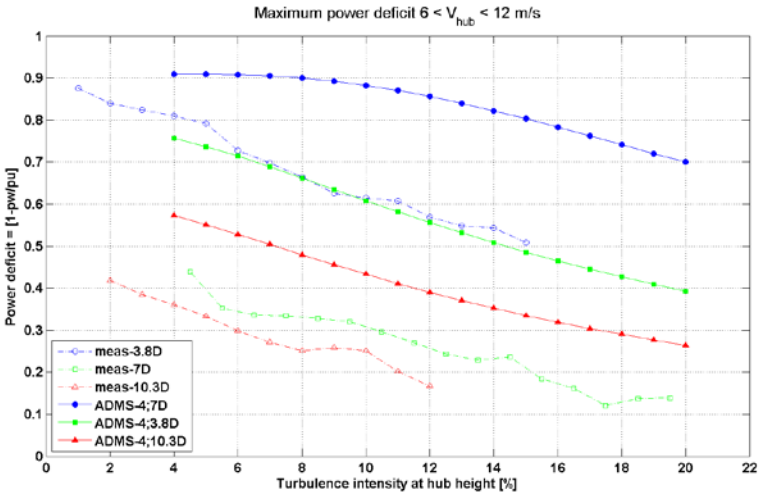

Figure 39: Maximum power deficit for 5MW wind turbines with 3.8D, 7D and 10.3D spacing, simulated with ADMS 4.

4.4.1.3: Tjæreborg D=60m, 2-D flow field (Figure 40):

The 2MW/60m wind turbine, surrounded by two masts, was previously operating in Tjæreborg Enge [24]. A detailed wake analysis based on measurements was used for this validation. Wind speed measurements recorded in the wake of the wind turbine at hub height were compared with simulated results for three mean wind speeds; V_{hub} = 6, 8 and 10 m/s, respectively. In the computations the ambient turbulence intensity was in the range 6-8%, and computed and measured velocity deficits are shown in Figure 40.

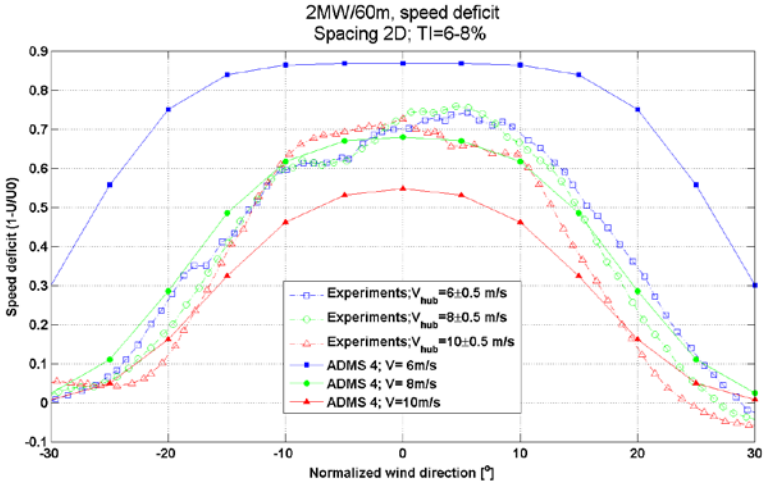

Figure 40: Comparison of measured and computed (ADMS 4) velocity deficit at hub height, 2D downstream of the turbine.

4.4.1.9: Tjæreborg NM80, 2½-D flow field (Figure 41 and Figure 42):

The NM80 2.5MW wind turbine, which is located in the Danish Tjæreborg Enge wind farm, was equipped with an adapted LIDAR system for measuring the wake characteristics [24].

A comparison of the wake deficit and turbulence intensity resolved in a meandering frame of reference 2.5D downstream of the 80m turbine has been performed for a hub mean wind speed of 9.1 m/s and a 6% ambient turbulence intensity in Figure 41 and Figure 42.

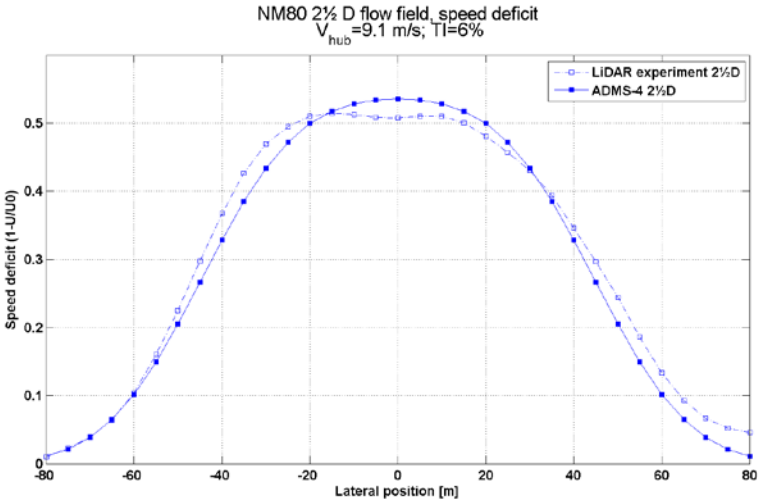

Figure 41: Comparison of measured and calculated (ADMS 4) near wake deficit at 9.1 m/s and 6% ambient turbulence.

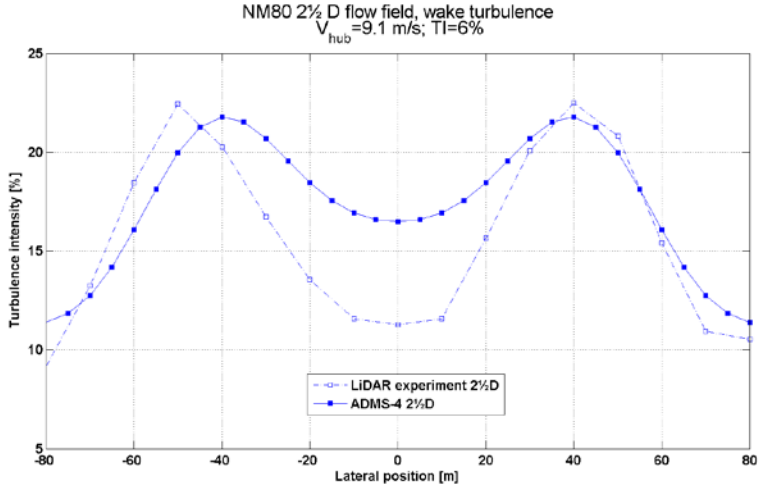

Figure 42: Comparison of measured and calculated (ADMS 4) near wake turbulence at 9.1 m/s and 6% ambient turbulence.

4.4.3.1. OWEZ wind farm performance (Figure 43):

The Offshore Wind farm Egmond aan Zee (OWEZ) in the Netherlands consists of 36 × 3 MW Vestas V90 wind turbines arranged in 4 parallel rows. The wind farm has one mast located outside the wind farm, which can be used to determine the inflow conditions for some flow sectors [24]. The power deficit along row of turbines has been determined for SE flow sector and compared to simulation results in Figure 42 for the rows[1] of turbines.

1 *Row 2-4 has a gab equal to a "missing turbine" between turbine 4 & 5.*

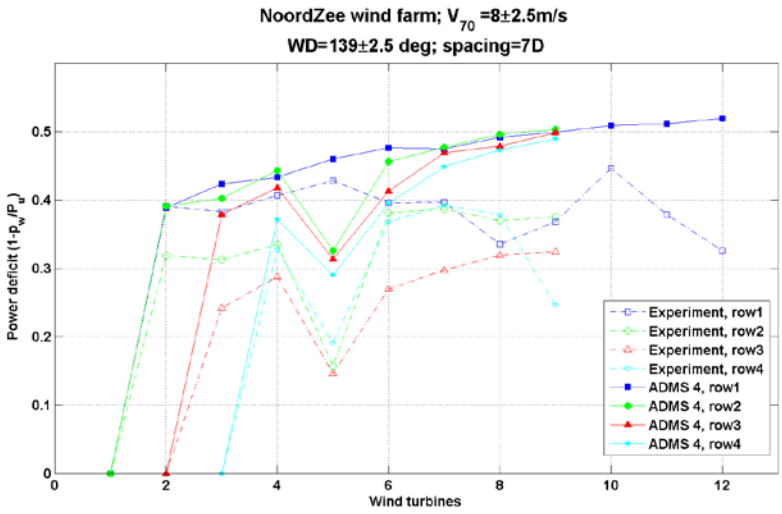

Figure 44: Comparison of measured and calculated (ADMS 4) power deficit inside the OWEZ wind farm, for a narrow sector and a wind speed interval of 5.5 – 10.5 m/s.

4.4.3.3.Nysted park performance (Figure 45):

The Nysted offshore wind farm in Denmark consists of 72 × 2.3 MW Bonus 82m wind turbines arranged in a regular layout. The wind farm includes 4 masts located outside the wind farm, which can be used to determine the inflow conditions [24]. The power deficit along the row of turbines has been determined for western flow sector and compared to simulation results in Figure 45 for three different flow directions.

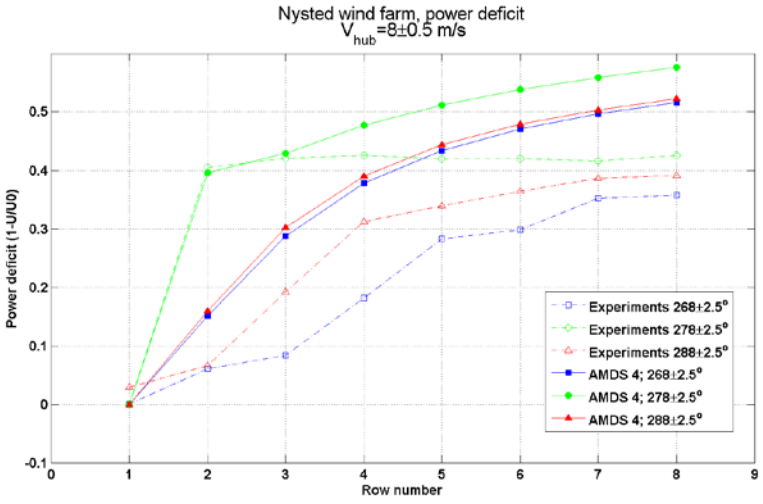

Figure 45: Comparision of measured and calculated (ADMS 4) power deficit inside Nysted wind farm for three narrow flow sectors along a line of wind turbines at 8 m/s inflow.

Dynamic wake meandering model (DWM; RISOE.DTU)

The DWM model has been tested against two sets of full scale measurements encompassing both power production and wind turbine fatigue loading associated with selected load sensors.

4.4.1.1.Maximum power deficit vs. TI (Figure 46):

The purpose of this validation is to clarify the influence of ambient turbulence on power deficits. The wind turbine has 5MW nominal power. Results are presented for three downstream distances: 3.8D (blue lines); 7D (green lines); and 10.3D (red lines). DWM results in Figure 46 are represented by full lines and "filled" symbols, and experiments are represented by dashed lines and "open" symbols.

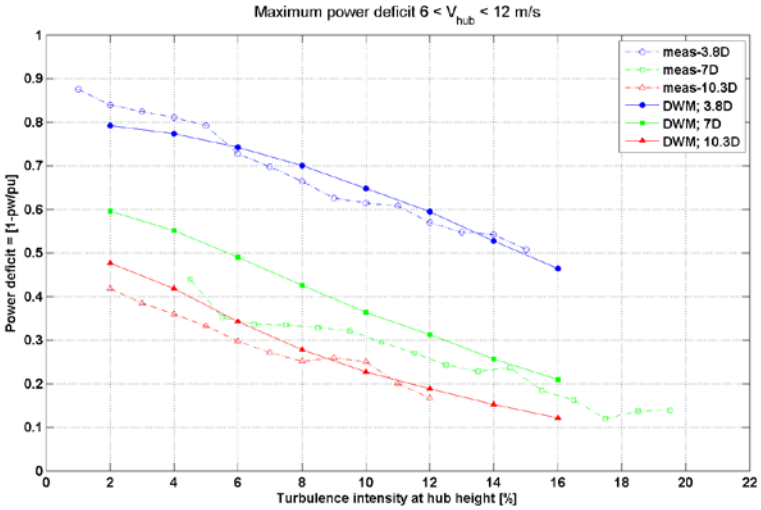

Figure 46: Maximum power deficit for 5MW wind turbines with 3.8D, 7D and 10.3D spacing, simulated with DWM.

4.4.2.1. OWEZ wind farm, fatigue loads (Figure 47, Figure 48 and Figure 49):

The Offshore Wind farm Egmond aan Zee (OWEZ) in the Netherlands consists of 36 × 3 MW Vestas V90 wind turbines arranged in 4 parallel rows. The wind farm has one mast located outside the wind farm, which can be used to determine the inflow conditions for some flow sectors [24].

The DWM model implementation in the HAWC2 code [133] was validated by comparing simulated results with experimental results from wind turbine wt07 located in the wind farm. The cases are used to verify the equivalent fatigue load range for free undisturbed flow and for a 7D spacing wake case with 5 upstream wake generating turbines. Two different S-N slopes have been used: m=10 representing the blade properties; and m=4 representing tower proper*ties.* The simulation results are presented in a draft journal paper [77], and 4 figures with simulated and measured results has been included below.

The measured and simulated 1Hz normalized equivalent fatigue loads for the blade root bending moment are shown on Figure 47 as function of the nacelle wind speed for 2 flow cases – free undisturbed inflow as well as wake

affected inflow corresponding 5 upstream turbines with an interspacing of 7D.

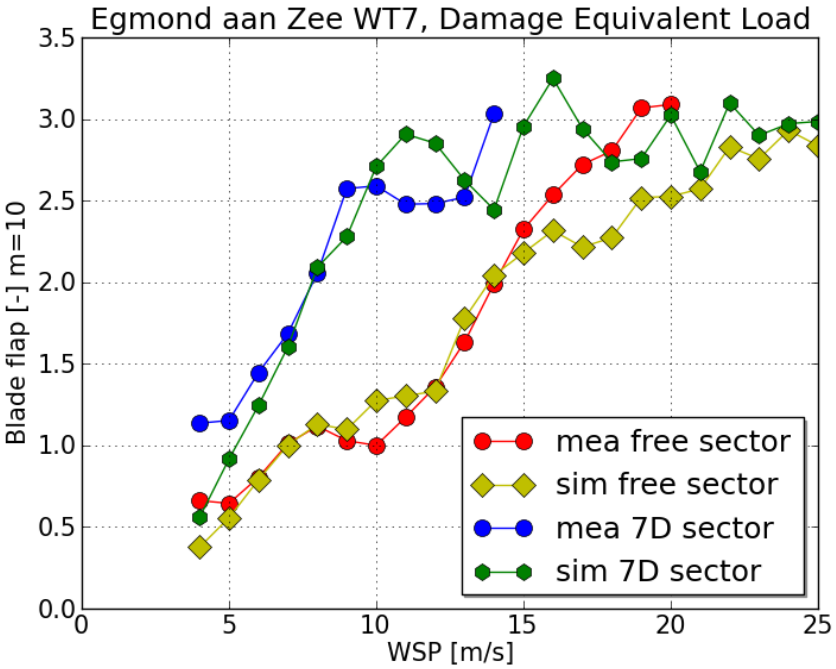

Figure 47: 1Hz normalized equivalent flap moment representing free flow and 7 D spacing for the V90 inside NoordZee wind farm.

The measured and simulated 1Hz *normalized* equivalent fatigue loads for the tower top torsion at level 61.5 m are shown as function of the nacelle wind speed for 2 flow cases in Figure 48 (i.e. free undisturbed inflow and 7D spacing, respectively).

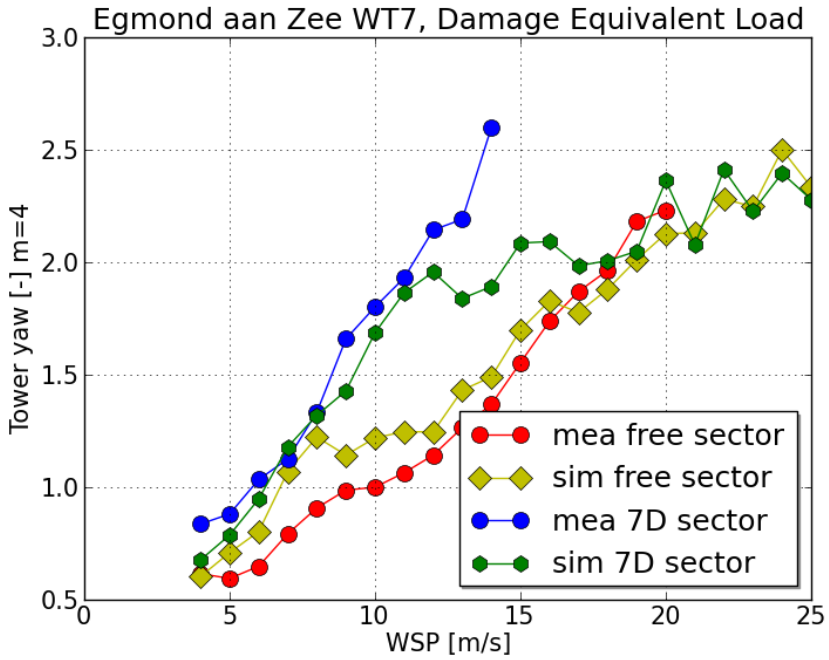

Figure 48: 1Hz normalized equivalent tower top torsion representing free flow and 7 D spacing for the V90 inside NoordZee wind farm.

The measured and simulated 1Hz *normalized* equivalent fatigue loads for the tower tilt[2] at level 17m are shown on Figure 49 as function of the nacelle wind speed for the 2 flow cases (i.e. free undisturbed inflow and 7D spacing, respectively).

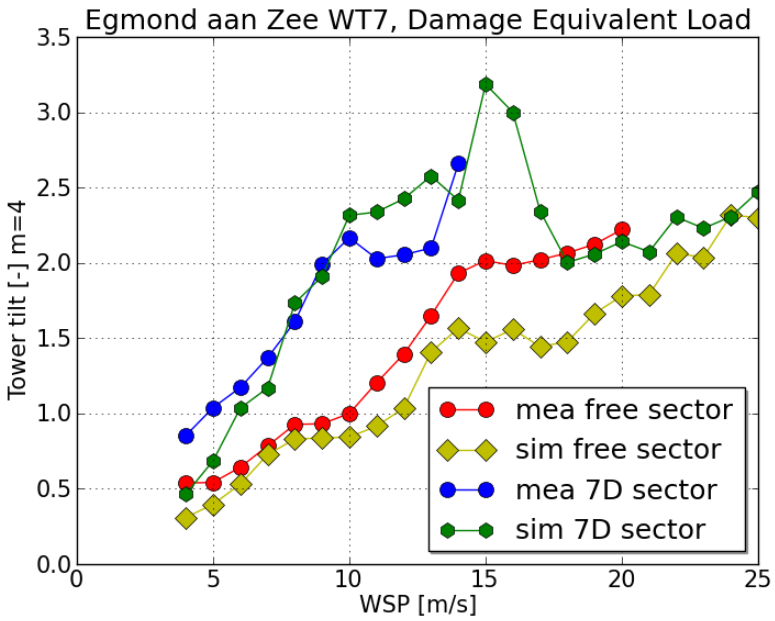

Figure 49: 1Hz normalized equivalent tower TILT, representing free flow and 7 D spacing for the V90 inside NoordZee wind farm.

2 The tower tilt is equal to the tower bending – in the wind direction.

GH Bladed with dynamic wake meandering model (BLADED; GL)

The GH Bladed [122] with the "dynamic wake meandering" wake simulation module is verified by comparing with full-scale Horns Rev measurements.

4.4.2.2 Horns Rev, fatigue loads (Figure 50, Figure 51 and Figure 52):

Horns Rev offshore wind farm is located west of Denmark and consists of 80 × 2MW Vestas V80 80m wind turbines arranged in a regular layout. WT14 has been instrumented for structural load measurements.

The DWM model implementation to GH Bladed has been validated with measurements from wind turbine wt14 in case of equivalent fatigue load range for free undisturbed inflow as well as 7D, 9.4D and 10.4 D wake inflow. Two different S-N slopes have been used, where m=12 represents the blade properties and m=4 represents the tower properties. The simulation results are presented in a conference paper [104] and here are included 3 figures with simulated and measured results.

The measured and normalized simulated 1Hz equivalent fatigue loads for the blade root bending moment are shown on Figure 50 as function of the nacelle wind speed for 4 flow cases: free undisturbed inflow; wake inflow characterized by 7D; 9.4D; and 10.4 D spacing. All the results are simulated with *GH Bladed* and the *dynamic wake meandering model.*

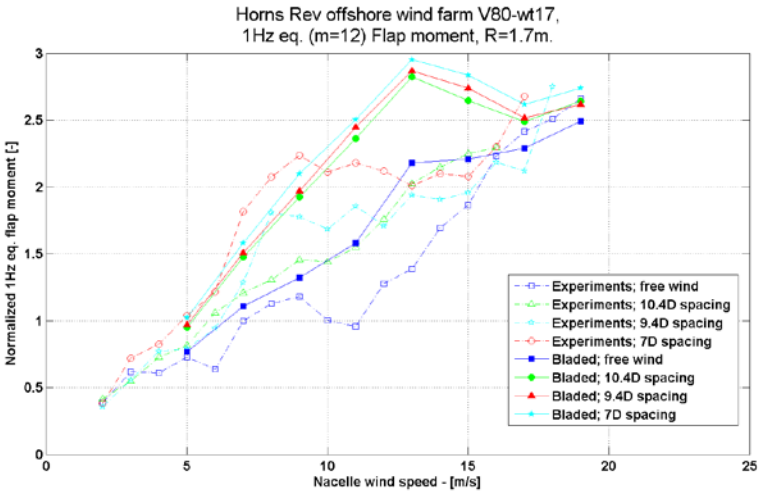

Figure 50: V80-wt14 normalized 1Hz equivalent (m=12) flap moment at free inflow, 7D, 9.4D and 10.4D spacing.

The measured and simulated 1Hz normalized equivalent fatigue loads for the tower tilt at level 13m are shown on Figure 51 as function of the nacelle wind speed for 4 flow cases: free undisturbed inflow; wake inflow characterized by 7D; 9.4D; and 10.4 D spacing. The normalized equivalent TILT fatigue moment values are derived as root-mean-square values from the bending moments at direction 229° and 319°, respectively.

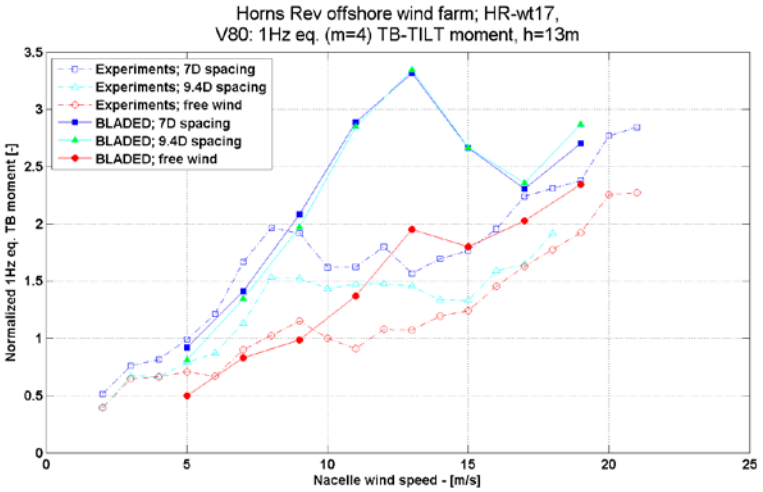

Figure 51: Horns Rev, V80-wt14 normalized 1Hz equivalent (m=4) tower TILT moment, h= 13m at free inflow, 7D and 9.4D spacing.

The measured 1Hz normalized equivalent fatigue loads (m=12) for the blade root bending moment are shown on Figure 52 as function of wind direction for a (nacelle) wind speed of 9 m/s. The simulated values, extracted from Figure 50, are shown for 5 distinct directions corresponding to free undisturbed inflow; wake inflow characterized by 7D; 9.4D; and 10.4D spacing in a western sector.

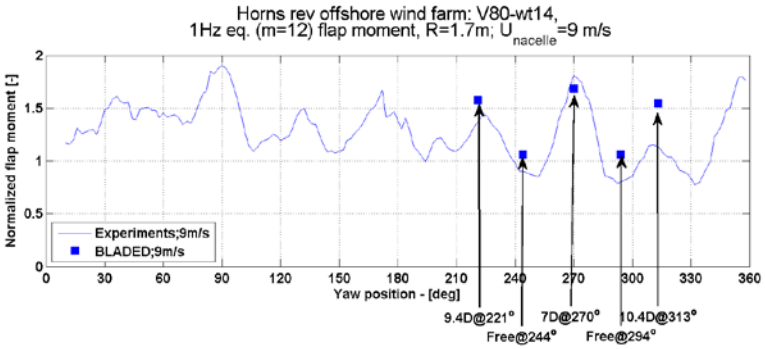

Figure 52: V80-wt14 normalized 1Hz equivalent (m=12) flap moment as function of wind direction for 9 m/s with reference to the nacelle wind speed.

Acknowledgements

- *Horns Rev:* We would like to acknowledge VESTAS A/S, Vattenfall AB and DONG Energy A/S for providing data from the Horns Rev wind farm;
- *Nysted:* We would like to acknowledge Siemens Wind Power, DONG Energy A/S and E.On Sweden for providing data from the Nysted wind farm;
- *NoordZee/Egmond Aan Zee:* We would like to acknowledge VESTAS A/S and NoordZeeWind B.V. for providing data from the NoordZee wind farm;

- *Tjæreborg:* We would like to acknowledge VESTAS A/S, Vattenfall AB and DONG Energy A/S for providing data from the Tjæreborg Enge wind turbines;
- *Vindeby:* We would like to acknowledge Siemens Wind Power and DONG Energy A/S for providing data from the Vindeby wind farm.

4.5 WP5 – Cost models

The synthesis of all required sub-models in the optimization platform (cf. Section 4.6) is performed by formulating an object (or penalty) function for the optimization problem. In the framework of TOPFARM this penalty function is formulated in economical terms, from which the need for cost models arises. The developed cost model complex [58] contain models describing *financial costs* as well as models describing wind farm *operating costs*, each of which in turn consists of a number of separate sub-models.

These models are tailored for application in the TOPFARM project in the sense that only costs *depending on wind farm topology and control* (including wind turbine foundations, production and loading) are of relevance. In the context of TOPFARM we will denote these costs as *variable* costs, contrary to *fixed* costs which are, in this framework, e.g. cost of planning and projecting of the wind farm, cost of the land available for the intended wind farm project, price of turbines, civil engineering costs to roads connecting the wind farm with the surrounding community (but not internal road infrastructure), price of cabling from the wind farm to the main grid (but not the internal grid infrastructure), etc.

The fixed costs may be included in the penalty function, but as seeking the stationary points for this functional involves gradient behavior only, the fixed costs will not influence the global optimum of the penalty function. Therefore only models for variable costs are considered.

Financial costs

The variable part of the total wind farm investment costs, C, may be expressed as [58]

$$C = CF + CI + CT + CE \ , \tag{12}$$

where CF is the cost of foundations, CI the cost of installation, CT the costs of civil engineering infrastructure, and CE denotes electrical infrastructure costs.

For onshore sites CI is in general variable in the sense that it depends on the accessibility of the individual wind turbine location, which in turn depends on the wind farm topology. For off-shore sites, the installation costs may depend on the water depth. For the demonstration optimizations performed in Section 4.7 and Section 4.8, respectively, we will assume that CI is constant. For the onshore case this is motivated by the fact that the onshore site is characterized by flat and homogeneous terrain. For the off-shore case we consider CI constant, because the water depths in question varies only moderately, and consequently the same installation equipment and effort in human resources is needed for all possible locations.

Civil engineering infrastructure denotes in the present context transportation infrastructure within an onshore wind farm (i.e. establishment of the necessary roads to access the turbines and enable installation of these). The cost of civil engineering infrastructure is in general a variable cost that depends on the orography of the terrain, the soil conditions, etc. However, as already mentioned the onshore site considered in Section 4.8 is characterized by homogeneous conditions, and consequently *CT* can be considered as constant in the present context.

Based on the considerations above, the variable part of the total wind farm investment costs may be simplified as

$$C = CF + CE \tag{13}$$

for the optimization study of the Middelgrunden and Coldham/Stags Holt wind farms.

Cost of foundation is in general a variable cost in the sense that it depends on the soil conditions and/or the water depth at the location of each individual turbine. For the present study we will, however, consider *CF* as constant for the onshore case, as homogeneous terrain conditions prevails. For the *onshore case*, the wind farm investment costs may therefore be further simplified by dispensing with the cost of the foundation. For the *off-shore case* we will assume that the investment costs depends on water depth only, and that *CF* can be expressed as

$$CF = \sum_{i=1}^{N_T} CT_i(x_i, y_i) , \tag{14}$$

where CT_i is the cost of foundation for the *i*'th wind turbine, (x_i,y_i) is the position of the *i*'th turbine in a Cartesian grid, and N_T is the total number of turbines in the wind farm considered. For the water depths relevant for the present off-shore case we will more specifically assume that CT_i depends linearly with the water depth as

$$CT_i(x_i, y_i) = CT_r + \Delta h(x_i, y_i) CT_g \ , \tag{15}$$

where the reference foundation cost CT_r equals equals 20% of the total turbine cost and refers to a reference water depth of 8 m, the gradient foundation cost per meter deviation from the reference water depth, CT_g, equals 2% of the total turbine cost, and $\Delta h(x_i,y_i)$ is the deviation of the water depth at location (x_i,y_i) from the reference water depth measured in meters.

The electrical infrastructure costs associated with the wind farm includes *cables* connecting the individual turbines to the wind farm transformer as well as expenses related to the *cable laying*. These expenses will depend on the distance between turbines and the site conditions. The cost of the electrical infrastructure is modelled as

$$CE = \int_C c(x, y) ds \ , \tag{16}$$

where $c(x,y)$ is the cabling cost per running meter, C is the cabling trace connecting all turbines in the shortest possible way, and ds is an infinitesimal curve element on the trace. Note, that for a more detailed modelling, the best strategy is not necessary to base the cabling on the shortest possible cabling, but rather on the cheapest possible cabling. This is elaborated on in more detail by [58], where such a formulation is derived.

As indicated we decompose $c(x,y)$ as

$$c(x,y) = c_c(x,y) + c_l(x,y)\,, \tag{17}$$

with $c_c(x,y)$ being the cable cost pr. running meter, and $c_l(x,y)$ being the cable laying cost pr. running meter. The assumed prices for cable costs are specified in Table 6.

In DDK/m	**Onshore**	**Offshore**
Cable	2000	1000
Installation	3000	1000
Total	50000	2000

Table 6: Assumed prices for cable costs (1DKK = 0.14EUR).

Electrical cables used to connect the wind turbines to the grid can carry different voltages. According to the voltage of the cable, a limited number of wind turbines can be connected per cable. These types of design limits are not considered in the present work. The idealized cables considered in the present cost modelling are assumed to be able to be able to carry all the electricity of the wind turbines connected through them. However, it should be noted that this type of considerations could have a significant impact on the cost modelling and thus on the optimization process and the final optimal solution. Such limitations should therefore be considered in future work.

Operational costs and value of production

We have adapted the philosophy of only *relative expenses* being of interest in a wind farm optimization context, and we will expand this concept to include also considerations on the relationship between rate of inflation and relevant interest rates as done in [58]. The financial balance, *FB*, expressed in [58] operates with a split of the total (variable) investment on consortium loans and consortium financial assets, respectively. To simplify matters, we will here consider the investment to be financed by loans only. Introducing two financial parameters – both referring to a one year period – the rate of inflation, r_i and the interest rate that the wind farm consortium has to pay for loans (i.e. price of money in banks or by other investors) and assuming interest of loans to be paid N_L times a year, the financial balance may thus be expressed as

$$FB = WP_n - C\left(1 + \left(\frac{r_{c1} - r_i}{N_L}\right)\right)^{XN_L}\,, \tag{18}$$

with X denoting the wind farm life time in years, and net value of the power production, WP_n, defined as

$$WP_n = WP - CD - CM \ , \tag{19}$$

where WP is the value of the wind farm power production over the wind farm lifetime, CD is the cost of fatigue driven turbine degradation, and CM is the costs of maintenance. For convenience, we have interpreted all operating costs (i.e. CD and CM) as referring to year Zero, with the implicit assumption that the development of these expenses over time follows the inflation rate, and that the inflation rate is the natural choice for the discounting factor transforming these running costs to *net present value*. We have also, through equation (4), implicitly referred the value of the wind farm power production over the wind farm lifetime, WP, to year Zero.

The cost of (fatigue) degradation of the turbines is accounted for by linear writing off [58]. For a particular structural member, identified by S, the *mean* cost of fatigue load degradation is presumed proportional to the *mean* accumulated equivalent moment, associated with a suitable component "hot spot", caused by turbine operation during the lifetime of the wind farm. We introduce the mean *relative degradation* as

$$D_S = \frac{M_{Sa}}{M_{Sd}} \ , \tag{20}$$

with subscript S referring to structural member S, and where M_{Sa} and M_{Sd} are the (mean) accumulated and the design equivalent moments, respectively. Using equation (6), the *cost of degradation*, CD_S, is defined as

$$CD_S = P_S D_S \ , \tag{21}$$

with P_S denoting the price of the particular structural component.

In the formulation of maintenance costs we apply a probabilistic failure criterion. Assuming the component equivalent moment resistance to be described by a log-Gaussian distribution [58], the *cost of maintenance*, CM_S, related to the structural member S, is approximated as

$$CM_S = W_{R+1} \times P_{S_r} F\left(D_S ; \mu_{S,(R+1)}, \sigma_{S,(R+1)}\right) + P_{S_r} \sum_{j=1}^{R} F\left(D_S ; \mu_{S,j}, \sigma_{S,j}\right) , \tag{22}$$

where P_{Sr} denotes the replacement cost (i.e. cost of the physical replacement and additional expenses originating the derived production loss), R is the maximum number of allowable replacements defined by the designer, and W_{R+1} is a weight factor large enough to assure that more than R replacements is unfavorable for the optimal wind farm topology. $F(D_S; \mu_{S,j}, \sigma_{S,j})$ is the log-Gaussian cumulative distribution function (CDF) with distribution parameters μ_j and σ_j. The j'th distribution parameter set is related to the mean component resistance, $E[M_{Sr}]$, and variance of the component resistance, $VAR[M_{Sr}]$, through the respective mean and variance of the relative degradation measure as

$$\sigma_{S,j} = \sqrt{Ln\left(\frac{VAR[M_{Sr}]}{j^2 M_{Sd}{}^2} + 1\right)}\,, \tag{23}$$

and

$$\mu_{S,j} = Ln(j) - \sigma_{S,j}^2\,. \tag{24}$$

The costs of degradation, described in equation (10), and the costs of maintenance, described in equation (11), are straight-forwardly generalized to all main components on all turbines within the considered wind farm as

$$CD = \sum_{N_T}\sum_{S} P_S D_S\,, \tag{25}$$

and

$$CM = \sum_{N_T}\sum_{S} CM_S\,, \tag{26}$$

respectively.

4.6 WP6 - Optimization platform

The sub-models developed in the WP's 1, 2, 3 and 5 have been synthesized into an optimization platform. Referring to Section 4.5, this synthesis has been obtained by formulating the objective function for the optimization problem in economical terms – more precisely in terms of a financial balance expressing the difference between the wind farm income (power production) and the wind farm expenses (i.e. financial expenses, O&M expenses, cost of turbine fatigue load degradation). With this setting, the purpose of the optimization algorithm is to alter the wind farm layout so that the financial balance attains its (global) optimum.

Optimization engine

The Risø-DTU in-house code, HAWTOPT, is used as the optimization engine. The HAWTOPT program has been developed at Risø National Laboratory from 1994 and onwards, and is predominantly used for optimization of wind turbines, and in particular aerodynamic design of wind turbine rotors [126], [127], [128]. However, HAWTOPT contains a general purpose optimization tool with several different optimization algorithms as options.

In the optimization context, the financial balance becomes the objective function with the wind farm layout being described as design variables. Constraints are then subsequently defined to limit the domain spanned by the design variables into a feasible region. The constraints are both explicit limits on the individual wind turbine coordinates as well as integral values resulting from calculation in addition to the cost function. These could e.g. be maximum allowable turbine loads, minimum distance between turbines, power quality, etc.

The optimization problem is defined within a Matlab environment, and during the optimization Matlab is acting as the working horse of the optimization. This means that when a new design vector (i.e. the wind farm layout) is generated by HAWTOPT, it is subsequently passed on to Matlab. Matlab then calculates the cost function, which is returned to HAWTOPT. As the optimization process is iterative, a significant number of cost function evaluations are needed before the optimization is done resulting in an optimized wind farm layout. In the present implementation, two optimizations algorithms of HAWTOPT are used:

1. The Sequential Linear Programming (SLP) method, which is a linear program within a linear sub-space of the design space. Move-limits are applied in all dimensions to ensure smooth convergence. The move-limits are adaptive and automatically adjusted according to the convergence toward an optimum on basis of the rate of convergence [119]. The SLP approach typically has an attractive rate of convergence and is therefore efficient in terms of the number of cost function evaluations necessary. However, this is at the expense of being sensitive to local minima. In a non-linear design space, there is no guarantee to reach at a global optimum.
2. The Simple Genetic Algorithm (SGA) is a genetic algorithm based on the original work of Goldberg [130] in which the design variables are converted into chromosomes (binary strings). Using an analogy to the theory of evolution, individual parents mate and create children by use of the genetic operators, crossover and mutation. Automatic Fitness scaling is used and constraints are included by a penalty formulation [129]. The SGA approach has a much slower rate of convergence compared with the SLP approach, but the advantage is that if the SGA method is run for a sufficient number of iterations, it will reach the *global* optimum.

The combination of the SGA and SLP approaches is appealing if the SGA method is used as an initial optimization using a coarse resolution of the design variable, and when an optimum is reached the gradient based SLP method can be used to refine the result using a finer resolution for the design variables. In this way, the global optimality advantage of the SGA is combined with the accuracy of SLP.

Design space reduction

Keeping the number of design variables as low as possible is the key to keep the computational costs at a minimum, since more design variables slows down convergence and requires more objective function evaluations. There are in general three different approaches to the mapping of the wind farm layout into design variables:

1. Defining a structured and regular pattern for the turbines. This can be done by using a structured grid, for example as rows and columns with fixed spacing but also as a sinusoidal pattern. In this way, the number of necessary design variables can be reduced to a just a few.
2. Using the unstructured turbine x and y coordinates directly as design variables resulting in two design variables for every turbine.

3. Using a transformation of the wind farm *x-y* domain into a single parameter as it is explained in more detail below. This has the advantage that turbines cannot end up outside of the domain, and it is therefore not necessary to define constraints to make sure that turbines stay in the feasible region. Especially the SGA method and other native unconstrained methods will benefit from this type of mapping by avoiding the use of a penalty function, which inevitably reduces the rate of convergence.

In the present implementation, the 2nd mapping is used with the SLP algorithm and the 3rd mapping is used with the SGA algorithm.

Multi-fidelity optimization approach

In order to speed up the convergence of the optimization, we have adopted a multi-fidelity approach. The idea is to carry out the largest part of the optimization using simpler/faster cost functions and coarse resolution, and to refine progressively the results by increasing the resolution of the domain and the complexity of the models. Three levels of increasing complexity and precision are ultimately proposed (see Table 7 below).

Table 7: Schematics of the multi-fidelity optimization approach

Fidelity Level	**1st**	**2nd**	**3rd**
Electricity sales	Stationary wake + Power curve	HAWC2-DWM Database	HAWC2-DWM Simulations
Fatigue costs	No	HAWC2-DWM Database	HAWC2-DWM Simulations
Foundation costs	Yes	Yes	Yes
Electrical Grid costs	Yes	Yes	Yes
Optimization algorithm	SGA	SLP or SGA+SLP	SLP
Domain discretization	Coarse	Fine	Fine
Wind speed and direction bin size	Coarse	Fine	Fine

However, the present implementation focuses on the first two levels of the sketched multi-fidelity optimization approach only. The first level addresses production explicitly, but fatigue loading only implicitly in the sense that loading and production performance is correlated. The second level addresses both fatigue loading and production explicitly. Component fatigue degradation costs and the derived operation and maintenance costs take as inputs the life-time equivalent fatigue loads of different wind turbine components. These fatigue loads are in principle to be calculated on basis of aeroelastic simulation of all wind turbines at all possible wind speeds and wind directions (i.e. level the three approach).

However, the complexity and resource requirements of this task can be significantly reduced under the assumption that only the closest turbine is contributing significantly to the inflow wake effect for a particular wind direction. Under this assumption it is possible to build a database of generic wake load cases with parameters such as the inflow wind speed, the ambient the turbulence intensity, the distance from the upstream wind turbine, and the azimuth angle between the wind turbines and the wind direction. Such a database needs a huge amount of simulations to reasonably cover all possible types of wake load cases. For the present implementation, 7436 simulations of 600 seconds were computed on Risø DTU cluster using the aeroelastic code HAWC2 [133] combined with the DWM model [47].

Two types of position constraints are enforced: 1) domain boundaries; and 2) interspacing between arbitrary two turbines in the farm should exceed one rotor diameter. These constraints are, however, enforced differently for the SGA and the SLP methods.

Domain boundaries

Some external factors to the wind farm optimization can limit the possible locations of the wind farm (e.g. ship routes, bird migration path, protected areas). For this reason it is necessary to be able to restrain the possible positions of the wind turbines to a feasible domain. In the present implementation the boundaries of the domain are defined by a polygon. Depending on how the design variables are defined, the boundaries of the domain are enforced differently. The SLP algorithm uses unstructured design variables for each direction of the possible turbine coordinates. To restrain the locations of the turbines, a norm is calculated of the distance between each turbine and the domain boundaries. If all the wind turbines are within the domain, then the norm becomes the distance from the boundary to the closest wind turbine. If one or more wind turbines are outside of the boundaries, the norm sums the negative distance between the boundary and the outlying wind turbines. A constraint is therefore put on this norm, enforcing the optimization algorithm to ensure that it is positive.

As the SLP algorithm is a gradient based method, it requires differentiable constraints, and it is unable to handle a binary norm (inside/outside). The advantage of the norm presented is that it is fully differentiable, so that the SLP algorithm knows in which direction it needs to change the design variables to increase the norm.

The SGA algorithm is, however, not very efficient with constraints, because they need to be added as a penalty to the objective function. Therefore, a more effective method is to use a more clever design variable mapping that limits the possible layout candidates by defining the design variables as an index on a list of points located inside the boundaries of the domain (see Figure 53).

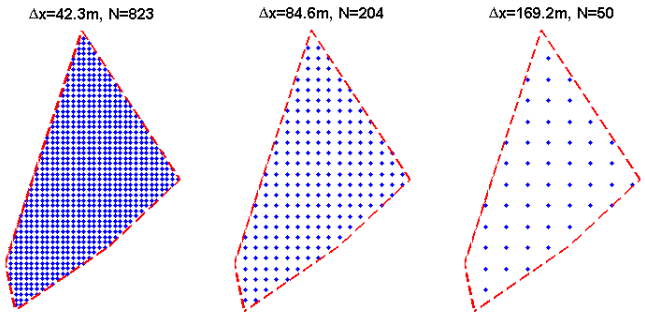

Figure 53: Discretization of the domain with different spacing.

The advantage of this approach is that the wind turbine positions are automatically bounded inside the polygon domain, and consequently there is no need to apply a constraint on the wind turbine position. Furthermore, it is possible to control the spacing between the possible locations, and consequently limiting the number of possible wind farm layout N_F to

$$N_F = \prod_{i=1}^{M} (N_L - i), \tag{27}$$

where M is the number of turbines and N_L the number of possible locations. The spacing of the grid therefore directly links with the speed of convergence of the genetic algorithm. Moreover, this approach gives a number of design variables equal to the number of turbines, which is reducing by a factor two the number of combinations and speeding up further the convergence.

This type of design variable definition would perform poorly with gradient based method, as it would only allow some 1D displacement of the wind turbines in the direction of the indexing. However, a global approach such as a genetic algorithm is not affected by the indexation of the positions.

Minimum Distance between Wind Turbines

There is a practical minimum distance under which two wind turbines are two close to each other to operate under normal conditions. For instance, two turbines next to each other can obviously not operate if they are at a distance lower than one rotor diameter from each other. There is a need to enforce this constraint to avoid unrealistic solutions. The two different optimization approaches should handle this constraint differently, as it is also the case for the domain boundaries.

The approach for the gradient based SLP is to define a norm quantifying the distance between each turbines and their closest neighboring turbine. Similarly to the domain boundary norm, this norm is positive when the minimum distance between turbines is larger than the minimum allowable distance. The minimum distance is selected as one rotor diameter to ensure clearance of the wind turbine rotors. In this case, the norm returns the minimum distance between two turbines in the wind farm layout. In the case where two or more wind turbines are violating this constraint, the norm returns the negative sum of all the distances between pairs of turbines that fail to meet the criteria. The mathematical expression of the norm is given as follows:

$$\text{Norm} = \begin{cases} \min_{i,j}(\overline{WT_i - WT_j}), \text{ when no turbine fail} \\ \sum(\overline{WT_i - WT_j} - MinD), \quad \forall(i,j) \in \text{Failing Turbines} \end{cases} \tag{28}$$

Similarly to the domain boundary norm this norm is differentiable, and it shows in which direction the optimization algorithm needs to move turbines to increase the norm.

Since the SGA is not performing well with constraints, a different approach is taken here. The mapping by itself ensures that turbines cannot be located at a closer distance than one rotor diameter except for the case where the turbines are located exactly on top of each other. In this special case, it is assumed that one of the wind turbines is not operating. This reduces the power production of the wind farm and thereby the component of the financial balance originating from electricity sales. However, all other costs are assumed unchanged. This has the same effect as a penalty function, but with the scaling of the penalty directly affecting amounts used in the financial balance.

4.7 WP7 - Optimization of the Middelgrunden wind farm

The potential of the developed topology optimization platform is demonstrated on the Danish offshore wind farm Middelgrunden, which is located in Øresund close to the coast line of Copenhagen.

The Middelgrunden site

The Middelgrunden wind farm is composed of 20 Bonus B80 2MW wind turbines with a rotor diameter of 76 m and a hub height of 64 m. In the baseline design the wind turbines are arranged in an arc with 2.3D turbine inter-spacing (see Figure 55).

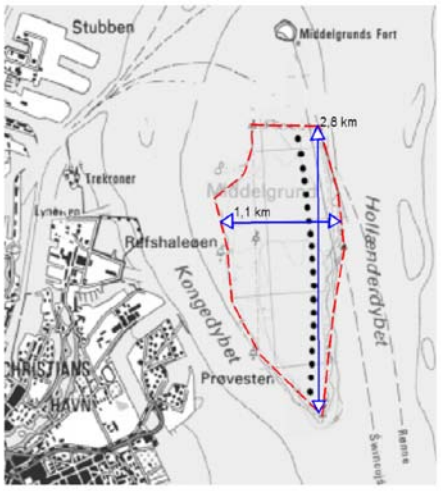

Figure 54: Allowed wind turbine region [25].

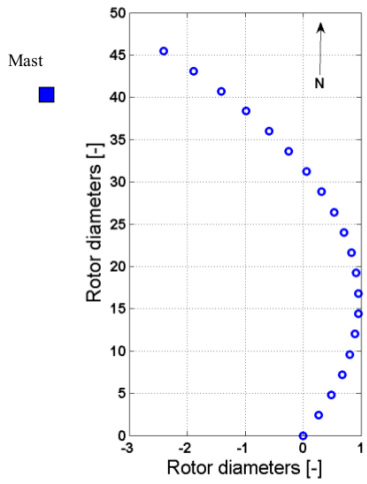

Figure 55: Middelgrunden layout [25].

The wind farm is located on an area elevated relatively compared to the averaged surrounding water depth of this location. The limits of the area, where wind turbines are allowed to be erected, are following closely the limits of the elevated area of the wind turbine site (see Figure 54).

Detailed information about the wind climate of Middelgrunden is available in a TOPFARM report by Hansen [25]. The wind speed distribution for a

number of wind sectors are used together with the turbulence intensity distribution to form the necessary inputs required for setting up the computation. Figure 56 shows the wind speed distribution and Figure 57 shows the turbulence intensity distribution.

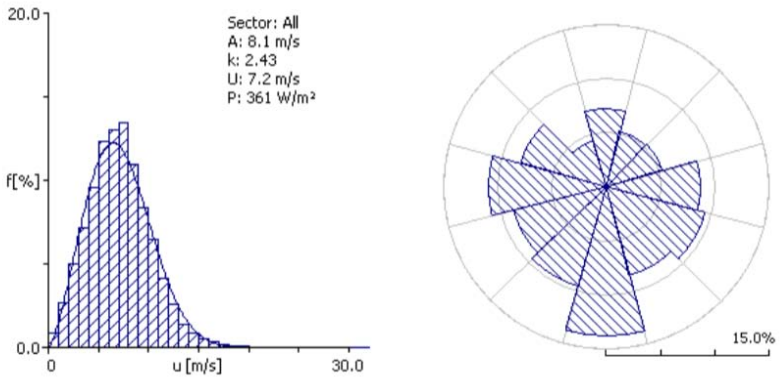

Figure 56: Middelgrunden wind speed distribution [25].

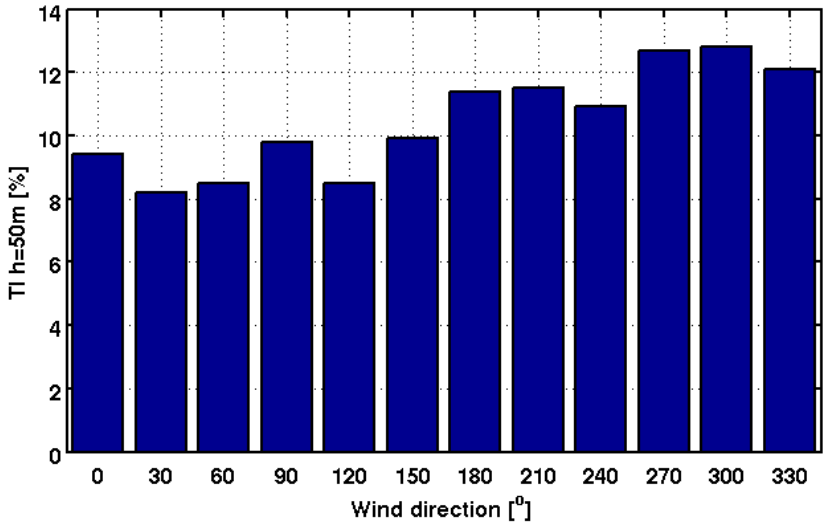

Figure 57: Middelgrunden turbulence intensity distribution [25].

The base line design

Based on the wind farm layout in Figure 55 and the wind climate specified in Figure 56 and Figure 57, the power production and turbine loads could be calculated for each of the turbines. Figure 58 shows the corresponding contour plots that were generated on basis of the values for the individual turbines. Due to the location of the turbines on an arch, it is difficult to obtain contour lines and therefore difficult to really see the difference between the turbines. However, it is clear that it is the turbines to the very south that show the highest power production. The total energy efficiency is calculated to 83.9%, where this is would be 100% for a stand-alone reference turbine. It is obvious that the dense spacing between the turbines has a consequence on the energy efficiency. For the tower base moments, it is also the turbines to the south that display the lowest loading.

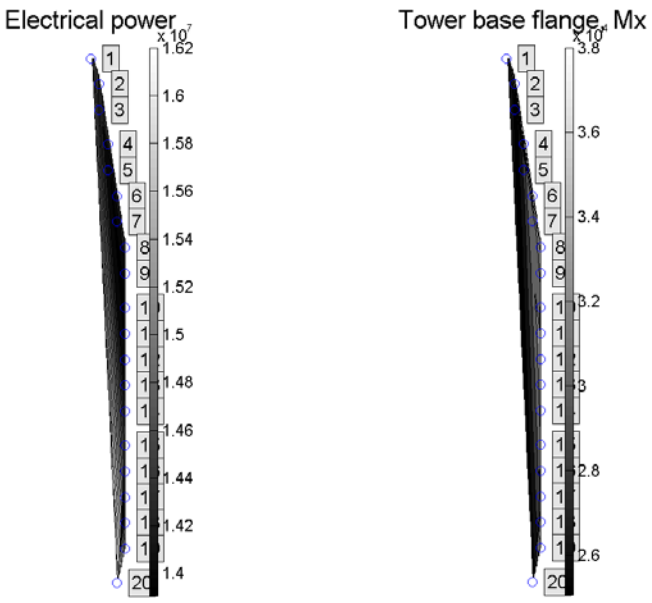

Figure 58: Energy production contour plots (left) and tower base over-turning bending moment (right) for the Middelgrunden baseline topology.

Figure 59 shows the financial balance components for each of the turbines and in addition the average for all turbines. The values shown for each component are normalized to the value of the energy production for a stand-alone turbine. Furthermore, the energy production is expressed as a power loss by using the energy efficiency rather than the energy production. In this way, all the different components express a loss in the financial balance, and the total sum of all losses needs to be counterbalanced by the value of the energy production from a similar number of solitary turbines.

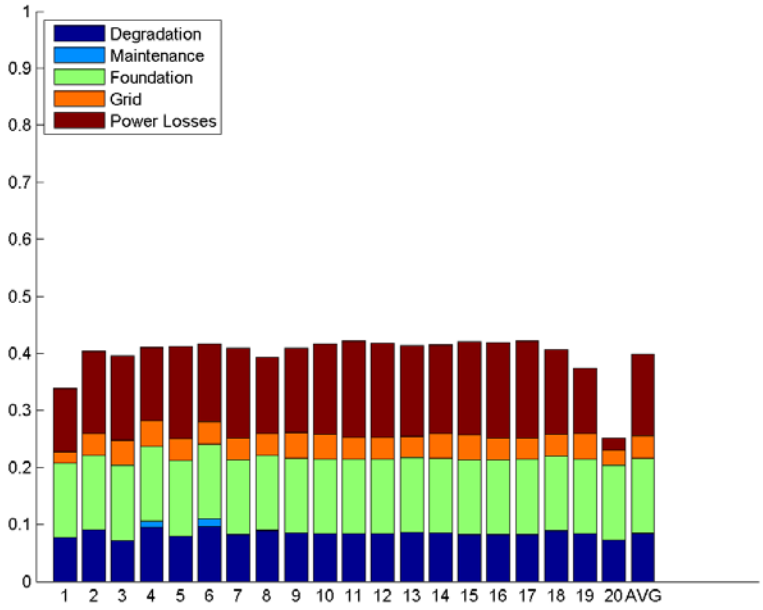

Figure 59: Financial balance components for each turbine for the Middelgrunden baseline topology.

Optimization result

The first level of optimization was obtained using SGA in 1000 iterations, and subsequently the second level used SLP for 20 iterations. Further iterations could not improve the financial balance. Compared to the baseline topology, the initial SGA optimization resulted in an improvement of the financial balance of 0.6 M€, and the SLP warm start resulted in a total improvement of the financial balance equal to 2.1 M€.

Figure 60 shows the convergence of the objective function (i.e. the negative financial balance) for the two levels of multi-fidelity optimization considered. The SGA clearly shows convergence. Due to the nature and principle of this algorithm, it converges in steps. Convergence is very stable but slow, and after approximately 525 iterations there appears to be only insignificant improvement of the objective function. Despite the many iterations performed, it cannot be excluded that further reductions of the objective function could have been possible.

The SLP algorithm was used for 20 iterations, after which no further improvement of the solution is possible. Convergence for the SLP run is not smooth, in that severe kinks are seen for the value of the objective function between iterations. The move-limits are intensively adjusted during the optimization, and despite the kinks a trend towards reducing the objective function is seen.

The 20 turbines result in 40 design variables and combined with constraints on turbine spacing and domain boundaries, the optimization problem is very complex. This explains the kinky appearance of the convergence, where the non-linearity of the optimization problem makes the size of the move-limits a challenge for the SLP algorithm.

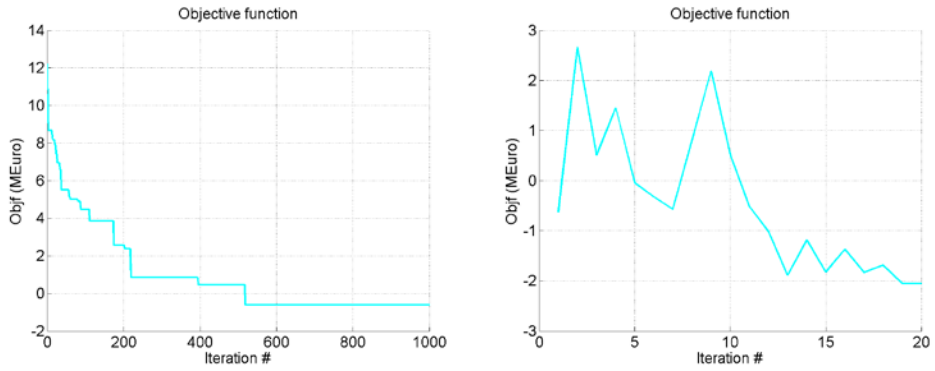

Figure 60: Optimization convergence from SGA (left) and SLP warm start on basis of SGA result (right).

The large difference between the financial balance after applying the SGA algorithm on the one hand and the financial balance after the adding the SLP refinement on the other hand can be explained by the penalty function applied on the minimum distance between turbines in the SGA algorithm, which reduces the power production of the wind farm. Because of the local nature of the SLP algorithm it is able to comply more efficiently with the constraint on the minimum distance, by simply displacing the turbines to close to each others.

Figure 61 shows the resulting wind farm topology layout together with the changes in the financial balance caused by the optimization. The optimized solution is fundamentally different from the baseline layout, in that the turbines are no longer arranged on line with a limited spacing between turbines. The resulting layout makes use of the counterpart of the feasible domain, and the turbines are not placed in a regular pattern. A closer look on the financial balance changes in Figure 61 shows that the foundation costs have not been increased, because the turbines have been placed at shallow water. The major changes involve energy production and electrical grid costs, respectively.

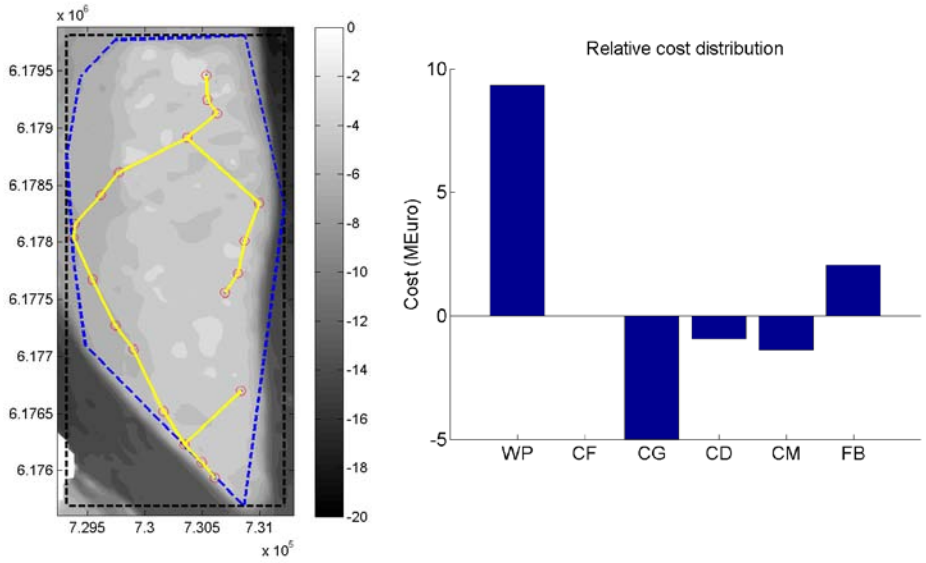

Figure 61: Optimum wind farm layout (left) and financial balance cost distribution relative to baseline design (right).

Figure 62 shows the details of the financial balance components for each of the turbines and Figure 63 shows how energy production and lifetime equivalent tower base over-turning moment changes mutually between the turbines in the wind farm.

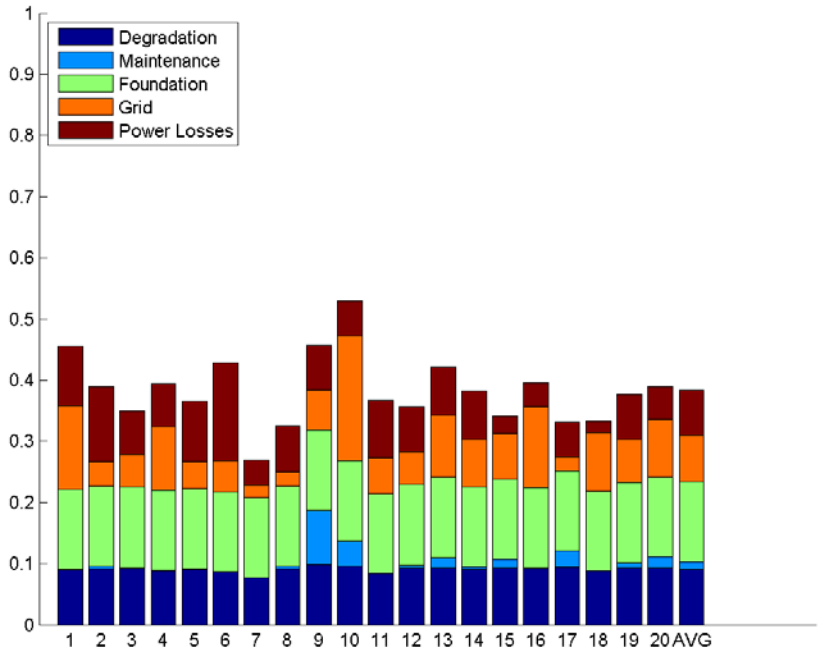

Figure 62: Financial balance components for each turbine.

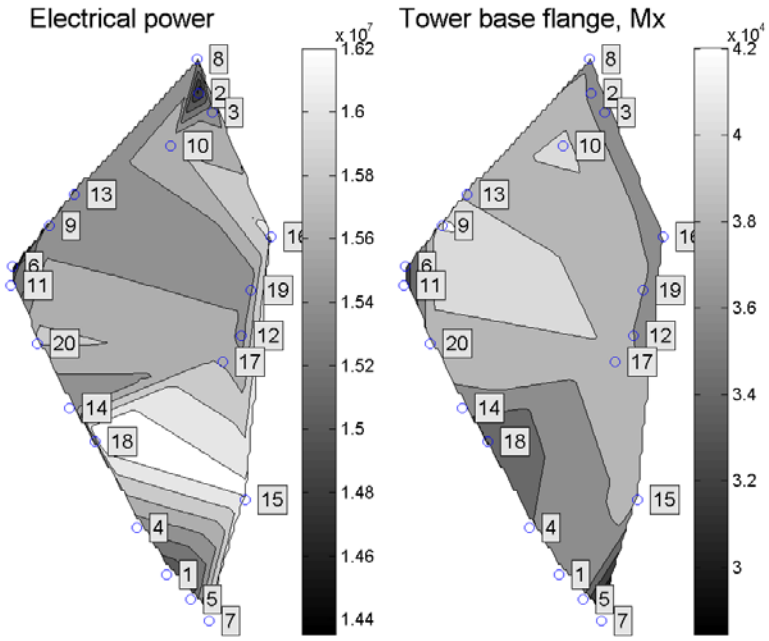

Figure 63: Contour plots of energy production (left) and tower base over turning bending moment (right).

It appears from Figure 62 that a few turbines, e.g., 9 and 10, have high O&M costs in contrast to the initial baseline layout, whereas most turbines have high annual energy efficiency. Turbine 10 has a relatively high energy production and a relatively high tower based flange moment, probably due to

the wake meandering of turbine 13 and 9. This shows that the fatigue loads can have an important influence on the financial balance, which would not be captured by an optimization purely based on the power production.

The dark areas to the left in Figure 63 show turbines having comparatively lower energy production efficiency, and the light areas to the right in Figure 63 show turbines with comparatively higher tower base loads. The fact that there seems to be some of the turbines that have comparatively high degradation and O&M costs is supported by the contour plot showing a few "problem areas" in the wind farm. Also a few "problem areas" appear for the energy production. The optimization result therefore leaves an open a question mark on whether the *global* optimum was found. It is likely that adjustments in some of the areas in the wind farm can lead to further improvements of the financial balance, but it is not likely that a significant change in the value of the improvement is obtainable.

4.8 WP8 - Optimization of the Coldham and Stags Holt wind farms

In addition to the Middelgrunden offshore wind farm, the potential of the developed topology optimization platform is demonstrated on the U.K. onshore wind farm Coldham/Stags Holt wind farm located in between March and Wisbech in Cambridgeshire.

The Coldham/Stags Holt site

The Coldham/Stags Holt wind farm is in reality two wind farms "merged" and consists of a total of 17 Vestas V80 wind turbines with a rotor diameter of 80 m rotor diameter and a hub height of 60 m. The baseline layout and the boundary enclosing the area restriction of the optimization are shown in Figure 64.

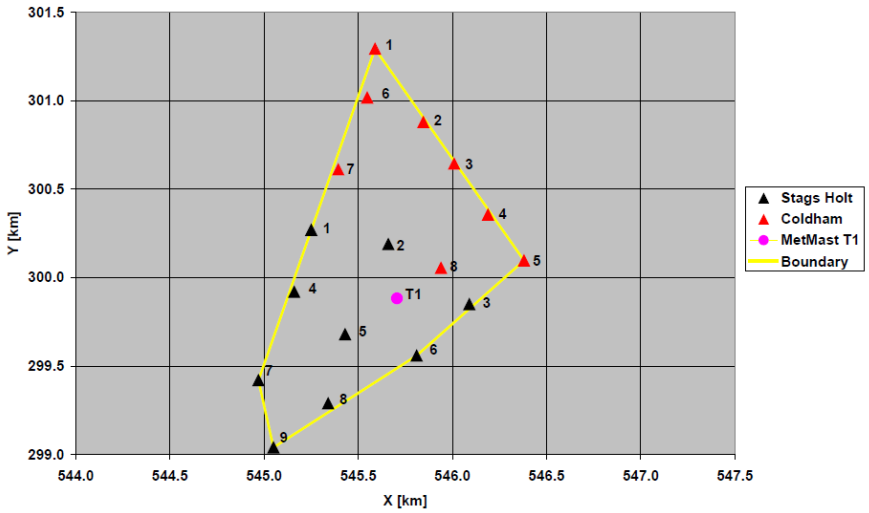

Figure 64: Coldham/Stags Holt layout and allowed area for wind turbine erection [117].

The wind farm is located on land at flat terrain. Foundation costs are therefore not relevant to the optimization, because they can be considered as topology independent, and consequently they can be legitimately omitted from the cost function.

Detailed information about the wind climate of Coldham/Stags Holt, including the full description of the wind climate, can be found in a TOPFARM technical report [117]. The wind rose and turbulence intensity distribution are illustrated in Figure 65.

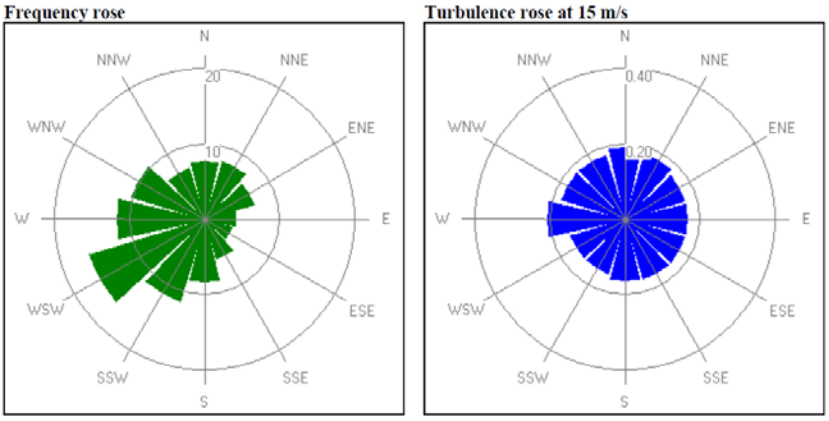

Figure 65: Coldham/Stags Holt wind rose and turbulence rose [117].

Figure 66 shows contour lines of power production and tower base overturning moments generated on basis of the values for the individual turbines. The wind rose in Figure 65 defines South-West as the dominating wind direction, which seems to be the direction with the smallest projected areas of the wind farm due to the defined boundary. It can be seen that energy production is highest towards the South-West corner and reduces toward North-East with the turbines 13 and 17 having the lowest power production. The tower base moment follows this trend but with highest loads for the turbines 2, 5, 11 and 12 forming the central area of the wind farm. The total energy efficiency is calculated to 89.4% relative to 100% which is a stand-alone reference turbine at the same wind climate. The relatively dense spacing between the turbines is causing the energy efficiency to drop compared to the ideal value.

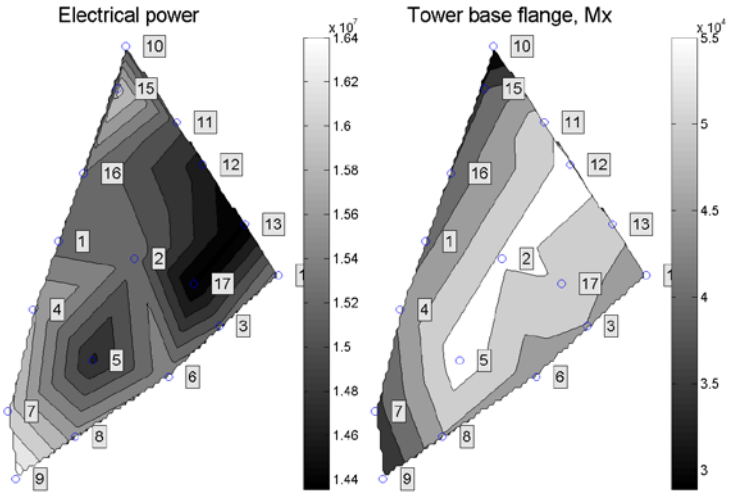

Figure 66: Contour plots of energy production (left) and Tower base over turning bending moment (right) for the Coldham/Stags Holt baseline layout.

Figure 67 shows the financial balance components for each of the turbines and also the average for all turbines normalized to the value of the energy production for a stand-alone turbine. The energy production is expressed as a power loss by using the energy efficiency rather than the energy production. In this way, all the different components express a loss in the financial balance, and the total sum of all losses needs to be counterbalanced by the value of the energy production. It can be seen that there is a large variation in the power loss coefficient, as some turbines have a very little loss, whereas others have significant losses. The turbines 5, 12, 13 and 17 are having the highest losses, which is caused by operation in wake conditions for predominantly more time than for example turbine 9. It can be seen that the electrical grid costs are in general small, and it is also noteworthy that many turbines have a non-zero maintenance coefficient, indicating that turbine spacing is limited.

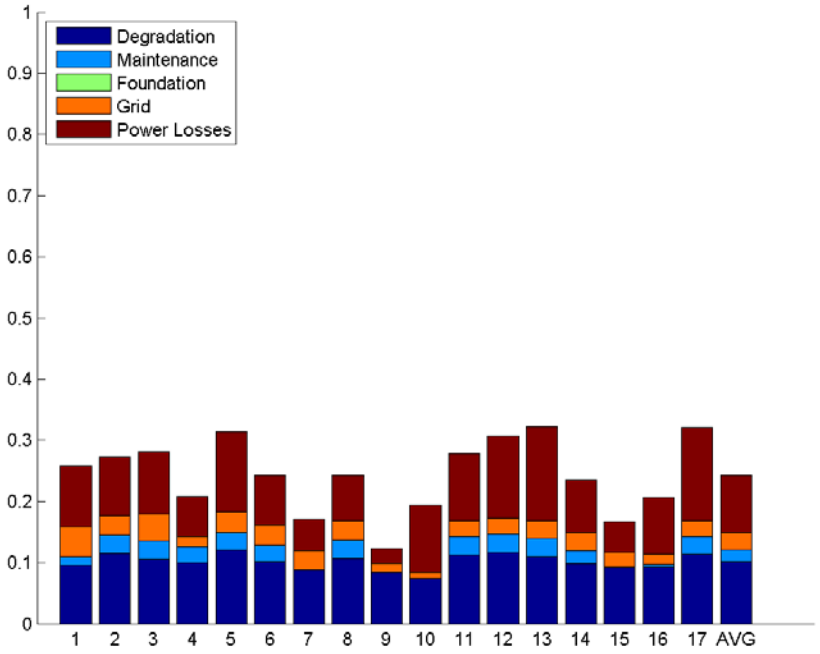

Figure 67: Financial balance components for each turbine for the Coldham/Stags Holt baseline layout.

Optimization results

The first level of optimization used SGA for 1000 iterations followed by the second level applying SLP for additionally 30 iterations. Further iterations could not improve the financial balance. The initial SGA based optimization resulted in an improvement of the financial balance of 1.5 M€, and the SLP warm start finally resulted in a total improvement of the financial balance of 3.1 M€ compared with the baseline layout.

Figure 68 shows the convergence of the objective function (i.e. the negative financial balance) for the two levels multi-fidelity optimization considered. The SGA clearly shows convergence. Due to the nature and principle of this algorithm, it converges in steps. Convergence is very stable but slow, and

after approximately 750 iterations there appears to be only insignificant improvement of the objective function. Despite the many iterations performed, it cannot be excluded that further reductions of the objective function could have been possible.

The SLP algorithm was applied in additionally 30 iterations, after which no further improvement of the solution was possible. Convergence of the SLP run is not smooth in that quite some kinks are seen for the value of the objective function between iterations. The move-limits are intensively adjusted during the optimization, and despite the kinks a trend towards reducing the objective function is seen.

The 17 turbines result in 34 design variables, and despite that this is less than for the Middelgrunden case, it remains a challenge for the SLP algorithm to arrive at convergence. Move-limits are adjusted and both the boundary and the turbine spacing constraints are difficult to handle in the many dimensions spanning the feasible region of the optimization.

The difference in financial balance between the two optimization levels is caused by the SLP being able to improve energy production significantly by fine-tuning each turbine position and at the same time reducing grid costs.

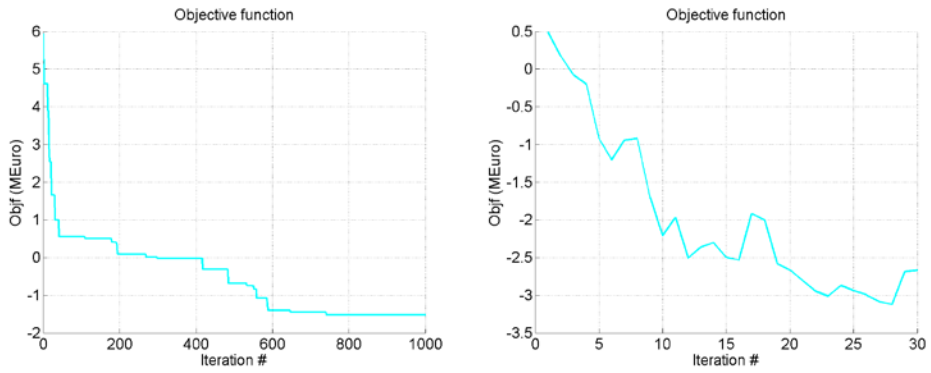

Figure 68: Optimization convergence from SGA (left) and warm start on basis of SGA result (right).

Figure 69 shows the resulting wind farm layout together with the changes to the financial balance caused by the topology optimization. The solution is not fundamentally different from the baseline layout. The turbines are not as regularly laid out but rather on different connecting strings, which seems to utilize the electrical grid costs better and even allow for improving energy production. The financial balance in Figure 69 shows that the total improvement of the financial balance is contributed to by all components including turbine degradation and O&M.

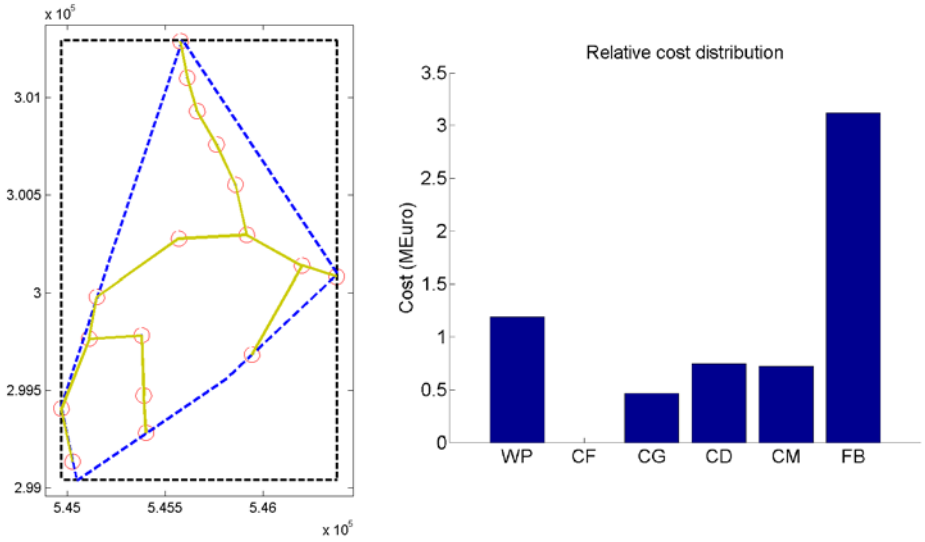

Figure 69: Optimum wind farm layout (left) and financial balance cost distribution relative to baseline design (right).

Figure 70 shows the details of the financial balance components for each of the turbines and Figure 71 shows how energy production and lifetime equivalent tower base over-turning moment changes between mutually the turbines in the wind farm.

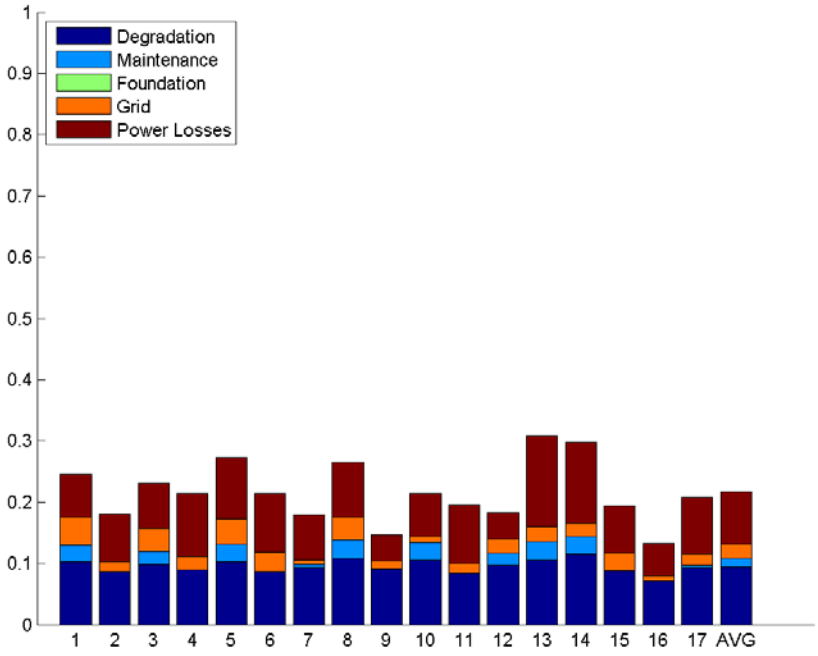

Figure 70: Financial balance components for each turbine.

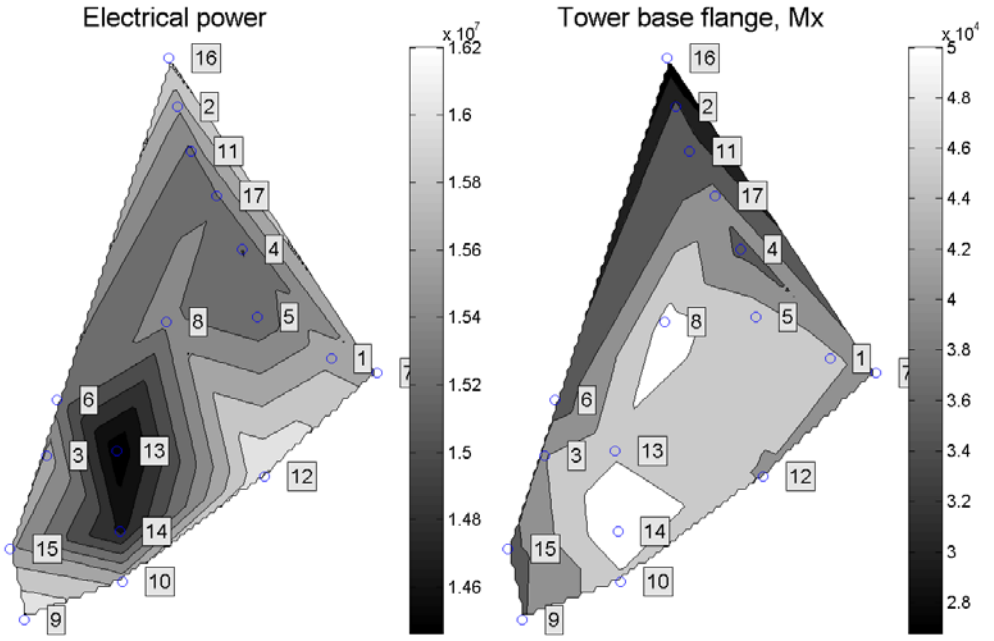

Figure 71: Contour plots of energy production (left) and tower base over turning bending moment (right).

It is seen from Figure 71 that some of the turbines have significantly worse financial balance than efficient ones in the resulting wind farm layout. It is in general the turbines on the edge of the wind farm that show the most efficient financial balance.

5 PROJECT EVALUATON

The TOPFARM project has successfully addressed the goals put forward in the original formulation of the project, and the results achieved are expected to have significant impact on the end-user segment (wind farm developers, utility companies, wind turbine manufactures, certification bodies, ...), as well as on the wind energy research sector in general.

For the first time it has been demonstrated that it is possible to conduct a thorough topology optimization of wind farms on a rational basis, in the sense the *optimal economical performance* of the wind farm over its life time is achieved. This has been done by formulating the objective function for the optimization in economical terms, essentially expressing the balance between – on the one hand – capital costs, operation and maintenance costs, costs related to component fatigue lifetime consumption and – on the other hand – the income from power production output.

The required input for this objective function is obtained from detailed aeroelastic computations of the individual wind farm wind turbines. Crucial factors in this respect are the overall (ambient) wind climate at the wind farm site, the position of the individual wind turbines, the wind turbine characteristics, the resulting internal wake affected wind farm wind climate, and the wind turbine control/operation strategy for wind turbines interacting through wakes.

The design space for the optimization is large and complex, and to enable the optimization without posing outrageous requirements on computer resources, a major challenge for the project has been to develop *fast approximate* models and yet preserve the essential physics of the problem. This challenge has been met on all levels ranging from the wind farm wind field simulation to the aero-elastic simulation and the optimization approach.

The developed innovative sub-models push present technological boundaries, and the TOPFARM results have the potential to assure a significant jump forward in future wind farm layout as well as in wind farm turbine design and reliability – and, in addition, the potential for contributing to future design regulations for wind farm design.

6 PROJECT DISSEMINATION AND REFERENCES

During the course of the TOPFARM project exploitation and dissemination of results has taken place regularly both *internally* among the project partners and *externally*. As for the *external* dissemination of results, reports, publications in scientific journals and presentations at international conferences/workshops have been the predominant approach – and a large number of presentations, reports and journal papers have resulted.

A prominent additional effort was the organization of the Euromech Colloquium 508 on Wind Turbine Wakes. The colloquium was scheduled on October 20-22, 2009, at E.T.S.I. Industriales of the Universidad Politécnica de Madrid. UPM was the main organizer, assisted by the RISOE-DTU that acted as co-organizer. 50 papers were submitted for presentation at the colloquium, and each of these is briefly described in [19].

The colloquium attracted 69 participants. Most of these were representatives of European Companies involved in Wind Energy that were interested in wakes, and wanted to learn from this meeting the latest developments within this topic. Later comments indicated that their expectations had been fulfilled.

The colloquium dealt with wake models, turbulence closure models, turbine aerodynamics and near wake, influence of topography and atmospheric characteristics on wakes, modification of the atmospheric boundary layer by arrays of wind farms, experimental work, interpretation of measurements, wake meandering, offshore wind farms, large wind farms, strategies for control, fatigue, loads and optimization. The colloquium was thus organized in ten sessions, each with approximately five papers.

Summarizing the internal and external dissemination of results, the following publications, presentations, and activities relates fully, or in part, to the TOPFARM project:

[1] Aubrun, S., Tchouaké, T.F., Espana, G., Larsen, G.C., Mann, J. and Bingöl, F. (2010). Comparison between wind tunnel and field experiments on wind turbine wake meandering. Presented at: iTi Conference on Turbulence IV. Bertinoro (IT).

[2] Bechmann, A. and Sørensen, N.N. (2008). CFD simulation of the MEXICO rotor wake. EWEC conference, March 2009. Paper is available from the TOPFARM team-site.

[3] Bechmann, A., Sørensen, N.N. and Zahle, F. (2010). CFD simulations of the MEXICO rotor. Wind Energy, Published online in Wiley Online Library (wileyonlinelibrary.com). DOI: 10.1002/we.450.

[4] Bingöl, F.; Trujillo, J.J.; Mann, J. and Larsen, G.C. (2008). Fast wake measurements with LiDAR at Risø test field. 14. International symposium for the advancement of boundary layer remote sensing, Risø (DK), 23-25 June. IOP Conf. Ser.: Earth Environ. Sci. (2008) 1, 012022 (9 p.).

[5] Bingöl, F., Mann, J. and Larsen, G.C. (2010). Lidar Measurements of Wake Dynamics, Part 1: One Dimensional Scanning. Wind Energy **13**, 51-61.

[6] Buhl, T., Larsen, T.J. and Carlén, I. (2009). A method to formulate a feasible optimization problem taking into account not only energy production but also aeroelastic loads, control strategies and installation costs. Risø-R-1705(EN).

[7] Buhl, T., Carlén, I. and Larsen, G.C. (2009). Wind farm optimization with structured and un-structured grids. Euromech Colloquium 508 on Wind Turbine Wakes, Madrid, 20-22 October, 2009. Extended abstract published in ISBN 978-84-7484-220-3, pp. 95.

[8] Buhl, T. and Larsen, G.C. (2010). Wind farm topology optimization including costs associated with structural loading. The Science of making Torque from Wind June 28-30, 2010, FORTH, Heraklion, Crete, Greece.

[9] Cabezón, D., Sanz, J., Martí, I., Crespo, A. and Migoya, E. (2009). Comparison of turbulence models for the CFD simulation of wind turbine wakes in the Atmospheric Boundary Layer. Euromech Colloquium 508 on Wind Turbine Wakes, Madrid, 20-22 October, 2009. Extended abstract published in ISBN 978-84-7484-220-3, pp. 14-15.

[10] Cabezon, D., Migoya, E. and Crespo, A. (2010). Comparison of turbulence models for the CFD simulation of wind turbine wakes in the atmospheric boundary layer. Submitted for publication in Wind Energy.

[11] Carlén, I. (2008). TOPFARM - Next generation design tool for optimization of wind farm topology and operation (Optimal styrning och layout för stora vindfarmer). Elforskdagen 2008, http://www.elforsk.se/nyhet/seminarie/elforskdagen_08/elfdag_08.html.

[12] Carlén. I. (2009). Presentation of current (TOPFARM) and future activities (proposed) addressing dynamic wind farm modelling, at the Swedish Vindforsk III's planning Workshop, March 5, Göteborg, Sweden.

[13] Carlén, I. (2009). TOPFARM - A study on Wind Sector Management. Euromech Colloquium 508 on Wind Turbine Wakes, Madrid, 20-22 October, 2009. Extended abstract published in ISBN 978-84-7484-220-3, pp. 94.

[14] Carlén I. and Ivanell S. (2009). Optimization and Control of Wind Farms. Presentation given at the conference "Forskning om vindkraft i fokus", Stockholm 25th November (in Swedish).

[15] Carlén, I. (2010). Some simple concepts for dynamic Wind Sector Management of wind farms, Teknikgruppen report TG-R-1006, Teknikgruppen AB.

[16] Carlén I. (2010). Concepts for Wind Sector Management control of wind farms. Report TG-R-10-02, Teknikgruppen AB.

[17] Carlén, I. (2009). Simulering och optimering av vindparker" (in Swedish). Elforsk rapport 09:23.

http://www.vindenergi.org/Vindforskrapporter/09_23_rapport.pdf.

[18] Carlén I. (2011). Control Strategies - Reports of task results, Deliverable D8. Teknikgruppen AB.

[19] Crespo, A., Larsen, G.C. and Migoya, E. (2009) (Editors). Extended Abstracts for Euromech Colloquium 508 on Wind Turbine Wakes, Sección de Publicaciones de la Escuela Técnica Superior de Ingenieros Industriales de Madrid, Madrid, Libro. ISBN 978-84-7484-220-3.

[20] Crespo, A., Migoya, E., Prieto, J.L., Jiménez, A. and García, J. (2010). Study of isolated wakes and their superposition in wind farms, using different turbulence models. V European Conference on Computational Fluid Dynamics, ECCOMAS CFD 2010, Mini-symposium on Computational Wind-Farm-Wake-Aerodynamics, Lisbon, Portugal, 14–17 June. Book of abstracts ISBN: 978-989-96778-0-7.

[21] Crespo, A., Migoya, E., Jiménez, A., García, J., García, A., Prieto, J.L. and Muñoz, J. (2010). UPM contribution to WP1 of TOPFARM project. Universidad Politécnica de Madrid.

[22] Dellwik. E. (2009). Presentation of various Danish wind energy activities (among these OPFARM activities) at the Swedish Vindforsk III's planning Workshop, March 5, Göteborg, Sweden.

[23] Hansen, K.S., Larsen, G.C., Mann, J. and Enevoldsen, K. (2009). LiDAR measurements of full-scale wind turbine wake characteristics. EWEC2009, Marseille, France.

[24] Hansen, K.S. (2009). Wake measurements for code validations, Deliverable D11: EU – TOPFARM, MEK-FM 2009-01, Department of Mechanical Engineering, Technical University of Denmark.

[25] Hansen, K. (2010). Definition of local wind climate for Middelgrunden, DK. Deliverable D17: EU – TOPFARM. Technical report.

[26] Hansen, K.S., Larsen, G.C., Mann, J. and Enevoldsen, K. (2009). LiDAR measurements of full-scale wind turbine wake characteristics. EWEC 2009, European Wind Energy Conference, 16-19 March, Marseille. Unpublished.

[27] Hansen, K.S., Larsen, G.C., Mann, J. and Enevoldsen, K. (2009). LiDAR measurements of full-scale wind turbine wake characteristics. Euromech Colloquium 508 on Wind Turbine Wakes, Madrid, 20-22 October. Extended abstract published in ISBN 978-84-7484-220-3, pp. 55-56.

[28] Hansen, K.S., Larsen, G.C., Bingöl, F., Mann, J. and Trujillo, J.J. (2008). LIDAR measurements of wind turbine wake meandering. Wake workshop, Oldenburg (DE), 30 June - 2 July. Unpublished.

[29] Hansen, K.S. and Larsen, G.C. (2008). Full scale wake measurements. VindKraftNet seminar on wakes, Copenhagen (DK), 16 September. Unpublished.

[30] Hansen, K.S. (2009). Wake measurements for code validations; Deliverable D11: EU TOPFARM. MEK-FM 2009-01, June 2009, DTU, 36p.

[31] Hansen, K.S., Larsen, G.C., Mann, J. and Enevoldsen, K. (2009). LiDAR measurements of full-scale wind turbine wake characteristics. Euromech Colloquium 508 on Wind Turbine Wakes, Madrid, 20-22 October. Extended abstract published in ISBN 978-84-7484-220-3, pp. 55-56.

[32] Hansen, K.S. (2010). Local wind climate at Middelgrunden, Deliverable D17: EU – TOPFARM. Department of Mechanical Engineering, Technical University of Denmark.

[33] Heath, M.A., Hendriks, H.B. and Veldkamp, H.F. (2009). Cost modeling for wind farm design optimization. Garrad Hassan report 12803/BR/06, Garrad Hassan and Partners Limited.

[34] Hunt, J. (2009). Mesoscale and turbulence effects on wind farms. Euromech Colloquium 508 on Wind Turbine Wakes, Madrid, 20-22 October, 2009. Extended abstract published in ISBN 978-84-7484-220-3, pp. 42.

[35] Ighil, T.A. (2009). Analysis of Taylor's "frozen turbulence" hypothesis and the possible feed-back of wind turbines on large scale lateral turbulence. Internal report Risø-DTU report.

[36] Ivanell, S., Mikkelsen, R.F., Sørensen, J.N. and Henningson, D. (2008). Stability analysis of the tip vortices of a wind turbine**.** Presented at Aerospace Sciences Meeting and Exhibition, 7 - 10 January 2008, Reno, Nevada.

[37] Ivanell, S., Sørensen, J.N., Mikkelsen, R. and Henningson, D. (2009). Analysis of Numerically Generated Wake Structures, Wind Energy, Vol. 12(1), p. 63-80.

[38] Ivanell, S., Mikkelsen, R., Sørensen, J.N. and Henningson, D. (2009). ACD modelling of wake interaction in Horns Rev wind farm. Euromech Colloquium 508 on Wind Turbine Wakes, Madrid, 20-22 October, 2009. Extended abstract published in ISBN 978-84-7484-220-3, pp. 83.

[39] Ivanell, S., Mikkelsen, R., Sørensen, J.N. and Henningson, D. (2010). Stability analysis of the tip vortices of a wind turbine. Submitted for publication in Wind Energy.

[40] Ivanell, S., Mikkelsen, R., Sørensen, J.N., Hansen, K.S. and Henningson, D. (2010). The impact of wind direction in atmospheric BL on interacting wakes at Horns Rev wind farm. Presented at TORQUE2010 The science of making torque from wind. Heraklion, Crete, Greece.

[41] Johansen, N.A. (2009). Verification of simulated fatigue loads on wind turbines operating in wakes, Master Thesis Report MEK-FM-EP 2009-10 (to be published).

[42] **J**iménez, A. et al. (2008). Application of a simplified LES model to characterize the wake deflection of a wind turbine in yaw. Wake workshop, Oldenburg (DE), 30 June - 2 July. Unpublished.

[43] Jiménez, A., Migoya, E., García, J., Crespo, A. and Prieto, J.L. (2009). Analysis of the wake meandering using a LES method. Euromech Colloquium 508 on Wind Turbine Wakes, Madrid, 20-22 October, 2009. Extended abstract published in ISBN 978-84-7484-220-3, pp. 20-21.

[44] Jiménez, A., Crespo, A. and Migoya, E. (2009). Application of a LES technique to characterize the wake deflection of a wind turbine in yaw. Wind Energy, accepted for publication 20-10-2009.

[45] Jiménez, A., Migoya, E., Esteban, M., García, J., Giménez, D. and Crespo A. (2009). Influence of topography and wakes on wind turbulence. Measurements and interpretation of results. Euromech Colloquium 508 on Wind Turbine Wakes, Madrid, 20-22 October, 2009. Extended abstract published in ISBN 978-84-7484-220-3, pp. 61.

[46] Jiménez, A., Migoya, E., Esteban, M., García, J., Giménez, D. and Crespo, A. (2010). Influence of topography and wakes on wind turbulence. Measurements and interpretation of results. Submitted for publication in Wind Energy.

[47] Larsen, G.C., Madsen, H.Aa., Thomsen, K. and Larsen, T.J. (2008). Wake Meandering - A Pragmatic Approach. Wind Energy, **11**, pp. 377–395.

[48] Larsen, G.C., Madsen, H.Aa., Bingöl, F., Mann, J., Ott, S., Sørensen, J., Okulov, V., Troldborg, N., Nielsen, M., Thomsen, K., Larsen, T., and Mikkelsen, R. (2007). Dynamic wake modeling, Risø-R-1607(EN), Risoe National Laboratory, Technical University of Denmark.

[49] Larsen, G.C., Aagaard Madsen, H., Larsen, T.J. and Troldborg, N. (2008). Wake modeling and simulation. Risø-R-1653(EN), 28 p.

[50] Larsen, G.C., Aagaard Madsen, H., Larsen, T.J., Mann, J., Bingöl, F. and Trujillo, J.J. (2008). The dynamic wake meandering (DWM) model and its future perspectives. VindKraftNet seminar on wakes, København (DK), 16 September. Unpublished.

[51] Larsen, G.C. (2009). Ainsley's eddy viscosity formulation revised. Paper in preparation.

[52] Larsen, G.C., Madsen, H.Aa., Larsen, T.J., Mann, J. and Bingöl, F. (2009). TOPFARM – background, vision … and challenges. Workshop on Offshore Wind Farms. IEA, Task 23 – Offshore wind energy technology and deployment. February 25-26, Risø DTU, Risø Campus, Roskilde, Denmark. Unpublished.

[53] Larsen, G.C., Mann, J., Ighil, T.A. and Mouritzen, A.S. (2009). Do wind farms influence large scale turbulence? Euromech Colloquium 508 on Wind Turbine Wakes, Madrid, 20-22 October. Extended abstract published in ISBN 978-84-7484-220-3, pp. 38-40.

[54] Larsen, G.C., Larsen, T.J., Madsen, H. Aa., Mann, J., Peña, A., Hansen, K.S. and Jensen, L. (2009). The dependence of wake losses on atmospheric stability characteristics. Euromech Colloquium 508 on

Wind Turbine Wakes, Madrid, 20-22 October. Extended abstract published in ISBN 978-84-7484-220-3, pp. 35-37.

[55] Larsen, G.C., Larsen, T.J., Madsen, H. Aa., Mann, J., Peña, A., Hansen, K.S. and Jensen, L. (2010). The dependence of wake losses on atmospheric stability characteristics. To be submitted for publication in Wind Energy.

[56] Larsen, G.C., Madsen, H.Aa. and Troldborg, N. (2009). A tailored eddy viscosity closure consistent with the Dynamic Wake Meandering philosophy. Euromech Colloquium 508 on Wind Turbine Wakes, Madrid, 20-22 October, 2009. Extended abstract published in ISBN 978-84-7484-220-3, pp. 73-74.

[57] Larsen, G.C. (2009). A simple stationary semi-analytical wake model, Risø-R-1713 (EN).

[58] Larsen, G.C. (2009). A simple generic wind farm cost model tailored for wind farm optimization. Risø-R-1710(EN).

[59] Larsen, G.C. (2010). TOPFARM – background, vision … and challenges. Aeolus-seminar, 08-02-2010, Kastrup, Copenhagen.

[60] Larsen, G.C., Hansen, K.S., Mann, J., Enevoldsen, K. and Bingöl, F. (2010). Full-scale measurements of wind turbine wake turbulence. Proceedings of Torque 2010 - The science of making torque from wind, pp. 391-405, Heraklion, Greece.

[61] Larsen, G.C. (2010). TOPFARM – next generation design tool for optimization of wind farm topology and operation ... background, vision and challenges. The Science of making Torque from Wind June 28-30, 2010, FORTH, Heraklion, Crete, Greece.

[62] Larsen, G.C., Hansen, K.S., Troldborg, N., Mann, J., Enevoldsen, K. and Bingöl, F. (2010). A first attempt to characterize the structure of wake turbulence using a combined experimental and numerical approach. Presented at: iTi Conference on Turbulence IV. Bertinoro (IT).

[63] Larsen, G.C. (2010). From solitary wakes to wind farm wind fields – a simple engineering approach. Risø-R-1727(EN).

[64] Larsen, G.C., Madsen, H.Aa, Larsen, T.J., Troldborg, T., Buhl, T. and Réthoré, P.-E. (2011). TOPFARM – philosophy, results and outlook. EWEA 2011.

[65] Larsen, G.C. et al. (2008). TOPFARM First Periodic Report, June 2008. Risø DTU – National Laboratory for Sustainable Energy.

[66] Larsen, G.C. et al. (2008). TOPFARM Second Periodic Report, December 2008. Risø DTU – National Laboratory for Sustainable Energy.

[67] Larsen, G.C. et al. (2009). TOPFARM Third Periodic Report, June 2009. Risø DTU – National Laboratory for Sustainable Energy.

[68] Larsen, G.C. et al. (2009). TOPFARM Forth Periodic Report, December 2009. Risø DTU – National Laboratory for Sustainable Energy.

[69] Larsen, G.C. et al. (2010). TOPFARM Fifth Periodic Report, June 2010. Risø DTU – National Laboratory for Sustainable Energy.

[70] Larsen, G.C. et al. (2010). TOPFARM Sixth Periodic Report, December 2010. Risø DTU – National Laboratory for Sustainable Energy.

[71] Larsen, G.C. et al. (2011). TOPFARM Publishable Final Activity Report, January 2011. Risø DTU – National Laboratory for Sustainable Energy.

[72] Larsen, T.J., Aagaard Madsen, H. and Larsen, G.C. (2008). Simulation of loads on wind turbines operating in wakes. Vinddag 2008, Dansk Forskningskonsortium for Vindenergi, Risø (DK), 25 November. Unpublished.

[73] Larsen, T.J., Aagaard Madsen, H. and Larsen, G.C. (2008). Comparison of design methods for turbines in wake. In: Bak, C. (ed.), Technical University of Denmark. Risø National Laboratory for Sustainable Energy (DK). Wind Energy Department. Research in aeroelasticity EFP-2007. Risø-R-1649(EN), pp. 83-92.

[74] Larsen, T.J., Larsen, G.C., Aagaard Madsen, H. and Thomsen, K. (2008). Comparison of design methods for turbines in wake. 2008 European Wind Energy Conference and Exhibition, Brussels (BE), 31 Mar - 3 Apr 2008. Unpublished. Paper available.

[75] Larsen, T.J. (2009). Distributed computing using the Hxgrid library. Risø-R-1709(EN).

[76] Larsen, T.J., Madsen, H.Aa., Larsen, G.C., Troldborg, N. and Johansen, N. (2009). Status on development and validation of the dynamic wake meandering (DWM) model. Euromech Colloquium 508 on Wind Turbine Wakes, Madrid, 20-22 October, 2009. Extended abstract published in ISBN 978-84-7484-220-3, pp. 70-72.

[77] Larsen T.J., Madsen H.Aa., Larsen G.C. and Hansen K.S. (2011). Validation of the Dynamic Wake Meander Model for Loads and Power Production in the Egmond aan Zee Wind Farm. Accepted for publication in Wind Energy.

[78] Machefaux, E. (2010). Wake analysis on full-scale LiDAR based Measurements. Internal Risø-DTU report.

[79] Madsen, H.Aa., Larsen, G.C., Troldborg, T. and Larsen, T.J. (2011). A quasi 3D computation of merging wakes using a boundary layer equation model approach. EWEA 2011. To be published.

[80] Madsen, H.Aa., Larsen, G.C., Larsen, T.J., Mikkelsen, R. and Troldborg, N. (2008). Wake deficit-and turbulence simulated with two models compared with inflow measurements on a 2MW turbine in wake conditions. In: Scientific proceedings. 2008 European Wind Energy Conference and Exhibition, Brussels (BE), 31 Mar - 3 Apr 2008. (2008) p. 48-53.

[81] Madsen, H.Aa., Larsen, G.C. and Larsen, T.J. (2009). Development and calibration of an engineering model for simulation of wake velocity deficits. Workshop on Offshore Wind Farms. IEA, Task 23 – Offshore wind energy technology and deployment. February 25-26, Risø DTU, Risø Campus, Roskilde, Denmark. Unpublished.

[82] Madsen, H.Aa., Larsen G.C., Larsen T.J., Troldborg N. and Mikkelsen R. (2010). Calibration and Validation of the Dynamic Wake Meandering Model for Implementation in an Aeroelastic Code. Journal of Solar Energy Engineering, Vol. 132 / 041014-1.

[83] Madsen, H.Aa., Larsen, G.C., Troldborg, N. and Larsen, T.J. (2009). A quasi 3D computation of multiple wakes using a boundary layer equation BLE model. Euromech Colloquium 508 on Wind Turbine Wakes, Madrid, 20-22 October, 2009. Extended abstract published in ISBN 978-84-7484-220-3, pp. 75-76.

[84] Mann, J. (2009). Presentation of various Danish wind energy activities (among these TOPFARM activities) at the scientific workshop "Large-Scale Wind Generated Power" hosted by Cornell University, 12-13 June 2009.

[85] Markou, H. and Andersen, P.B. (2009). Potential load reductions on megawatt turbines exposed to wakes using individual pitch wake compensator and trailing edge flaps. Euromech Colloquium 508 on Wind Turbine Wakes, Madrid, 20-22 October, 2009. Extended abstract published in ISBN 978-84-7484-220-3, pp. 77.

[86] Markou, H., Andersen, P.B., Larsen, G.C. (2010). Potential Load Reductions on Megawatt Turbines Exposed to Wakes using Individual Pitch wake Compensator and Trailing Edge Flaps. Wind Energy (special issue), DOI: 10.1002/we.431.

[87] McCann G.N. and King J.M. (2009). A comparison of the developed models with existing methods employed to estimate wind turbine fatigue loads within a wind farm for large off shore and simple terrain sites. Garrad Hassan report 12803/BR/04, Garrad Hassan and Partners Limited.

[88] McCann G.N. and King J.M. (2009). An investigation into the benefits of individual pitch control in alleviating wind turbine loading within a meandering wake flow. TOPFARM project WP3, Garrad Hassan report 12803/BR/05, Garrad Hassan and Partners Limited.

[89] McCann, G.N. (2009). Deliverable D5: EU-TOPFARM; A parameterisation of the wake wind field suited for detailed and rapid load prediction. Garrad Hassan report 12803/BR/02, Garrad Hassan and Partners Limited.

[90] McCann, G.N. (2009). Deliverable D4: EU-TOPFARM; A method to facilitate full aeroelastic modeling of a wind farm turbine based on detailed three-dimensional dynamic wake wind field simulation. Garrad Hassan report 12803/BR/01, Garrad Hassan and Partners Limited.

[91] McCann, G.N. (2009). Deliverable D6: EU-TOPFARM; An efficient way of approximating turbine fatigue loads within wind farms developed to scale with future wind energy plant trends. Garrad Hassan report 12803/BR/03, Garrad Hassan and Partners Limited.

[92] Migoya, E., Jiménez, A., Manuel, F. and Crespo, A. (2009). Stochastic simulation to study wake meandering using UPMPARK. Euromech Colloquium 508 on Wind Turbine Wakes, Madrid, 20-22 October, 2009. Extended abstract published in ISBN 978-84-7484-220-3, pp. 8-10.

[93] Migoya, E., Jiménez, A. and Crespo, A. (2009). Estudio no estacionario y del meandering de las estelas de un parque eólico. IX Congreso Iberoamericano de Ingeniería Mecánica Las Palmas de Gran Canaria, 17-20 November, 2009. Proceeding of the congress, pp. 146.

[94] Mikkelsen, R., Sørensen, J.N. and Øye, S. (2009). Meandering Wake Characteristic Derived from Actuator Line Simulations of Wind Turbine Wakes. Euromech Colloquium 508 on Wind Turbine Wakes, Madrid, 20-22 October, 2009. Extended abstract published in ISBN 978-84-7484-220-3, pp. 29.

[95] Mouritzen, A.S. (2010). DONG Energy's contribution to WP1, DONG Energy, PONDUS Doc. 757431 (2010-06-17).

[96] Neubert, A., Shah, A. and Schlez, W. (2010). Maximum yield from symmetrical wind farm layouts. DEWEK 2010, Bremen, 17-18 November.

[97] Morten, N. (2009). Stochastic simulation of wake meander and turbulence in a wind farm. Euromech Colloquium 508 on Wind Turbine Wakes, Madrid, 20-22 October, 2009. Extended abstract published in ISBN 978-84-7484-220-3, 80p.

[98] Okulov, V.L.; Sørensen, J.N. and Shen, W.Z. (2008). Refined Betz limit for rotors with a finite number of blades. Wind Energy, Vol. 11, pp. 415-426.

[99] Okulov, V. and Sørensen, J.N. (2008). An ideal wind turbine with a finite number of blades. Doklady Physics, Vol. 53(6), pp. 337-342.

[100] Okulov, V.L. and Sørensen, J.N. (2010). Maximum efficiency of wind turbine rotors using Joukowsky and Betz approaches. To appear in Journal of Fluid Mechanics.

[101] Ott, S. (2009). Fast linearized models for wind turbine wakes. Euromech Colloquium 508 on Wind Turbine Wakes, Madrid, 20-22 October. Extended abstract published in ISBN 978-84-7484-220-3, pp. 11-13.

[102] Rethore, P.-E., Fuglsang, P., Larsen, T.J., Buhl, T. and Larsen, G.C. (2011). TOPFARM wind farm optimization tool. Risø-R-1768(EN).

[103] Rethore, P.-E., Fuglsang, P., Larsen, G.C., Buhl, T., Larsen, T.J. and Madsen, H.Aa. (2011). TOPFARM: Multi-fidelity Optimization of Offshore Wind Farm. The 21st International Offshore (Ocean) and Polar Engineering Conference, ISOPE-2011, Maui, Hawaii, June 19-24.

[104] Schmidt, B. et al. (2011). Load validation and comparison versus certification approaches of the Risø Dynamic Wake Meandering (DWM) model implementation in GH Bladed, EWEA 2011. To be published.

[105] Stidworthy, A., Carruthers, D. and Hunt, J. (2011). A new approach to modelling mean flow and turbulence in wind turbine wakes and wind farm environments. EGU General Assembly 2011.

[106] Stidworthy, A., Carruthers, D. and Hunt, J. (2011). CERC activities during the TOPFARM project: Wind turbine wake modeling using ADMS. FM766/2011/1. Cambridge Environmental Research Consultants ltd.

[107] Stidworthy, A., Carruthers, D. and Hunt, J. (2011). CERC activities under WP8 of the TOPFARM project: Optimisation of the Stags Holt and Coldham wind farm in the UK. FM766/2011/WP8/1. Cambridge Environmental Research Consultants ltd.

[108] Sørensen, J.N. and van Kuik, G. (2009). Actuator disc momentum theory for low lambda rotors. Euromech Colloquium 508 on Wind Turbine Wakes, Madrid, 20-22 October, 2009. Extended abstract published in ISBN 978-84-7484-220-3, pp. 30-31.

[109] Sørensen, J.N., Mikkelsen, R., Troldborg, N., Okulov, V. and Ivanell, I. (2011). Simulation and Modeling of Turbulent Wind Fields in Wind Farms. DTU Mechanical Engineering contribution to TOPFARM Work Package 1. Technical University of Denmark.

[110] Troldborg, N., Sørensen, J.N. and Mikkelsen, R. (2009). Numerical Simulations of Wakes Operating in Sheared and Turbulent Inflow. Proc. EWEC 2009, European Wind Energy Conference, Marseille.

[111] Troldborg, N., Larsen, G.C. and Madsen, H.A. (2009). Numerical Simulations of Wake Interaction between Two Wind Turbines at Various Inflow Conditions. Euromech Colloquium 508 on Wind Turbine Wakes, Madrid, 20-22 October. Extended abstract published in ISBN 978-84-7484-220-3, pp. 23-25.

[112] Troldborg, N., Larsen, G.C., Madsen, H.Aa., Sørensen, J.N. and Mikkelsen, R. (2010). Numerical Simulations of Wake Interaction between Two Wind Turbines at Various Inflow Conditions. Submitted for publication in Wind Energy.

[113] Troldborg, N., Sørensen, J.N. and Mikkelsen, R. (2009). Numerical simulations of wake characteristics of a wind turbine in uniform inflow. Wind Energy, **13**, 86-99. doi: 10.1002/we.3452009.

[114] Trujillo, J.J., Bingöl, F., Larsen, G.C., Mann, J. and Kuehn, M. (2009). Lidar Measurements of Wake Dynamics, Part 2: Two Dimensional Scanning. Wind Energy (2010) Published online. DOI:10.1002/we.402.

[115] Trujillo, J.J., Bingöl, F., Larsen, G.C., Mann, J. and Kühn, M. (2008). LIDAR measurements of wind turbine wake dynamics and comparison with an engineering model. Wake workshop, Oldenburg (DE), 30 June - 2 July. Unpublished.

[116] Trujillo, J.J., Bingöl, F., Mann, J., Larsen, G.C. and Kühn, M. (2008). LIDAR measurement and modelling of wind turbine far-wake dynamics. In: Book of abstracts. 9. German wind energy conference (DEWEK 2008), Bremen (DE), 26-27 Nov 2008, pp. 17-20

[117] Veldkamp, D. (2010). Data for Stags Holt/Coldham wind farm, UK. Deliverable D19: EU – TOPFARM. Technical Report, Vestas Global research.

7 REFERENCES

[118] Ainslie, J. F. (1985). Development of an eddy viscosity model for wind turbine wakes. Proceedings of 7th BWEA Wind Energy Conference.

[119] Arora, J.S. (2004). Introduction to Optimum Design. Elsevier-direct, ISBN 9788131201275.

[120] Bingöl, F. (2005). Adapting a Doppler laser anemometer to wind energy. M.Sc. Thesis Project.

[121] Bingöl, F., Mann, J. and Larsen, G.C. (2007). Laser measurements of wake dynamics. EWEC2007, Milan, Italy.

[122] Bladed Theory Manual, Version 4.0, Garrad Hassan & Partners Ltd, United Kingdom, 2010.

[123] Cleine, J.W. (1993). TNO Results of Sexbierum Wind Farm; single wake measurements. TNO document number 93-082.

[124] Crespo, A.; Chacon, L.; Hernandez, J.; Manuel, F. and Grau, J. (1994). UPMPARK: a parabolic 3D code to model wind farms. Proc. EWEC 1994, European Wind Energy Conference, Thessaloniki, 454-459.

[125] Database of Wind Characteristics; http://www.windata.com/

[126] Fuglsang, P. and Madsen, H.Aa. (1995). Optimization of Stall Regulated Rotors. Proc. ASME Wind Energy – 1995, Houston, Texas, SED-Vol 16, pp. 151-158.

[127] Fuglsang P. and Madsen H.Aa. (1999). Optimization method for wind turbine rotors. J. Wind Engineering and Industrial Aerodynamics Vol. 80 No 1-2, pp. 191-206.

[128] Fuglsang P. and Thomsen, K. (2001). Site Specific Design Optimization Of Wind Turbines. ASME J. Solar Engineering, Vol. 123, pp 296-303.

[129] Goffe, Ferrier and Rogers (1994). Global Optimization of Statistical Functions with Simulated Annealing. J. of Econometrics, vol. 60, no. 1/2, Jan./Feb. 1994, pp. 65-99.

[130] Goldberg, D.E. (1989). Genetic Algorithms in Search, Optimization & Machine Learning, New York: Addison-Wesley, ISBN 0201157675.

[131] Hansen, K.S. (2010). 3 x 3 x 1 Flow cases at NoordZee wind farm - Draft version, UPWIND WP8, DTU-MEK; Unpublished.

[132] Jonkman, J., Butterfield, S., Musial, W. and Scott, G. (2009). Definition of a 5-MW reference wind turbine for offshore system development, Tech. Report NREL/TP-500-38060, National Renewable Energy Laboratory (NREL).

[133] Larsen T.J. and Hansen A.M. (2006). Influence of Blade Pitch Loads by Large Blade Deflections and Pitch Actuator Dynamics Using the New Aeroelastic Code HAWC2. Proc. EWEC 2006, Athens.

[134] Larsen T.J. and Hansen, A.M. (2007). How 2 HAWC2, the user's manual. Risø-R-1597(ver. 3-1)(EN), 70p.

[135] Mann J. (1994). The spatial structure of neutral atmospheric surface-layer turbulence. Journal of Fluid Mechanics, 273, 141-168.

[136] Michelsen, J.A. (1994). Block Structured Multigrid Solution of 2D and 3D elliptic PDE's. Report AFM 94-06, Dept. of Fluid Mechanics, Technical University of Denmark, DTU.

[137] Mikkelsen, R., Sørensen, J.N. and Troldborg, N. (2007). Prescribed Wind Shear Modeling Combined with the Actuator Line Technique. EWEC, Milan.

[138] Shinozuka, M. and Jan, C.M. (1972). Digital Simulation of random Processes and Its Applications. Journal of Sound and Vibration, Vol. 25. No. 1, pp. 111-128.

[139] Sørensen, J.N. and Shen, W.Z. (2002). Numerical modeling of Wind Turbine Wakes. Fluids Engineering, Vol. 124, Issue 2.

[140] Sørensen, N.N. (1995). General Purpose Flow Solver Applied to Flow over Hills, PhD thesis, Risø-R-827(EN), Risø National Laboratory.

[141] Troldborg, N. (2008). Actuator Line Modeling of Wind Turbine Wakes, PhD Dissertation, MEK-PhD 2008-03, Technical University of Denmark.

[142] Ganander, H. (2003). The use of a Code-generating System for the Derivation of the Equations for Wind Turbine Dynamics, Wind Energy, Vol. 6, Issue 4, pp. 333-345.

[143] Bossanyi, E.A. (2004). Developments in Induvidual Blade Pitch Control. EWEA 04/2004.

[144] Andersen. P.B. (2009). Advanced load alleviation for Wind turbines using Adaptive Trailing Edge Flaps: Sensoring and Control. PhD Thesis, Risø-DTU.

[145] Jonkman, J. (2005). NREL 5MW Baseline Wind Turbine. NREL/NWTC: 1617 Cole Boulevard, Golden, CO80401-3393, USA.

[146] Thomsen, K., Madsen, H.Aa., Larsen, G.C. and Larsen, T.J. (2007). Comparison of methods for load simulation for wind turbines operating in wake. Journal of Physics: Conference Series, **75**. DOI:10.1088/1742-6596/75/1/012072.

[147] Nieslony, A. (2010). Rainflow counting function for Matlab. Matlab file exchange website.

Risø DTU is the National Laboratory for Sustainable Energy. Our research focuses on development of energy technologies and systems with minimal effect on climate, and contributes to innovation, education and policy. Risø has large experimental facilities and interdisciplinary research environments, and includes the national centre for nuclear technologies.

Risø DTU
National Laboratory for Sustainable Energy
Technical University of Denmark

Frederiksborgvej 399
PO Box 49
DK-4000 Roskilde
Denmark
Phone +45 4677 4677
Fax +45 4677 5688

www.risoe.dtu.dk